ABSTRACT

SAMU, VIVEK. Nondestructive Length Estimation of Pile Foundation through Effective Dispersion Analysis of Reflections. (Under the direction of Dr. Murthy Guddati).

This dissertation introduces a newly developed method called the Effective Dispersion Analysis of Reflections (EDAR) to effectively estimate the length of unknown foundations. The key idea of the method is based on accurately capturing the dispersion of waves as they propagate through a pile and is applicable to both longitudinal and bending waves. Specifically, the measured accelerations at two distinct locations on the pile due to hammer impact is processed using EDAR methodology resulting in an estimate of the pile length (foundation depth).

Firstly, EDAR is derived through simple one-dimensional bar and Bernoulli-Euler beam models and validated through laboratory testing. The analysis hinges on examining the oscillations in phase difference that are due to reflections, as a function of a newly defined quantity called effective wavenumber, which is essentially a scaled wavenumber. Laboratory experiments on concrete filled steel tubes (CFST) on loose soil conditions resulted in accurate length estimates with less than 5 percent error.

Secondly, based on the success in the lab EDAR was extended to field piles. The original EDAR method is based on processing dispersive bending wave signals in the frequency-effective wavenumber domain, thus eliminating the need to perform peak picking that is difficult due to over-distortion of reflected signals. While the method was successful in laboratory settings, preliminary field validation resulted in significant errors. After careful examination of the wave physics, it is discovered that both longitudinal and transverse waves need to be carefully included in EDAR analysis. Specifically, it is shown that the initial arrival is dominated by transverse waves, while the reflections are dominated by longitudinal waves, owing to significant attenuation of transverse waves due to compacted soil around the pile. This observation led to a refined EDAR methodology and accurate estimation of embedded pile depth in field settings (less than 10 percent error).

Finally, all the factors that influence EDAR including accurate measurement, other boundaries such as pile top and damage in the pile were examined through synthetic beam models as well as preliminary laboratory and field testing.

© Copyright 2019 by Vivek Samu

All Rights Reserved

Nondestructive Length Estimation of Pile Foundations through Effective Dispersion Analysis of Reflections

by
Vivek Samu

A dissertation submitted to the Graduate Faculty of
North Carolina State University
in partial fulfillment of the
requirements for the degree of
Doctor of Philosophy

Civil Engineering

Raleigh, North Carolina
2019

APPROVED BY:

_____	_____
Dr. Murthy Guddati Committee Chair	Dr. Shamim Rahman
_____	_____
Dr. Mervyn Kowalsky	Dr. Ralph Smith

DEDICATION

Amma, Appa and Akka.

BIOGRAPHY

Vivek Samu was born and brought up in the city of Chennai, Tamil Nadu in India, son of Samu Shanmugasundaram and Sornavalli Nageswaran. He joined undergraduate in Civil Engineering in National Institute of Technology, Tiruchirapalli in 2008 and received Bachelor's in Technology degree in August 2012. Upon completion of his undergraduate degree, he joined North Carolina State University and earned his Master of Science in Civil Engineering with specialization in Structural engineering in 2015. He continued on to pursue his Doctor of Philosophy in Civil Engineering with a minor in Applied Mathematics and this dissertation is a result of the research conducted.

ACKNOWLEDGMENTS

I would like to express my deep gratitude to my advisor Dr. Murthy Guddati for his patient guidance, encouragement and useful critiques of this research work. His valuable suggestions have helped me progress and improve as a researcher over the course of my graduate studies.

I would like to thank Dr. Mervyn Kowalsky, Dr. Shamim Rahman and Dr. Ralph Smith for serving as members of my advisory committee. I would also like to specially thank Dr. Mervyn Kowalsky and Dr. Diego Aguirre Realpe for allowing me to perform tests on piles built for their research at North Carolina State University.

I would also like to thank Mr. Mike Knapp and Mr. Hiram Henry from Alaska Department of Transportation and Mr. Mohammed Mulla and Mr. Chris Krieder from North Carolina Department of Transportation for their continued support in identifying and help in testing of the field piles.

Many thanks to my fellow graduate students Dr. Hao Hu, Dr. Ali Vaziri, Srikrishnan Madhavan, David Zabel, Abhinab Bhattacharjee, Abdelrahman Elmeliegy, and Sriram Guddati who helped me during several laboratory and field tests. I would also like to thank all my friends at North Carolina State University and elsewhere who have supported me throughout my graduate school.

I would like to thank Keerthana for her unrelenting support and love throughout this journey.

Finally, I would like to thank my mother, father, and my sister Sudha for their unconditional love, and support throughout my life.

TABLE OF CONTENTS

LIST OF TABLES

LIST OF FIGURES

Chapter 1

Introduction

The 2017 report card for America's Infrastructure by American Society of Infrastructure (ASCE) [1], reports that one in eleven of the nation's bridges are rated as structurally deficient and the average age of the nation's over 600,000 bridges is 43 years. Also, almost 39% of existing bridges are 50 years or older. Thus, the need for structural health monitoring of bridges in terms of maintenance, repair and rehabilitation is becoming more and more critical. Pile Foundations are the most common type of deep foundations for bridges and are used for various conditions such as loose soil, large loads from structure, lack of space for shallow foundation. The capacity of a pile foundation is directly related to its embedded depth. Reduction in the effective depth of the foundation, especially due to scour, may cause significant reduction in strength and thus compromises the safety of the structure. National Bridge Inventory reports that there are more than 27,000 bridges with unknown foundation as of 2016, which could be potentially scour susceptible. Several other bridges over land are also expected to have unknown foundation and missing or incomplete records [2]. The scour safety of the bridge cannot be determined until the depth of foundation is known, and in most cases the records do not exist. Also, for bridges over land, repair and rehabilitation require information about the foundation elements. Hence it is beneficial to evaluate the effective embedded length of pile.
Detailed studies by the Florida state department of transportation [3], Olson et all [4] and Rausche [5] , contain a comprehensive list, with basic description, of most of the methods used for estimation of unknown foundation depth. The available methods can be categorized broadly into evidence based and nondestructive evaluation methodologies. Evidence based techniques involve static back calculation method based on pile design procedures and artificial neural network (ANN) specially built based on the available data for a region to arrive at unknown foundation information. Nondestructive evaluation methodologies are further categorized as surface techniques and borehole techniques.

Surface techniques comprise of several different NDE methodologies such as the sonic echo, impulse response, ultra-seismic, bending wave (short kernel) method, ground penetrating radar, and dynamic foundation response. Sonic-echo, impulse-response and their extension, ultraseismic methods have been widely used for a variety of situations such as integrity/condition

assessment, damage identification and length evaluations (see e.g. [6]–[15]). Lack of access to the pile top, and inability to induce purely longitudinal wave modes, increase the complexity in the analysis. Sonic echo and impulse response methods require information about the wave propagation velocity in the pile. While typical values based on the pile material are used, this introduces an inherent error in the estimates. This was addressed by the ultraseismic method which uses several sensors along the side of the pile to identify the initial arrival and reflections with higher confidence. This procedure requires multiple sensors and sufficient spacing between sensors which might not be available for piles with limited exposed lengths. Additionally, inducing a combination of both longitudinal and flexural waves increase the complexity in the patterns observed and subsequent analysis.

The idea of using lateral impact inducing flexural waves, rather than the conventional longitudinal waves from the impact-echo method, was introduced by Holt and Douglas [16] and later explored by other researcher [17]–[19]. Lateral impact imparts most energy into bending waves that are dispersive in nature. The analysis of dispersive waves is much more complicated than non-dispersive waves such as longitudinal waves; unfortunately, longitudinal waves are not excited well due to lateral impact and it is essential to deal with dispersive flexural waves. Holt and Douglas introduced the Short-Kernel Method (SKM) to process the response from dispersive flexural waves to obtain the travel time information, which is used to estimate the embedded length of the pile. SKM consists of choosing a kernel of a particular frequency, generally the dominant frequency of impact, and obtaining a cross correlation between the kernel and the signal. The plot of the cross correlation is known as the short kernel plot. This plot contains information about that particular frequency (frequency of the kernel) from the signal and the time difference between consecutive peaks is used to obtain the velocity of wave propagation. Using the known distance between the sensors, the velocity of propagation is determined by picking the first arrival peaks. This velocity obtained was used for the embedded part of the pile, along with the travel time calculated from the reflection peak to find the embedded length of the pile. This approach is completely based on the time of travel and does not take into account the effect of the soil and changes in wave velocity for the free and the embedded parts. Choosing the kernel frequency and picking the peaks that correspond to the initial wave arrival and reflected wave arrival can be complicated even for an experienced user [20]. Other signal processing technique based on combined time-frequency analysis (Hilbert Huang Transforms) was used for the

dispersive flexural waves by Farid [21]. Subhani et al. [22] used a combination of SKM and continuous wavelet transform (CWT), which is another time-frequency analysis technique, to estimate the embedded lengths of electricity poles and observed significant error margins in both the cases, up to 43% in some cases. Sheng-Huoo et al. [23] compares results from sonic echo test using CWT, in the context of longitudinal waves. All the above methods are purely based on signal processing and do not explicitly incorporate the dispersion properties of the waves. Essentially, all surface-based methods still rely on being able to get an identifiable reflection from the pile tip. This is specifically a problem whenever there is longer embedment depth and is compounded by the presence of stiffer soils due to the leakage of the waves into the soil. Also, complex foundation elements such as splices, embedded caps could potentially prevent the waves from reaching the pile tip and the reflection from these elements are not distinguishable giving a false length estimate.

The other class of nondestructive tests for pile foundations are borehole techniques, including parallel seismic, cross hole sonic, borehole sonic, borehole radar, borehole ultrasonic as well as induction testing and borehole magnetic for steel piles (see e.g. [4], [24]–[29]). All these tests require either a borehole alongside the pile foundation or a preinstalled test pipe in the pile and require expensive equipment. Even though these techniques are very reliable and applicable to a vast number of situations, using them to test a large group of piles is not practical due to the site requirements and cost. Thus, there is still a need for a quick, effective and cheaper techniques. These class of techniques are not used in the testing and evaluation of piles in this thesis and are not further explored.

Apart from NDE methods, other evidence based approaches such as reverse engineering based on static back calculation using the AASTHO design principles have also been used in practice [30]–[32]. Artificial Neural Networks (ANN) have also been used along with back calculation to extract information about unknown foundation and soil conditions depending on the availability of data in any region [3], [32], [33]. ANN have the advantage of providing estimates about unknown foundation by training the system based on the known information available in a region without need for conducting physical tests. They can also provide more information about the foundation and surrounding soil depending on the availability of information. But they are region specific and success at one region does not translate to others as the algorithm needs to be trained based on the region. Additionally, certain unknown foundation

locations do not have boring data and that requires conducting borings at bridges locations which is an added cost to the method. Unlike field evaluations, evidence-based methods are based on available data and previous design practices.

In spite of the extensive work on NDE of pile foundations, evaluation techniques are either not reliable in practical situations or expensive and prohibitive to scale for a large number of bridges and thus, there is a need for an effective method to estimate the embedded length of piles. The main objective of this work is to develop an easy, quick and effective methodology for reliably estimating the embedded length of pile foundation with minimal user intervention. We propose a new methodology called Effective Dispersion Analysis of Reflections (EDAR) that extracts the length information by carefully considering the physics of the wave dispersion and this methodology is the core of this thesis. EDAR incorporates the physical dispersion properties of the waves generated to estimate the length of the pile foundation.

The outline of the rest of the thesis is as follows. Chapter 2 presents the theory behind EDAR methodology, mathematical analysis based on simple bar and beam theories and initial laboratory validation of the methodology. Chapter 3 presents extension of EDAR to solid concrete field piles and the effect of soil which led to an improved length estimation procedure. Chapter 4 presents the details about the testing methodology, equipment selection and hammer characteristics which play an important role in obtaining useful data from testing. Chapter 5 presents the extension of the EDAR methodology to Concrete Filled Steel Tubes, aspects from both the laboratory and field application and preliminary work on quantifying the effects of other boundaries and damage in the pile. Chapter 6 presents the summary, conclusions and recommendations for future work.

Chapter 2

Nondestructive Method for Length Estimation of Pile Foundations through Effective Dispersion Analysis of Reflections

Abstract

A longstanding threat to bridge safety is the unknown foundation depths of bridges that are also identified as potentially susceptible to scour. According to the National Bridge Inventory, about 28,000 highway bridges with unknown foundation depths were recorded in 2016. Researchers have developed and investigated several methods over the years to determine embedded foundation lengths, including sonic echo/impulse response methods, bending wave method, various borehole methods, and many extensions and modifications of these methods. The borehole methods are considered reliable but expensive, and the surface-based methods are less expensive but lack the same level of reliability as the borehole methods. To address this problem, we have developed a new surface-based nondestructive test method that we call 'effective dispersion analysis of reflections' (EDAR). We show that EDAR is not only inexpensive, but also accurate and reliable. The method is based on accurately capturing the dispersion of waves as they propagate through a pile and is applicable to both longitudinal and bending waves. Specifically, EDAR processes measured accelerations at two distinct locations on the pile due to hammer impact, resulting in an estimate of the pile length (foundation depth): the analysis hinges on examining the oscillations in phase difference that are due to reflections as a function of wavenumber. We have validated EDAR using side impacts on concrete-filled steel tubes; the results consistently showed less than 5 percent error in a laboratory setting.

2.1 Introduction

Even after more than two decades of research and implementation ([34] ,[3]), the National Bridge Inventory reports that the United States has about 28,000 bridges with unknown foundation depths in 2016 that could be potentially susceptible to scour. The scour vulnerability of a bridge cannot be determined until the embedded depth of the foundation is known, and records that contain the total lengths of piles do not always exist. Thus, in order to evaluate the potential for scour, nondestructive evaluation (NDE) techniques are typically needed to estimate the length of embedded piles.

One class of NDE methods for pile foundations is borehole techniques, which include parallel seismic, cross-hole sonic, borehole sonic, borehole radar, and borehole ultrasonic methods as well as induction testing and borehole magnetic testing for steel piles (see [15], [24], [25], [27], [28], [35], [36] for examples). All these tests require either a borehole alongside the pile foundation or a pre-installed test pipe in the pile. They also require expensive equipment along with an experienced user to interpret the results. Even though these techniques are reliable and applicable to a vast number of situations, using borehole methods to test a large group of piles is not practical due to excessive costs and site limitations.

The other class of NDE methods is surface-based techniques, which do not require drilling boreholes. These methods include sonic echo, impulse response, ultra-seismic, and bending wave (short kernel) methods. Levy [6] and Dunn [7] pioneered work that led to the development of the sonic echo and impulse response techniques. Both methods are based on generating a longitudinal wave using a hammer impact on the top of a pile and analyzing the obtained response in the time domain for the sonic echo method and in the frequency domain for the impulse response method. Specifically, in time domain length estimates are obtained by identifying peaks associated with initial and reflected waves. This methodology became more prevalent after the advent of digital signal processing, starting with the work of Rausche et al. [8]. Several researchers have continued to use this methodology since then for a variety of situations [9]–[14]. Recent work by Rashidyan [37] investigated sonic echo type of methods for existing timber piles without top access (by vertically impacting on a metal block attached to the pile); however, other researchers determined that this method is not successful when testing steel H piles [31]. An extension of the sonic echo method using multiple sensors on the pile side, known as the ultra-seismic method, also has been established. All these surfaced-based methods rely on producing a wave that is dominated by longitudinal mode. However, due to the inaccessibility of the pile top, this process remains difficult because other types of waves (e.g., flexural waves) can also play a part in the data collected.

In order to try to solve the problems associated with an inaccessible pile top, Holt and Douglas first conceived the idea of using lateral impacts to induce flexural waves rather than using the impact-echo method to induce conventional longitudinal waves [16]. A lateral impact imparts most of the energy through bending waves that are dispersive in nature thus, it is essential to deal with dispersive flexural waves. To this end, Holt and Douglas [16] introduced

the bending wave or short kernel method to process responses from dispersive flexural waves to obtain travel-time information, which attempts to delineate the peaks through convolution, thereby enabling the application of simple travel-time algorithms. Although this idea is innovative, the choice of short kernel and subsequent peak selection is complicated, even for experienced users, resulting in subjective estimates with large errors (see e.g., [22]). Other techniques, such as Hilbert-Huang transform or continuous wavelet transform have been used by Subhani et al. [22], Farid [21] and Sheng-Hugo et al. [23]. All these techniques are based purely on signal processing and do not explicitly incorporate the underlying dispersion properties of the generated waves that could be utilized constructively to develop pile length estimation techniques.

Given both the advantages of using side impacts and the limitations associated with the existing processing techniques for flexural waves, we propose a new signal processing technique we call 'effective dispersion analysis of reflections' (EDAR). EDAR extracts length information by carefully considering the physics of wave dispersion, which has been ignored thus far in relevant methodologies. The experimental set-up for EDAR is identical to flexural wave testing, but the critical data processing step is fundamentally different and built on robust mathematical analysis that is, in turn, built on the precise dispersion relation that represent wave physics. We verified the proposed methodology using synthetic data and validated it using laboratory experiments.

The outline of the rest of the paper is as follows. Section 2.2 contains the problem definition and experimental set-up. A detailed derivation of the EDAR technique is given in Section 2.3, starting from simple longitudinal waves and leading to more complicated flexural waves. Section 2.4 contains the results from the laboratory validation effort, followed by conclusions in Section 2.5.

2.2 Problem Definition and Experimental Set-up

Pile foundations are made of various materials, such as timber, concrete, steel, or a combination thereof, and are either cast in place or driven deep into the soil. Many bridges have part of the pile exposed above the soil, terminating in the pile cap. The aim of this work is to estimate the embedded length of the pile using nondestructive testing. To achieve this aim, the pile foundation is excited by imparting a sharp strike using a hand-held hammer, and the

response is measured at a minimum of two locations in the foundation using sensors such as accelerometers or geophones. Depending on the location and type of excitation imparted to the pile, several types of waves can exist, such as longitudinal, flexural, and high order guided waves. Figure 2-1 presents a typical pile subjected to lateral impact, which is also the experimental set-up used in this study.

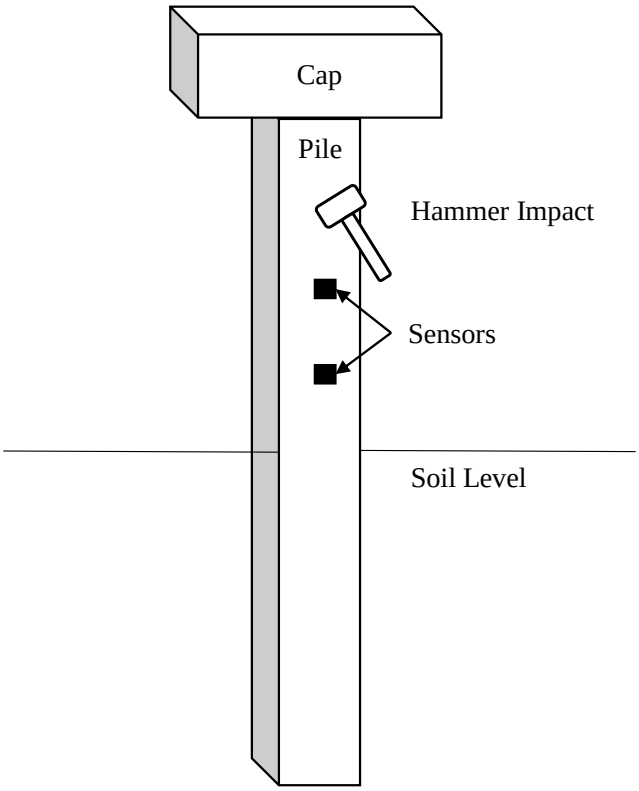

Figure 2-1: Pile and experimental set-up schematic.

We employed EDAR to process responses measured at two sensor locations along the length of a pile. EDAR can be applied for both longitudinal and flexural waves. Similar to the aforementioned surface-based methods, EDAR requires access to the exposed portion of the pile to record accelerations or velocity from a hammer impact at a minimum of two locations along the length of the pile. The major contribution of this paper (and how it differs from earlier methods) is the way the data are processed to estimate the length of a pile. Section 2.3 discusses the concept behind processing the data using the EDAR methodology.

2.3 Effective Dispersion Analysis of Reflections (EDAR): Theory

The fundamental concept of EDAR is based on the difference of individual phases between the responses measured at the two sensor locations. The basic theory is explained for both longitudinal and flexural waves, followed by verification using synthetic data and validation using laboratory experiments. EDAR presents a unique way to process the same response data that can be obtained from the ultra-seismic or short kernel (bending wave) methods to estimate the length of the pile by incorporating the physical dispersion characteristics of wave propagation. The phase difference between the responses at the two sensor locations in the frequency domain is given by

$$P_d = \text{Imag}\left(\log\left(u_2(\omega)\right) - \log\left(u_1(\omega)\right)\right) , \tag{2.1}$$

where $u_1(\omega)$ and $u_2(\omega)$ are the Fourier transforms of the responses (displacements, velocities or accelerations) obtained at the two sensor locations, respectively. The phase difference between the responses obtained at the two sensor locations in the frequency domain contains the product of theoretical wavenumber (k) and the lengths associated with the pile. Generally, the phase depends on the distance the wave has traveled before and after reflections from the various boundaries in the structure. Section 2.3.1 explains the characteristics of the phase difference and extraction of the pile length using simple theoretical models: Section 2.3.1.1 discusses wave propagation without reflections with the help of dispersion analysis, and Section 2.3.1.2 discusses the effects of the reflections and introduces the concept of EDAR plot.

2.3.1 Longitudinal waves in bar

2.3.1.1 Propagation without reflections

Longitudinal or axial waves are nondispersive in nature and thus exhibit minimal variation in the initial waveform observed in the time domain. Figure 2-2 shows the simplest case of an infinite bar in which a propagating wave traveling from left to right is encountered once by the two sensors.

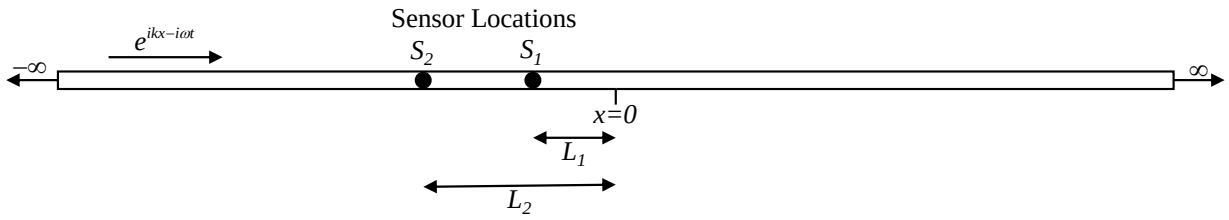

Figure 2-2: Schematic of infinite bar.

The second order differential equation describing the axial wave propagation in a homogeneous, linear elastic rod with Young's modulus E and density ρ is given by

$$-E\frac{\partial^2 u}{\partial x^2}+\rho\frac{\partial^2 u}{\partial t^2}=0\ , \tag{2.2}$$

which on transformation to frequency domain takes the form

$$-\frac{\partial^2 u}{\partial x^2}-{c_b}^2\omega^2\frac{\partial^2 u}{\partial t^2}=0\ , \tag{2.3}$$

where ω is the temporal frequency, c_b is the bar wave velocity and is given by $\sqrt{E/\rho}$, E is Young's modulus, and ρ is density. The solution of the equation in frequency domain takes the form

$$u(x,\omega)=Ae^{ikx}, \tag{2.4}$$

where k is the wavenumber. The wavenumber can be determined from the frequency by substituting Equation (2.4) into Equation (2.3), which gives the dispersion relation expressed as Equation (2.5).

$$k=\frac{\omega}{c_b} \tag{2.5}$$

Substituting Equation (2.4) in Equation (2.1) results in the phase difference:

$$P_d=k(L_2-L_1)=k\Delta L\ . \tag{2.6}$$

Thus, the phase difference is a product of the theoretical wavenumber (k) and the distance between the sensors (ΔL). Practically, the phase difference that is calculated from the sensor

responses results in wrapping between $-\pi$ and π . An important aspect of this method is to plot the phase as a function of a newly defined quantity called the 'effective wavenumber' (k_e), which is the wavenumber scaled by a material constant. Such scaling eliminates the need for the knowledge of material properties in estimating the length in this particular case (as well as in the more complicated case of Bernoulli-Euler beam theory in Section 2.3.2). In the specific case of a bar, because the theoretical wavenumber (k) in Equation (2.5) is directly proportional to the frequency, the effective wavenumber is simply defined as the frequency:

$$k_e^{bar} = \omega \ . \tag{2.7}$$

For reasons that will become clear after the reflections are analyzed in Section 2.3.1.2, the plot with the phase difference as the abscissa and the effective wavenumber as the ordinate is called the EDAR plot throughout the rest of the paper. The slope of the EDAR plot is governed by the distance between the sensors (ΔL) and the velocity of the wave propagation (c_b):

$$k_e^{bar} = \left(\frac{c_b}{\Delta L} \right) P_d \ . \tag{2.8}$$

The slope from Equation (2.8) would determine the value on the effective wavenumber axis at which the phase gets wrapped. The value at which the first wrapping occurs is called the cycle period (K_I) and is given by

$$K_I^{bar} = \frac{\pi c_b}{\Delta L} . \tag{2.9}$$

This is the first of the two periods associated with the phase and is a consequence of the initial arrival of the wave. Thus, the cycle is closely related to the time difference between the initial arrivals of the propagating wave at the two sensor locations. As an example, consider a model bar of infinite length with a wave propagation velocity of 1 m/s and lengths $L_1 = 3m$ and $L_2 = 3.5m$, thus making the distance between the sensors $0.5m$. Figure 2-3 presents the effective dispersion plot that is obtained using the solution form in equation (2.4). The first wrapping of phase occurs at 2π, as is expected from Equation (2.9).

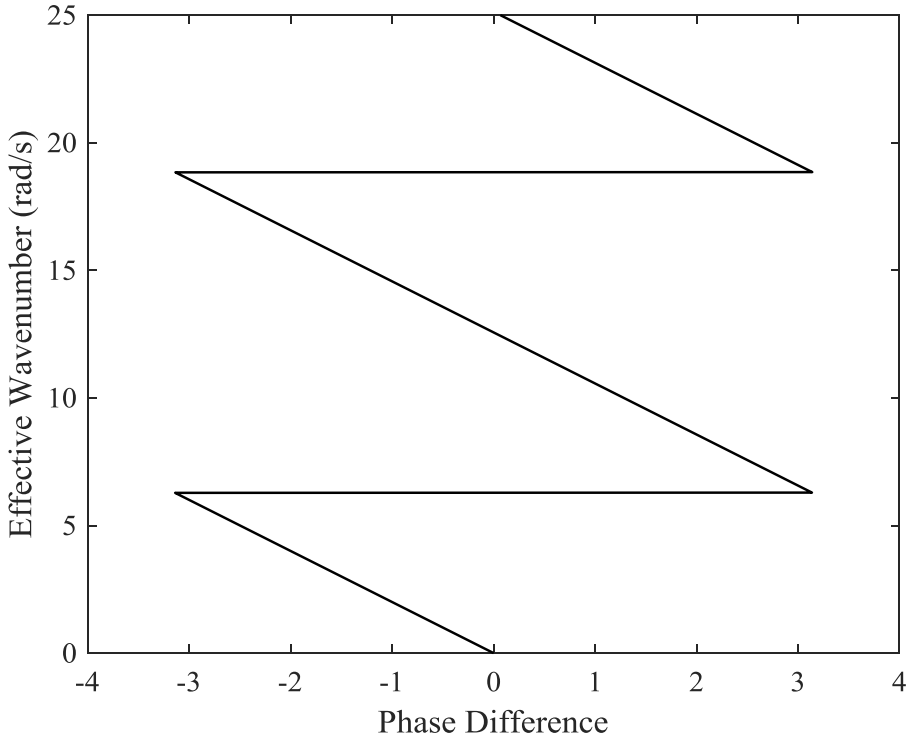

Figure 2-3: Effective dispersion plot for infinite bar: phase difference vs. effective wavenumber.

2.3.1.2 Effects of reflections and EDAR plot

Introducing a boundary at $x = 0$ makes the bar semi-infinite and results in a single reflection of the wave from the boundary; see Figure 2-4 that assumes a wave traveling from negative infinity towards the boundary where it gets reflected.

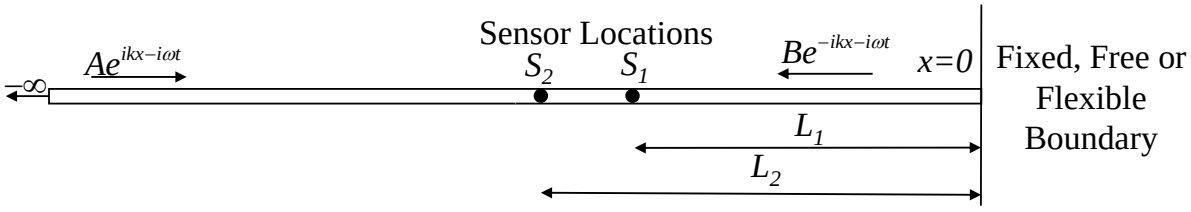

Figure 2-4: Semi-infinite bar: single reflection.

Without loss of generality, the displacement in the frequency domain anywhere in the bar can be assumed to be

$$u(x) = Ae^{ikx} + Be^{-ikx} \ , \tag{2.10}$$

where the first term on the right-hand side represents a forward propagating wave and the second term represents the reflected wave. Similar to the infinite case, a model bar with the same parameters are considered for a semi-infinite bar, but the displacement form in equation (2.10) is used to account for the reflection from the boundary (reflection coefficient of 0.5) that is introduced; Figure 2-5 presents the resultant EDAR plot that is computed for a semi-infinite bar. In addition to the cycle oscillations that are similar to those found for the infinite bar, smaller oscillations can be observed with a smaller period in the semi-infinite bar. These small oscillations, called 'wiggles', are a consequence of the wave being reflected at the boundary and can be utilized to estimate the location of the boundary.

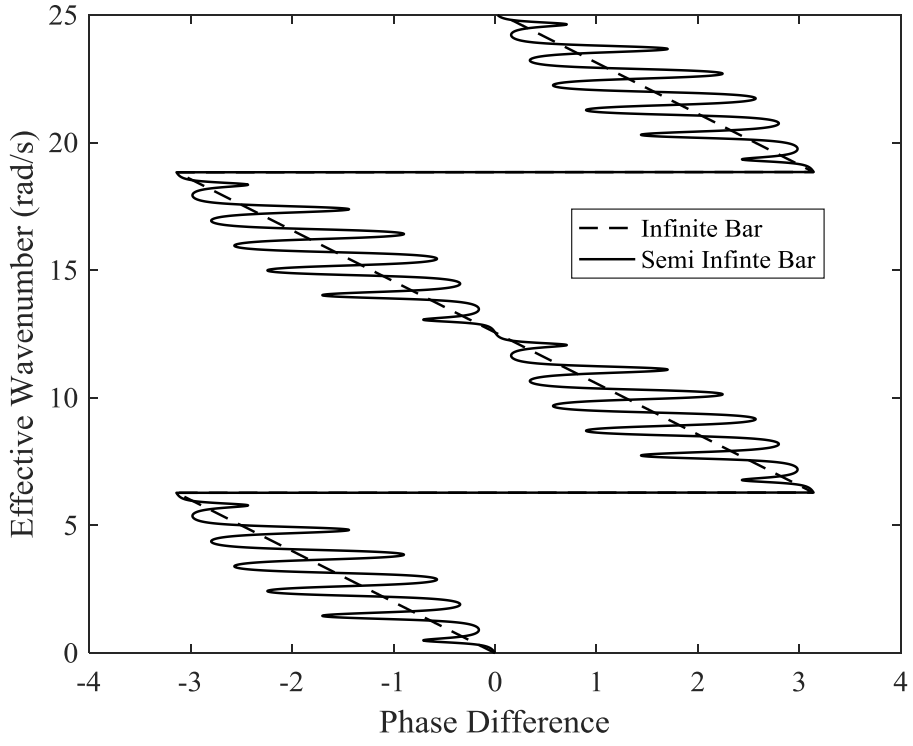

Figure 2-5: EDAR plot for semi-infinite bar superimposed on infinite bar.

The responses at the accelerometer locations S_1 and S_2 at distances L_1 and L_2, respectively, from the boundary are

$$u_1(L_1) = Ae^{ikL_1} + Be^{-ikL_1} \ , \tag{2.11}$$

$$u_2(L_2) = Ae^{ikL_2} + Be^{-ikL_2} . \tag{2.12}$$

Using these displacements, the phase difference can be calculated from Equation (2.1). The steps involved in calculating the phase difference analytically are shown here as Equations (2.13) through (2.15).

$$\frac{u_1}{u_2} = \left(\frac{Ae^{2ikL_1} + B}{Ae^{2ikL_2} + B} \right) e^{ik(L_2 - L_1)} \tag{2.13}$$

Taking the logarithm of the ratio shown in Equation (2.13) gives

$$log\left(\frac{u_1}{u_2} \right) = ik(L_2 - L_1) + log(Ae^{2ikL_1} + B) - log(Ae^{2ikL_2} + B) \ . \tag{2.14}$$

The imaginary part of Equation (2.14) is the phase difference. The imaginary part of the logarithm of a complex number is the argument of the complex number and thus

$$P_d = \underbrace{k(L_2 - L_1)}_{b_1} + \underbrace{\tan^{-1}\left(\frac{A\sin(2kL_1)}{B + A\cos(2kL_1)} \right)}_{b_2} - \underbrace{\tan^{-1}\left(\frac{A\sin(2kL_2)}{B + A\cos(2kL_2)} \right)}_{b_3} . \tag{2.15}$$

The periodic nature of P_d can be explained from the three terms b_1, b_2, and b_3. The first term is exactly the same as the one obtained for the infinite bar and, along with phase wrapping, gives rise to the cycles shown in the EDAR plot in Figure 2-3. The terms b_2 and b_3 are responsible for the smaller oscillations or wiggles observed in Figure 2-5. The trigonometric functions b_2 and b_3 can be shown to have a period of π/L_1 and π/L_2, respectively. Because the distance between the sensors is small compared to the length of the pile (L_1 is approximately equal to L_2 that is approximately equal to L^e), L^e is the distance between the midpoints of the sensors to the boundary. Thus, the period of the last two terms in Equation (2.15) in the theoretical wavenumber (k) space is given by

$$K_R^{bar} = \frac{\pi c_b}{L^e} \ . \tag{2.16}$$

One of the main practical concerns here is obtaining an accurate estimate of the wave velocity for the system under consideration. Often, pile foundations are old and deteriorated and knowledge about the construction material is hard to obtain. Examining the ratio of the cycle and wiggle periods helps resolve this issue. The ratio of the cycle and wiggle periods is

$$\frac{K_I^{bar}}{K_R^{bar}} = \frac{\pi c_b / \Delta L}{\pi c_b / L^e} = \frac{L^e}{\Delta L} \ . \tag{2.17}$$

Once the cycle and wiggle periods are calculated from the EDAR plot, the only unknown is length L^e, which can be computed without need for any other information about the pile. Because the plot effectively captures (a) the effect of the dispersion relation (simple in this case but can be more complicated for beams) and (b) the effect of reflections from the boundary, the plot and the ensuing analysis that result in Equation (2.17) are referred to as the 'effective dispersion analysis of reflections', hence, 'EDAR'.

The proposed EDAR technique is similar to the travel-time approach for nondispersive systems, where the travel time between sensors can be used to compute the wave velocity, which in turn can be used to compute the unknown boundary locations based on the arrival times of the reflections. The key advantage of the proposed EDAR method is that it can be extended to dispersive wave propagation, where travel-time approaches fail due to the significant distortion of the waves that is caused by dispersion. Section 2.3.2 provides details regarding this extension of EDAR.

2.3.2 Flexural waves in beams

Bending waves can be generated by a lateral impact to the pile. The test set-up for bending waves is exactly the same as for longitudinal waves and the responses are likewise measured at a minimum of two sensor locations. There are two main differences between the waves propagating in a bar and a beam. Firstly, along with the propagating waves, there exists evanescent waves, which decay exponentially. Due to this decaying nature, the effect of evanescent waves on measured reflections is negligible and does not have a significant effect on

EDAR processing. Secondly, the propagating waves are dispersive in nature as explained Equations (2.18) through (2.20) which is a critical for the formulation of the EDAR procedure. The governing differential equation for a homogeneous, linearly elastic Bernoulli-Euler (BE) beam is given by

$$EI\frac{\partial^4 v}{\partial x^4}+\rho A\frac{\partial^2 v}{\partial t^2}=0, \tag{2.18}$$

where v is the transverse displacement. Similar to the case for a bar, the general solution for Equation (2.18) can be given by

$$y=e^{ikx-i\omega t}\ . \tag{2.19}$$

Substituting Equation (2.19) in Equation (2.18) we get the dispersion relation between wavenumber and temporal frequency given by

$$k=\sqrt{\frac{\omega}{c_b r}}\ , \tag{2.20}$$

where c_b is the bar wave velocity and $r=\sqrt{I/A}$ is the radius of gyration. The phase velocity can be calculated from Equation (2.20); clearly frequency-dependent, resulting in wave dispersion, which distorts the waveform as it propagates through the length of the beam. This wave distortion makes peak-picking difficult and often impossible, thus making travel-time approaches difficult.

The dispersion relation shown in Equation (2.20) is the key to defining the effective wavenumber for EDAR, which is obtained by scaling the wavenumber. Specifically, the material constants and cross-sectional properties are dropped from Equation (2.20) to define the effective wavenumber:

$$k_e^{BE}=\sqrt{\omega}\ . \tag{2.21}$$

The above choice facilitates the estimation of length without prior knowledge about the material constants, as discussed below. Equation (2.21) also makes the relation between the phase difference and effective wavenumber linear, and thus, all the expressions relating to EDAR obtained for a bar become applicable to a beam. The cycle and wiggle periods computed using the above definitions are

$$K_I^{BE} = \frac{\pi\sqrt{c_b r}}{\Delta L} \ , \tag{2.22}$$

$$K_R^{BE} = \frac{\pi\sqrt{c_b r}}{L^e} \ . \tag{2.23}$$

Similarly, taking the ratios of the two periods, a length estimate of the pile (L^e) can be obtained as

$$L^e = \frac{K_I^{BE}\Delta L}{K_R^{BE}} \ . \tag{2.24}$$

Once the responses at the sensor locations are obtained, Equation (2.24) requires only the cycle period, wiggle period, and the distance between the sensors to obtain an estimate for the length of the member. The important modification is the definition of the effective wavenumber as the square root of the frequency, thus making the wiggle period constant and facilitating the extension of the bar length estimation shown in Equation (2.17) to the beam length estimation shown in Equation (2.24).

This method pertains specifically to BE beam theory. BE beam theory is simple, but not accurate for higher frequencies where the wavelength is of the same order as the beam thickness. However, the EDAR methodology can be extended to more sophisticated models, such as Timoshenko beam theory. The governing equation for a Timoshenko beam with Young's modulus E , density ρ , shear modulus G , area A , moment of inertia I , and Timoshenko shear coefficient κ is

$$\frac{EI}{\rho A}\frac{\partial^4 y}{\partial x^4} - \left(\frac{I}{A} + \frac{EI}{GA\kappa}\right)\frac{\partial^4 y}{\partial x^2 \partial t^2} + \frac{\partial^2 y}{\partial t^2} + \frac{\rho I}{GA\kappa}\frac{\partial^4 y}{\partial t^4} = 0 \ . \tag{2.25}$$

The corresponding dispersion relation is

$$\frac{EI}{\rho A}k^4 - \left(\frac{I}{A} + \frac{EI}{GA\kappa}\right)\omega^2 k^2 - \omega^2 + \frac{\rho I}{GA\kappa}\omega^4 = 0 \ . \tag{2.26}$$

EDAR can be used with any model for which the dispersion relation can be obtained either theoretically (Timoshenko) or numerically (guided wave propagation) by defining the effective wavenumber as the actual wavenumber obtained from the respective models. As models become more sophisticated, they more closely represent actual wave physics but at the same time lack the

simplicity of the bar or BE beam model. Different material properties regarding structure might be needed as opposed to not requiring any material properties as is the case with the simpler BE beam model. The EDAR procedure must be used cautiously, paying utmost attention to the frequency content under consideration and the validity of the underlying models. At lower frequencies, use of BE beam theory might be justified, but at higher frequencies, more robust models, such as Timoshenko beam theory or even more sophisticated models based on guided wave theory, may be required.

2.3.3 Synthetic examples for EDAR verification

In this study, a finite BE beam, with square cross section, was modeled with half spaces (HS) on the top and bottom with variable material properties to control the reflection coefficients and to treat reflections from different boundaries separately. Material damping was introduced by using complex values for the modulus of the pile (imaginary part was taken to be 5% of the Young's modulus). Table 2-1 presents the model BE beam properties and Figure 2-6 presents a schematic of the BE beam model with lengths.

Table 2-1: Model Bernoulli-Euler beam properties.

Property	Value
Young's Modulus	35 GPa
Density	2400 kg m/s^2
Poisson's Ratio	0.1
Cross section (square)	0.3048 m x 0.3048 m

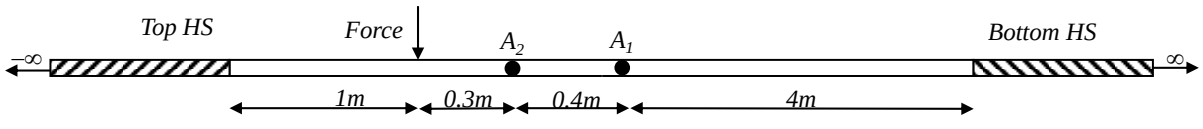

Figure 2-6: Schematic of Bernoulli-Euler beam model.

Example 1: The top HS is modeled such that it matches the beam to prevent reflections from the top. The bottom HS modulus is a large value to simulate a fixed end. Figure 2-7 presents the EDAR plot obtained from the BE model and Table 2-2 presents the BE model beam length estimates.

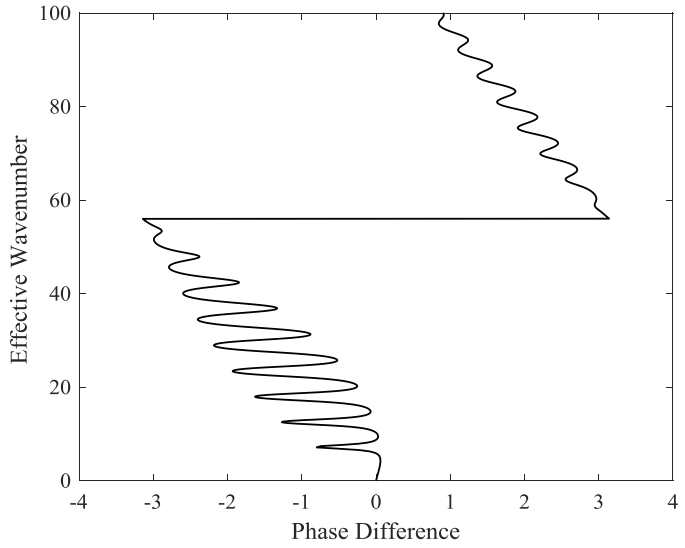

Figure 2-7: EDAR plot for synthetic Bernoulli-Euler beam experiment involving bottom reflections.

Table 2-2: Bernoulli-Euler beam model length estimate.

Cycle Period	Wiggle Period	Distance between sensors	Estimated Length (m)	Actual Length (m)	Error
64.49	6.2	0.4	5.66	5.7	-0.7%

Example 2: Both the top and bottom HS moduli are set to a large value to simulate a beam with fixed boundary conditions on both ends. Figure 2-8 presents the EDAR plot obtained from the BE beam model.

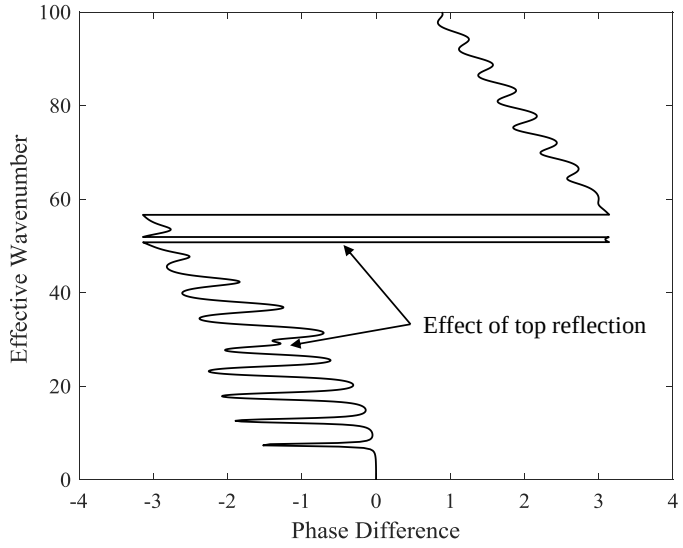

Figure 2-8: EDAR plot for Bernoulli-Euler beam model: bottom and top reflections.

Figure 2-8 shows the effect of the top reflection in the EDAR plot. Even though the top reflections disturbed the wiggle, the important aspect to note is the distinctive characteristics of the disturbances. They do not look similar to wiggles and can be ignored while calculating the wiggle period. This difference between the disturbances shown and wiggles is a consequence of the impact locations and the wave propagation direction. By using the unaffected wiggles in the EDAR plot, similar length estimates, as shown in Table 2-2, were obtained. Depending on the length to the top of the pile, there can sometimes be interference between the top effect and cycle period. This situation can be avoided by using multiple distances between the sensors, which we did during actual experimentation. We used four sensors instead of the two sensors required for EDAR. In this way, we built redundancy into the test and thus, the cycle and wiggle periods can be obtained from multiple sensor combinations.

2.4 Experimental Validation of EDAR

Following the successful verification of EDAR using synthetic data, we performed experiments at the Constructed Facilities Laboratory at North Carolina State University (NCSU) to validate the proposed EDAR. Figure 2-9 shows one of the concrete filled steel tube (CFST)

piles, installed as part of a different project at NCSU, which we used for initial testing. Table 2-3 presents the properties of the CFST.

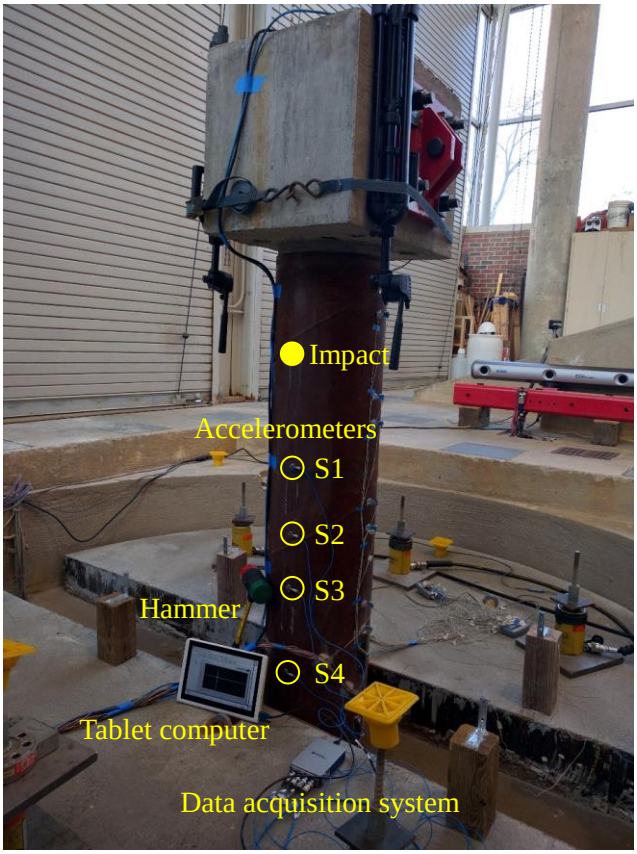

Figure 2-9: Concrete filled steel tube tested at NCSU.

Table 2-3: Properties of concrete filled steel tube.

Property	**Value (m)**
Total Length	5.92
Embedded Length	4.17
Cap Dimensions	0.6096 x 0.4572 x 0.4572
Concrete Diameter	0.292
Steel Thickness	0.0064

Accelerometers from PCB (352C33) and a data acquisition system from National Instruments (NI9232) were used respectively for sensing and recording the responses of CFST to a lateral impact from a small sledge-hammer. The impact is applied between the pile cap and top sensor, maintaining sufficient distance from the top sensor to prevent any overload. Figure 2-10 shows the equipment used for laboratory testing and Table 2-4 provides a summary of the equipment specifications.

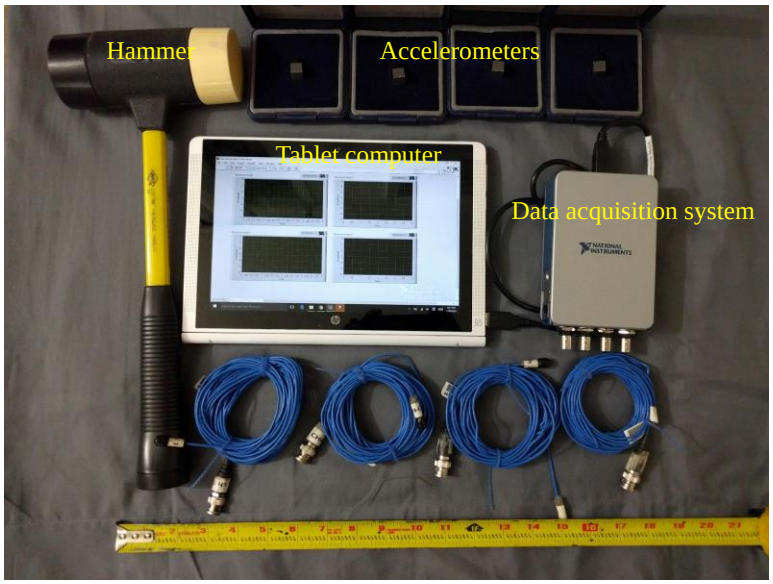

Figure 2-10: Equipment used for EDAR testing.

Table 2-4: Equipment specifications.

Equipment type	Model	Important specifications	
		Item	Range
Accelerometer	PCB 352C33	Frequency	0 to 10000 Hz
		Measurement Range	±50 g
		Sensitivity	100 mV/g
DAQ System	NI 9234 with USB chassis	Analog Input Resolution	24 Bits
		Sampling Rate	51.2 KS/s

Four accelerometers were used to build redundancy in the data obtained, giving six two-sensor combinations. The distances between the four sensors were 0.203, 0.152, and 0.254 m and are directly reflected in the cycle periods observed in the EDAR plots. Figure 2-11 presents the time domain plots of the accelerations obtained at the four sensor locations. Examining these time histories indicates that there are no clear peaks associated with incident and reflected waves, owing to the dispersion associated with flexural waves.

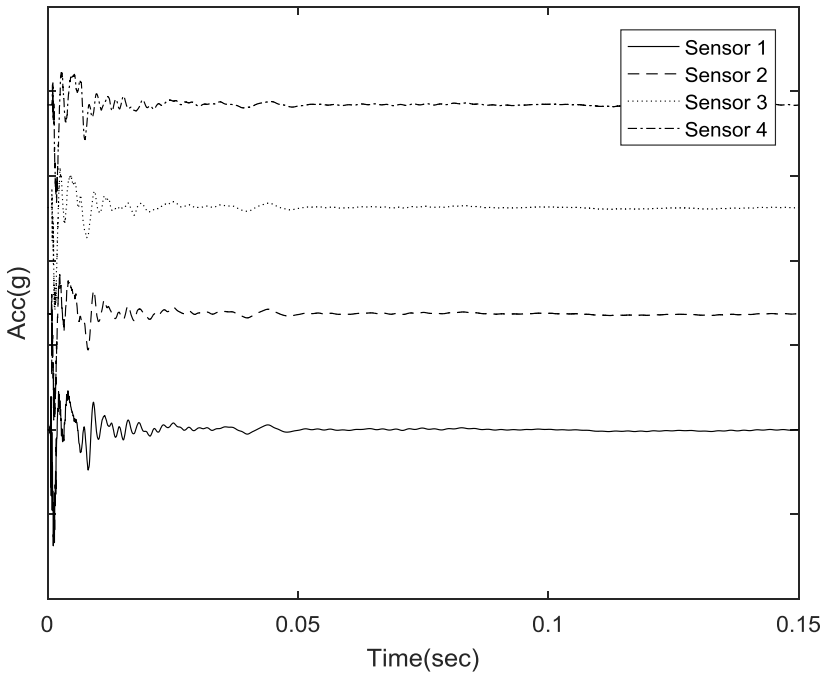

Figure 2-11: Experimental response: time domain.

Figure 2-12(a) presents EDAR plots that clearly show the cycles and wiggles which are as expected from the theory presented earlier in Section 2.3. Raw data from the tests were processed using an exponential window in the time domain to reduce noise effects and to facilitate peak-picking to find the wiggle period. The cycle and wiggle period were obtained as shown in Figure 2-12(b). Concrete with density 2400 kg/m^3, Young's modulus 33.37 GPa, Poisson's ratio 0.2 and steel with density 7800 kg/m^3, Young's modulus 210 GPa, Poisson's ratio 0.3 were used for computing the theoretical dispersion curves [38]. Figure 2-13 presents the theoretical dispersion relation computed based on BE and Timoshenko beam theories.

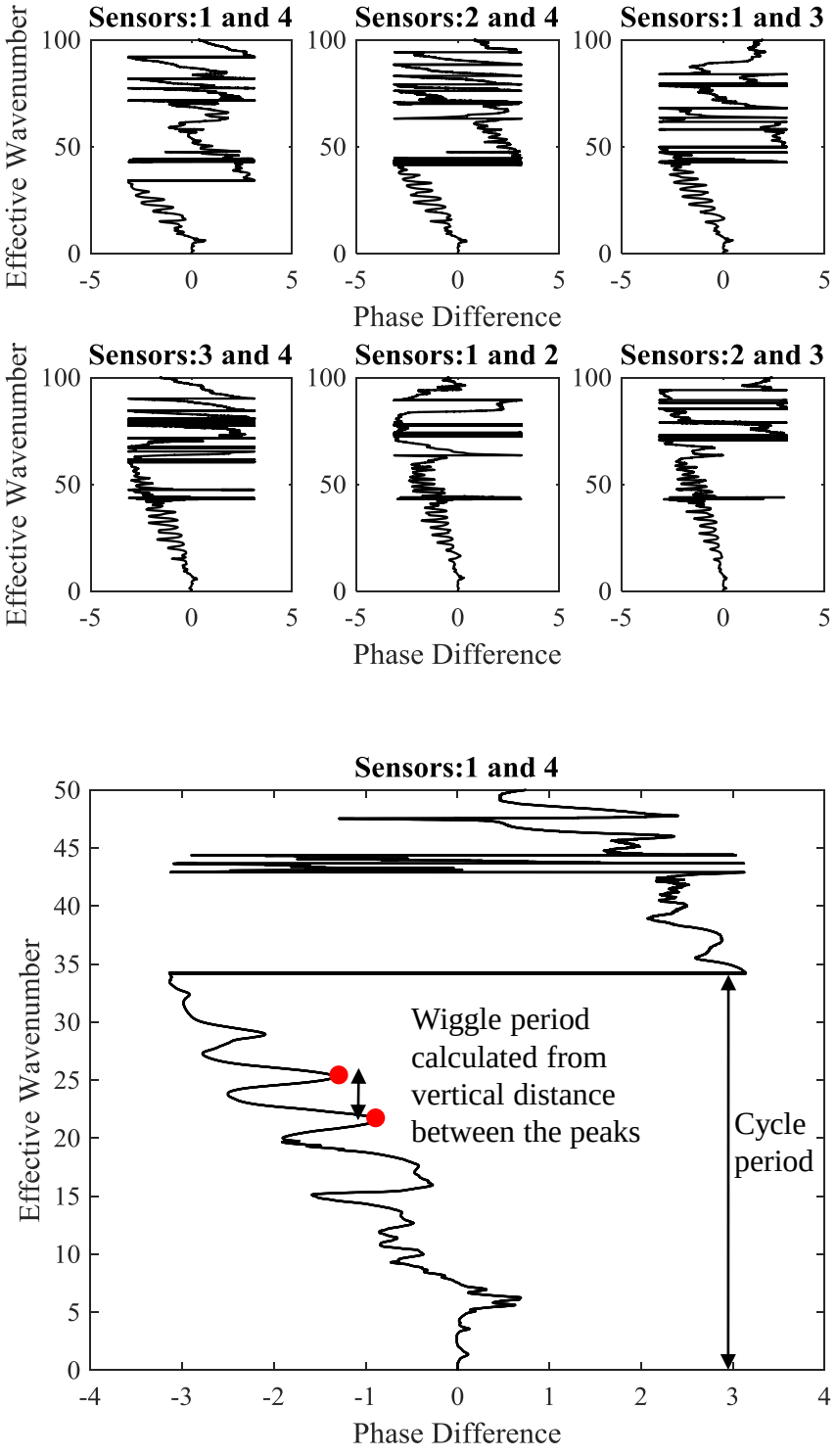

Figure 2-12: (a) Representative experimental EDAR plots (b) Finding wiggle and cycle period from EDAR plot.

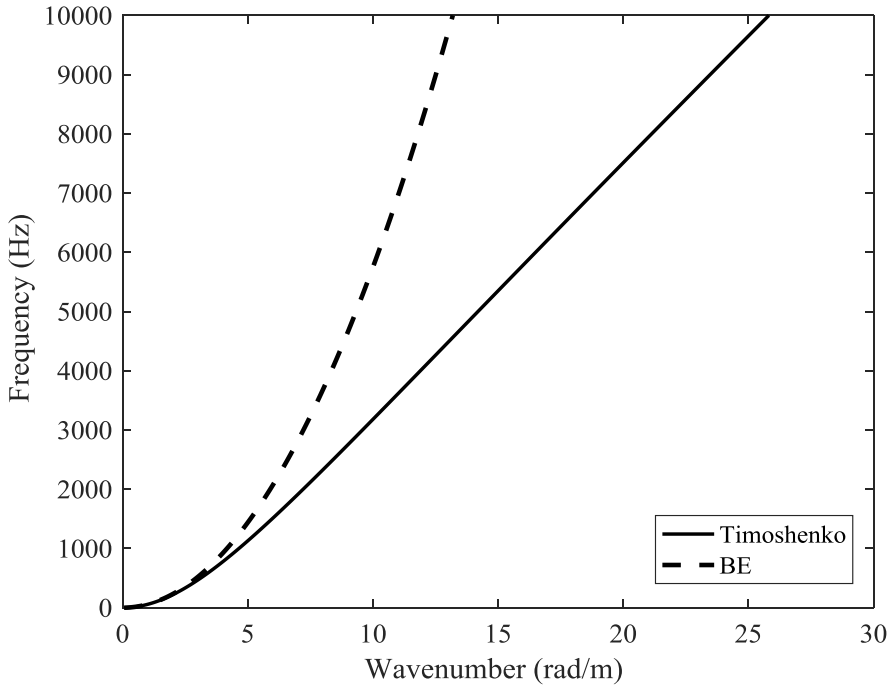

Figure 2-13: Theoretical dispersion relation: Bernoulli-Euler vs. Timoshenko beam theories.

It is well known that Timoshenko beam theory is more accurate than BE theory for higher frequencies, but at low frequencies the dispersion curves overlap for both models. Thus, using the lowermost wiggle in the frequency axis and cycle period between the farthest two sensors, a length estimate can be obtained.

Table 2-5: Length estimate from first observed wiggle using Bernoulli-Euler beam theory.

Cycle period	Wiggle period from lowermost wiggle	Distance between sensors	Estimated length (m)	Actual length (m)	Error
34.18	3.63	.6096	5.74	5.92	3%

Even though the estimated length presented in Table 2-5 is close to the actual length, with an error of 3 percent, many wiggles can be observed at different levels on the theoretical

wavenumber axis. Each of these wiggles were used to calculate the wiggle period and subsequently used to estimate the length. As explained earlier, the main difference between the BE and Timoshenko beam theories is the theoretical wavenumber axis, and thus, the cycle and wiggle periods are changed, as shown in Figure 2-14. In Figure 2-15, the length estimates obtained from each observed wiggle are plotted as a function of the frequency at each wiggle. Clearly, the BE beam theory estimates are a function of the frequency and increase as we move up the frequency. This frequency dependence is reduced greatly for estimates obtained using Timoshenko beam theory, and the average error percentage also is reduced significantly (see Table 2-6).

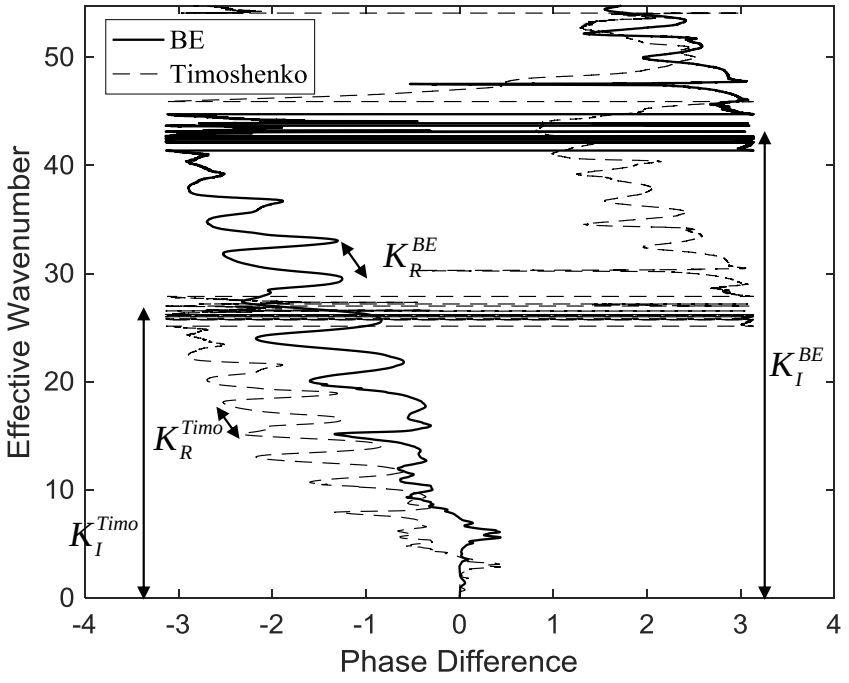

Figure 2-14: Comparison of Bernoulli-Euler and Timoshenko EDAR plots.

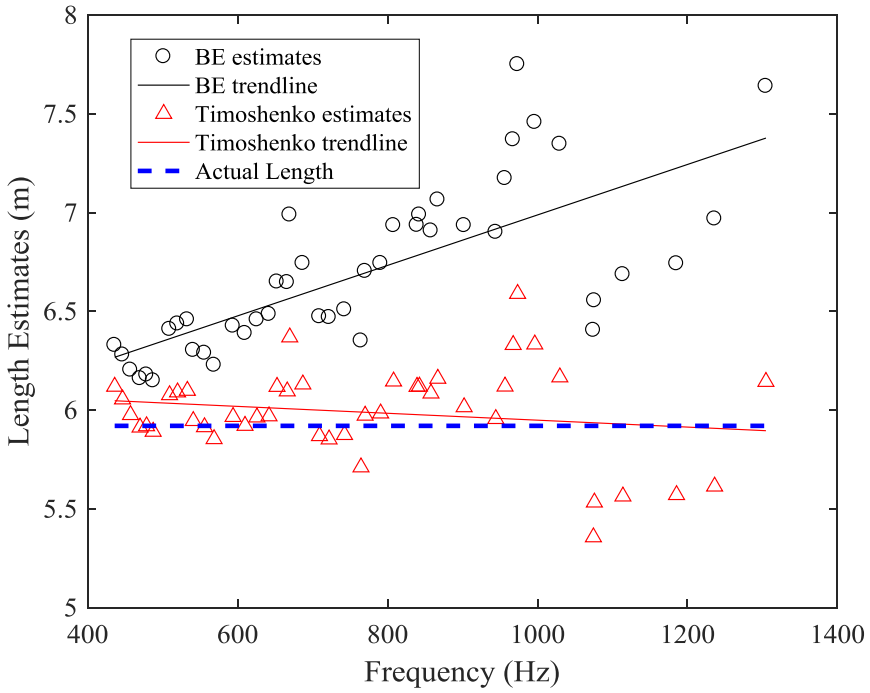

Figure 2-15: Length estimates as a function of frequency.

Table 2-6: Average length estimates.

	Bernoulli-Euler theory	Timoshenko theory	Actual length (m)
Estimate (m)	6.69	5.99	5.92
Error	13%	1.18%	

Unlike Timoshenko beam theory, BE beam theory does not require any information about the pile properties to calculate the effective wavenumber defined in Equation (2.21). However, BE theory leads to a less accurate representation of the exact physical system, and thus, the resulting estimates are less accurate. Therefore, depending on the availability of material property estimates and location of the wiggles in the frequency axis, one of the two theories can be used to obtain the length.

In a more general sense, waves that propagate inside a pile are ‘guided’ waves owing to their three-dimensional nature and reflections from all the boundaries of the pile. Various

research efforts conducted at Northwestern University by Finno [39], Hanifah [40], Chao [41], Wang [42], and Lynch [43] have considered the pile as a cylindrical wave guide to obtain the longitudinal, torsional, and flexural modes of vibrations and corresponding dispersion relation. The predominant modes in longitudinal and flexural waves are the first modes, namely L(0,1) and F(1,1), for frequencies excited via hammer impact, which gives us more confidence to use a 1-D wave propagation model.

2.5 Conclusion

A newly developed NDE methodology, EDAR, is introduced in this work. EDAR is based on obtaining the phase difference of responses at two different locations on a pile in the frequency domain as a function of a newly defined quantity called the 'effective wavenumber'. The effective wavenumber is a function of the dispersion relation of the model chosen to represent the physical system and the type of impact. The theory behind EDAR is based on longitudinal and flexural waves. We conducted experimental validation and found the pile length estimates to be consistently within a 5 percent error margin. EDAR methodology is based on the underlying physics of wave propagation and thus improves reliability for the results obtained. EDAR is currently being evaluated in the field, following its success in laboratory test conditions. Although we have demonstrated EDAR's effectiveness in estimating the length of a pile, the method should be extensible to other scenarios where the length of a member, e.g., an electricity pole, is to be determined. Future work is aimed at improving the estimates at higher frequencies and potential improvements using sophisticated guided wave models. The piles used in this study, despite being full scale, were relatively short in length compared to typical piles in the field. Also, the soil conditions for the tests were relatively loose, which could potentially have had a minimal effect on the EDAR estimations. Even though the methodology has been experimentally demonstrated to work for CFST piles, it should be applicable to other types of pile foundations as well. Such extension is left for future investigations.

Chapter 3

Nondestructive Length Evaluation of an Embedded Pile Using Lateral Hammer Impact: Combined Transverse and Longitudinal Waves

Abstract

This paper presents an important modification of the recently developed nondestructive testing method for estimating embedded depth of pile foundations – EDAR – effective dispersion analysis of reflections. The original EDAR method is based on processing dispersive bending wave signals in the frequency-effective wavenumber domain, thus eliminating the need to perform peak picking that is difficult due to over-distortion of reflected signals. While the method was successful in laboratory settings, preliminary field validation resulted in significant errors. After careful examination of the wave physics, it is discovered that both longitudinal and transverse waves need to be carefully included in EDAR analysis. Specifically, it is shown that the initial arrival is dominated by transverse waves, while the reflections are dominated by longitudinal waves, owing to significant attenuation of transverse waves due to compacted soil around the pile. This observation led to a refined EDAR methodology and accurate estimation of embedded pile depth in field settings.

3.1 Introduction

Missing records of bridges has been a longstanding issue and systemic problem in USA. Engineers have relied on several nondestructive evaluation techniques to obtain the crucial length information about bridge pile foundations, especially when they are classified as scour critical. There are still about 28,000 highway bridges with unknown foundations in 2016 that could be potentially susceptible to scour according to National bridge inventory. Several other bridges over land are also expected to have unknown foundation and missing or incomplete records [2]. Thus, there is a need for an easy and effective nondestructive methodology to estimate the length of pile foundations.

Several methods have been developed over the years which can be broadly classified into borehole-based methods and surface-based methods (see e.g., [4], [3]). Borehole-based methods include parallel seismic, cross-hole sonic, borehole radar, induction-field and borehole magnetic tests. Even though these methods provide reliable results for most foundation types, they are

often expensive and time-consuming due to the need for a borehole near the foundation. In contrast, surface-based methods rely on generating waves through an impact and recording the response at specific sensor locations. Testing is easier, but these methods do not provide the same level of reliability as borehole methods. Surface-based methods for length estimation purposes mainly include sonic echo, impulse response, ultraseismic and bending wave techniques. This paper discusses a newly developed methodology that utilizes multiple types of waves generated through a hammer impact.

One of the most widely used method for length estimation is the sonic echo or pulse echo method which involves impacting pile top leading to generation of longitudinal waves. This method has been standardized by ASTM (D5882-16) and several researchers have used this methodology in a variety of situations over the years (e.g., [9], [12], [37]). These waves are non-dispersive in nature i.e. all the frequencies travel at the same velocity. Thus, there is minimal distortion of the initial waveform in the time domain and peak picking can help determine the distance of wave propagation. This has been very successful for newly constructed bridges both for length estimation and integrity evaluations but has limitations for existing bridges due to reduced access to the top of the pile. Researchers have tried various methods to induce longitudinal waves without access to the top, but the recorded waveforms tend to be complicated to be able to process. Existing piles have much easier access to the sides of the piles and producing a lateral impact leading to flexural or bending waves is easier from the experimental and site perspective. Using lateral excitations for pile length estimation was introduced by Holt and Douglas [16]. Unlike longitudinal waves, flexural waves are dispersive in nature and thus distort as they propagate making any time domain processing of the signals complicated. In order to analyze these complicated signals, the bending wave or short kernel method was introduced. This method helps obtain travel-time information through convolution of the signal with a chosen kernel of specific frequency. The choice of kernel frequency and peak picking is still complicated even for experienced users leading to higher error percentages [22]. Other methods based on signal processing techniques have also been investigated (e.g., [21], [23]). Major drawback of these methods is that they are purely signal processing based methods and do not explicitly incorporate the underlying physics that causes wave distortion.

A new methodology called Effective Dispersion Analysis of Reflection (EDAR) was introduced recently by the authors [44]. EDAR is based on carefully examining the phase

difference between the responses obtained at two accelerometer locations, due to an impact applied to the side of the pile, as a function of a newly defined quantity called the effective wavenumber. Effective wavenumber is defined based on the physical dispersion of the wave generated from impact. Given this general definition of effective wavenumber, EDAR can be easily applied to both longitudinal and flexural waves. EDAR methodology was initially tested in the laboratory resulting in length estimates with errors less than 5% and its extension to a field piles is presented in this paper. In contrast with the success in the lab, preliminary application of EDAR for field data indicated significant underestimation of the embedded pile depth. A closer look at the physics of waves indicated that there is a significant effect of the compacted soil found in the field, necessitating a revision of the original EDAR methodology. Specifically, it is observed that the compacted soil causes differential attention of longitudinal and transverse waves. This paper is focused on a detailed discussion of the phenomenon, and a resulting modification to EDAR methodology that results in accurate estimation of embedded pile depths in field settings.

The outline of the paper is outlined as follows. Section 3.2 contains a brief introduction to the original EDAR methodology and a summary of laboratory validation. Preliminary length estimates obtained from direct application of EDAR to field data are presented Section 0. Section 3.4 contains the reasons for discrepancies in the initial length estimates, while Section 3.5 contains the modified EDAR methodology for compacted soils. The paper is concluded with field validation in Section 3.6, followed by concluding remarks in Section 3.7.

3.2 EDAR Preliminaries

Traditionally surface-based techniques have relied on generating a wave through a hammer strike at various locations on the exposed parts of the pile. The main two types of waves that are generated are the longitudinal and flexural/transverse waves. Depending on the type of hammer impact and the sensor orientation various waves can be recorded (Figure 3-1). Measuring axial accelerations for a top impact produces the clear signals in time domain that can be processed by picking peaks. This is also a consequence of the fact that longitudinal waves are non-dispersive. In contrast, lateral impact produces flexural waves that are dispersive and are distorted as they travel along the pile making any time domain interpretation of the results very complicated. To analyze such dispersive reflections, the authors have recently developed

Effective Dispersion Analysis of Reflections (EDAR), which has the potential to analyze both longitudinal and flexural waves with equal ease to obtain length information from the pile response.

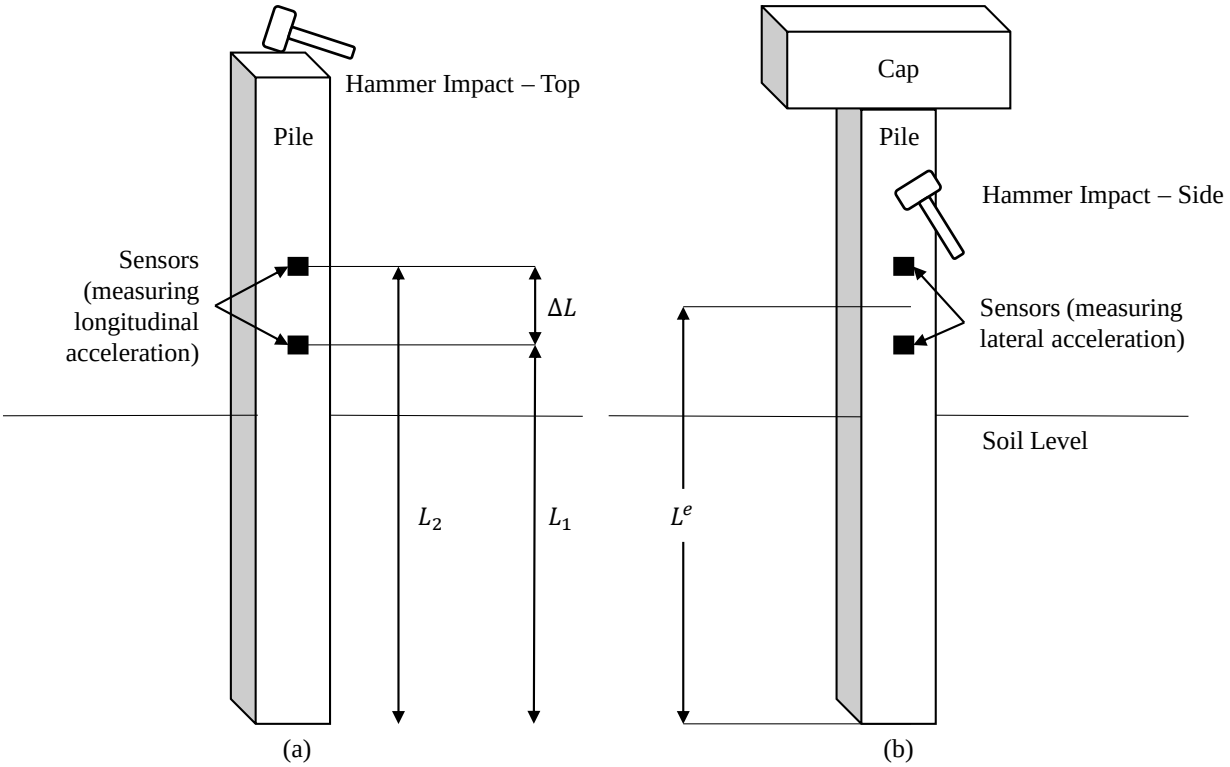

Figure 3-1: Pile setup (a) Top impact (b) Side impact.

3.2.1 Theory

EDAR requires a minimum of two sensors along the length of the exposed region of the pile either capable of measuring lateral or longitudinal accelerations. The impact should be above the top sensor and could be in either longitudinal or lateral direction. The phase difference (P_d) is defined by,

$$P_d = \text{Imag}\left(\log\left(u_2(\omega)\right) - \log\left(u_1(\omega)\right)\right), \tag{3.1}$$

where u_1 and u_2 are the frequency-domain representation of responses (accelerations, velocities or displacements) at the two sensor locations. We introduce the concept of effective

wavenumber, which is essentially a scaled wavenumber and is based on the dispersion relation of the propagating waves. For longitudinal waves, the wavenumber (k) and ω have a linear relationship with the bar wave velocity (C_b) as the proportionality constant:

$$k = \frac{\omega}{c_b}. \tag{3.2}$$

Correspondingly, effective wavenumber is defined as,

$$k_e = \omega, \tag{3.3}$$

which is proportional to the wavenumber but is independent of the wave velocity. This specific definition facilitates the estimation of the pile length without the need for the material properties of the pile, as explained below. The general form of wave propagating in a bar is given by,

$$u(x) = Ae^{ikx} + Be^{-ikx}. \tag{3.4}$$

Using the Equations (3.1) and (3.4), the phase difference can be derived as [44],

$$P_d = k\underbrace{(L_2 - L_1)}_{=\Delta L} + \tan^{-1}\left(\frac{A\sin(2kL_1)}{B + A\cos(2kL_1)}\right) - \tan^{-1}\left(\frac{A\sin(2kL_2)}{B + A\cos(2kL_2)}\right). \tag{3.5}$$

P_d is periodic in nature with two periodicities, defined as cycles and wiggles. The first term is the theoretical wavenumber scaled by the distance between the sensors (ΔL) which along with phase wrapping leads to cycle period as shown in *Figure 3-2*. The second and third term are responsible for the smaller oscillations called wiggles observed in *Figure 3-2*. The trigonometric functions have periods π/L_1 and π/L_2 which can be approximated to π/L^e , where L^e is the distance from midpoint of the sensors to the tip of the pile. A semi-infinite bar with lengths L_1=3 m, L_2=3.5 m as shown in Figure 3-1 and velocity of wave propagation c=1 m/s was simulated using the bar wave equation. The bar extends towards $-\infty$ with a boundary at the other end having a reflection coefficient of 0.5. The resulting EDAR plot is shown in Figure *3-2*.

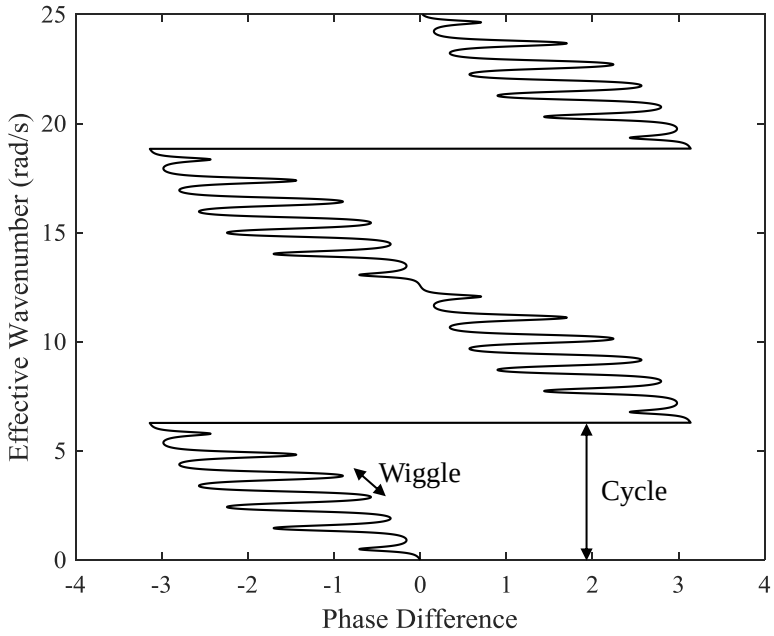

Figure 3-2: EDAR plots for Semi-Infinite bar with characteristic cycle and wiggle periods.

The cycle and wiggle periods shown in Figure 3-2 is given respectively by

$$K_I^{bar} = \frac{\pi c_b}{\Delta L} \ , \tag{3.6}$$

$$K_R^{bar} = \frac{\pi c_b}{L^e} \ . \tag{3.7}$$

The ratio of the cycle and wiggle periods is

$$\frac{K_I^{bar}}{K_R^{bar}} = \frac{L^e}{\Delta L} . \tag{3.8}$$

Once the cycle and wiggle periods are obtained from the EDAR plot, the only unknown in equation (3.8) is L^e can be calculated giving us an estimate of the pile length. This is very similar to travel-time approaches where the velocity of wave propagation is calculated based on travel time between sensors and pile length calculated from the travel time of the reflected wave. In addition to providing an easier and alternate analysis methodology for processing non-dispersive waves, the key advantage of EDAR is that it can be extended to dispersive waves in a beam, where the travel time approach fails due to significant distortion in the waves. Similar to the bar, the dispersion relation of a Bernoulli-Euler (BE) beam is given by

$$k = \sqrt{\frac{\omega}{c_b r}} \tag{3.9}$$

where $r = \sqrt{I/A}$ is the radius of gyration. The phase velocity is frequency-dependent, resulting in wave dispersion, i.e. distortion the waveform as it propagates through the length of the beam. We correspondingly define the effective wavenumber as the quantity proportional to the wavenumber but independent of the material and section properties:

$$k_e^{BE} = \sqrt{\omega}\,, \tag{3.10}$$

The above makes the relationship between phase difference and effective wavenumber linear and all the results described earlier for the bar can be directly applied to the BE beam. The length estimate of the pile can derived based on Equation (3.8) adapted to Bernoulli-Euler beam:

$$L^e = \frac{K_I^{BE} \Delta L}{K_R^{BE}}\ . \tag{3.11}$$

More sophisticated models can be used in place of B-E beam theory to more accurately represent the waves propagating in the piles. For example, theoretical wavenumber obtained from Timoshenko beam theory can be used as effective wavenumber to obtain the EDAR plot which modifies both the cycle and wiggle periods leading to an improved length estimate. The key in selecting the appropriate definition for effective wavenumber lies in carefully examining the type of waves and the range of frequencies in which the cycle and wiggle periods occur. If the propagating waves are predominantly longitudinal in nature, simple bar model can be used. If the waves are predominantly transverse in nature and wavelengths are significantly higher than the cross-sectional dimensions, use of BE beam theory can be justified (since the slenderness ratio would be large). Otherwise, the Timoshenko beam theory or even more sophisticated guided wave modelling may be needed to obtain accurate length estimates.

3.2.2 Laboratory testing

Two sensors are required for EDAR methodology but to build redundancy a four-channel USB-based data acquisition (DAQ) system and four accelerometers (PCB352C33) were chosen for testing the piles. Thus, a single impact produces six different EDAR plots from six sensor-pair combinations. The accelerometers were aligned such that they measure the lateral

acceleration of the foundation. Large sledge hammer (PCB 086D50) with hard and soft tips and a small sledge hammer (0.45 Kg) with hard, medium hard, medium and tough tips were chosen to impact the piles in between the cap and top sensor. The results for the hard tip of the large and small sledge hammers are presented here for the laboratory tests.

EDAR methodology was validated in laboratory testing using concrete filled steel tubes (CFST). The properties of CFST and other details of the laboratory test can be found in references [44] and [38]. Total length of the pile was 6.33 m with 4.22 m embedment. The concrete diameter was 0.292 m with a steel thickness of 0.00635 m. Four sensors, numbered one to four from top to bottom, were used with spacing of 0.2, 0.16, and 0.25 m. The distance from the midpoint of the sensors to the bottom of the cap is 1.1 m. Typical EDAR plot for two pairs of sensors are shown in Figure 3-3. The data shown in the time domain on the left does not immediately provide much information. On the other hand, the EDAR plots on the right clearly show cycles and wiggles, which can be used to estimate the embedded depth, as described below.

The periodicities explained earlier can be clearly seen in the EDAR plots for which the effective wavenumber was obtained using Equation (3.10). The data were analyzed using Timoshenko beam theory. The dispersion relation for Timoshenko beam with Young's modulus E, density ρ, shear modulus G, area A, moment of inertia I, and Timoshenko shear coefficient κ, is given by:

$$\frac{EI}{\rho A}k^4 - \left(\frac{I}{A} + \frac{EI}{GA\kappa}\right)\omega^2 k^2 - \omega^2 + \frac{\rho I}{GA\kappa}\omega^4 = 0 \tag{3.12}$$

The Timoshenko shear coefficient κ for a rectangular section can be obtained using [45],

$$\kappa = \frac{10(1+\nu)}{12+11\nu} \tag{3.13}$$

It is important to note that all the required details about the pile materials and their properties are readily available in the controlled laboratory setting. The cycle period was obtained between top and bottom sensors which are spaced at a distance 0.61 m. Multiple wiggles are often observed, and only clear wiggles are used and are plotted as function of frequency in Figure 3-4. A slight trend can be observed as a function of frequency which is also evident from the length estimates obtained from different frequency ranges as shown in Figure 3-4.

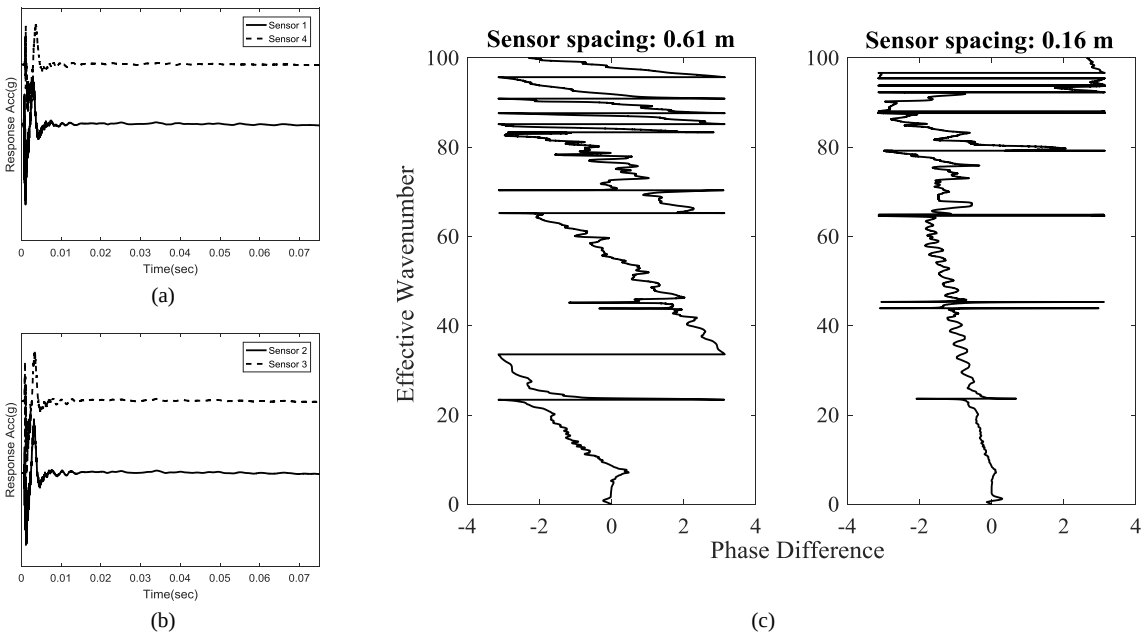

Figure 3-3: Laboratory pile (a) Time history at accelerometers 1 and 4 (b) Time history at accelerometers 2 and 3 (c) Representative EDAR plots.

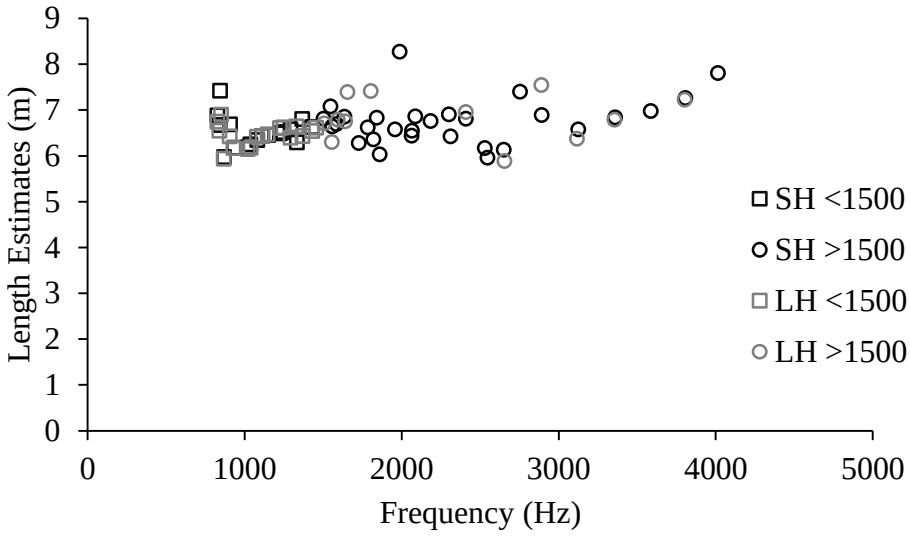

Figure 3-4: Wiggle period as a function of frequency for large (LH) and small (SH) sledge hammers hard tip.

Lower frequency estimates had lesser errors and it can be seen that the scatter gets bigger as we go higher up the frequency. Nevertheless, the overall trend of the estimates is fairly flat giving us a good average length estimate as shown in Table 3-1. Although there was not much variation between the results obtained from different hammer tips in the laboratory tests, hammer type and tip played an important role in the results obtained in the field as presented later.

Table 3-1: Length Estimates for laboratory pile.

Actual Length	Frequency Range	SH		LH	
		Average Estimate (m)	Error	Average Estimate (m)	Error
6.33	<1500 Hz	6.52	3 %	6.46	2.1 %
	>1500 Hz	6.75	6.6 %	6.85	8.2 %
	All	6.67	5.4 %	6.61	4.4 %

3.3 Observations from Field Testing

Newly driven solid concrete pile with 16" side in Rodanthe, Outer Banks NC, was used for preliminary field validation of the EDAR methodology. A particular bent with good access to the piles was selected and the piles had the length markings on them using which very accurate length of the exposed and embedded parts of the pile was calculated shown in Table 3-2. The pile cap was not yet constructed giving us complete access to the entire length of the exposed part of the pile. Pictures of the site and the specific pile tested are shown in Figure 3-5(a). A close up of the pile along with the sensor locations and test equipment is shown in Figure 3-5(b). Similar to the laboratory testing, four sensors were used along the length to measure the response of the pile to the hammer impact. The sensors were stud mounted using super glue to accurately measure the pile response. Similar to the laboratory tests multiple hammers with interchangeable tips (Figure 3-5 (b)) were used to impact the pile. Not all the hammer tips produced good data with observable wiggles. While multiple hammer tips produced usable data, small hammer with a tough tip was found to be most consistent and results from this hammer tests are presented (effect of hammer type of EDAR is currently under investigation and will be reported in the future).

Table 3-2: Field pile properties.

Property	**Value**
Design concrete compressive strength (Fc')	68.9 MPa
Estimated modulus (using AASHTO 5.4.2.4-3)	41.8 GPa
Cross section – square	0.4064 m
Total length	17.07 m
Top of pile to bottom-most sensor (pile 1)	1.74 m
Top of pile to bottom-most sensor (pile 2)	2.4 m

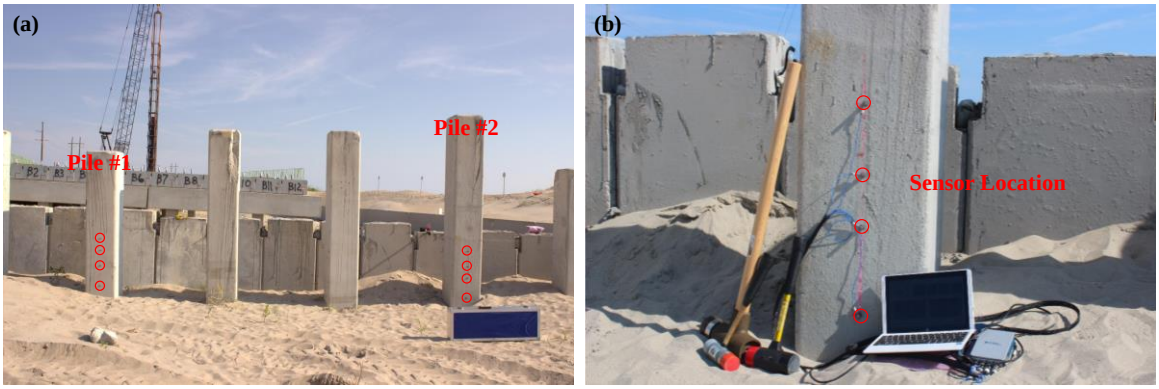

Figure 3-5: (a) Field piles (b) Equipment and sensor location.

Material properties to calculate the Timoshenko wavenumber are in general not readily available in case of unknown foundations. In this particular case though design strength is available from design drawing and used to obtain the initial estimates (a more robust procedure to obtain the material properties is outlined in Section 3.6.1). The density of concrete was assumed to be 2,400 Kg/m^3 and Young's modulus value was calculated as 41.8 GPa from the 28-day design compressive strength using AASHTO LRFD equation 5.4.2.4-3. Poisson's ratio of concrete is typically between 0.1 to 0.2 and is assumed to be 0.15 for this part of the analysis. Length estimates are obtained by analyzing the data obtained in the field using the same

procedure described for the laboratory data. Typical EDAR plot from the field is shown in Figure 3-6.

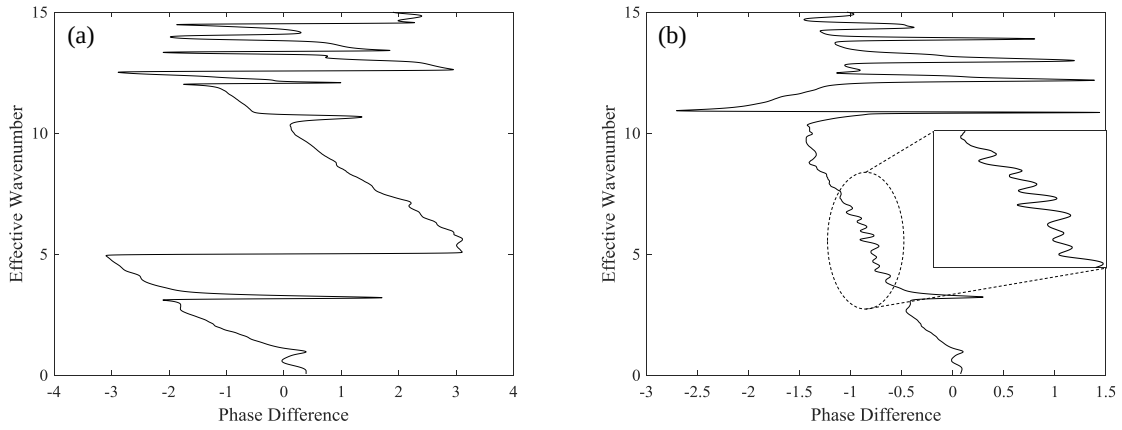

Figure 3-6: Representative EDAR plots from Pile 2 for (a) Sensor spacing of 0.62 m (b) Sensor spacing of 0.15 m

The cycle period was calculated from the sensor pair with farthest spacing (0.61 m for pile 1 and 0.62 m for pile 2) and wiggles are utilized from the data from all the sensor combinations. Scatter plot of the length estimates obtained are shown in Figure 3-7. The mean length estimate for pile 1 was 11.2 m which was 34.4% lesser than the measured length. The mean length estimate for pile 2 was 11.5 m which was 32.6% lesser than the measured length. Clearly, the length was significantly underestimated in both cases. This led to the further exploration on the effect of consolidated soil, which appears to be the main difference between laboratory and field conditions.

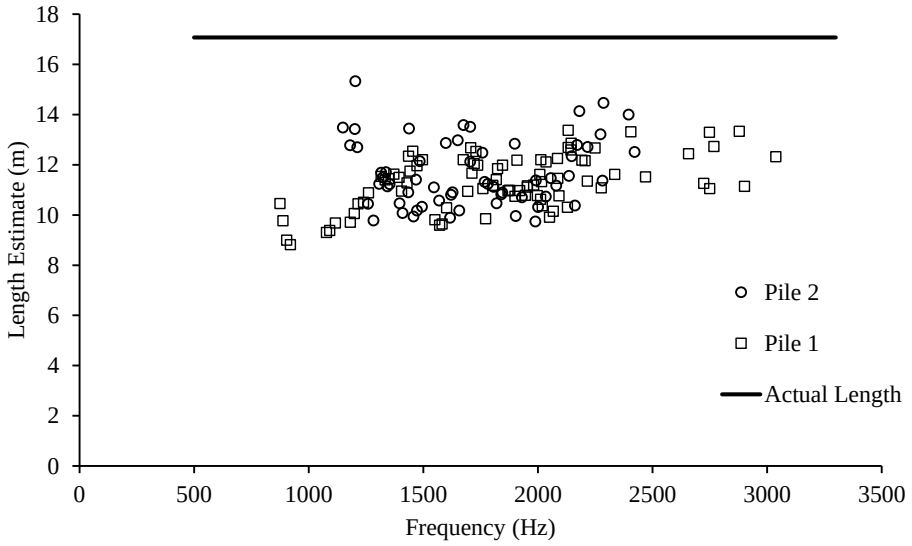

Figure 3-7: Initial field length estimates – significant underestimation.

Soil boring data and SPT tests conducted near the location of the pile revealed a fairly uniform loose fine sand until a depth of 14.63 m followed by medium to very dense silty sand up to a depth of 19.2 m. Pile 1 and 2 were embedded to a depth of 15.2 m and 14.5 m respectively and thus the pile tip is expected to have just breached the boundary between the loose and dense sand layers. This eliminates the possibility of reflections due to embedment into stiff soil layers at the pile depths estimated from EDAR procedure. The other effect is the attenuation of waves due to radiation damping coming from the soil (radiation of energy into unbounded soil). Careful investigation found that the transverse waves that were the focus of EDAR thus far, get attenuated by the soil. Instead, EDAR appears to capture the effect of reflected longitudinal waves, which are generated due to secondary Poisson's effect from lateral impact. The following sections contain a discussion of the effect of these longitudinal waves on EDAR as well as a modification of EDAR methodology that results in accurate estimates of embedded depths.

3.4 The role of longitudinal waves

Even though the pile is impacted laterally, several modes of vibration can be generated based on the frequencies that are excited. In general, the pile acts as a waveguide propagating the waves generated through the hammer impact. Modeling the pile as a cylindrical waveguide using

the previously mentioned properties of concrete with a radius of 0.2 m, the dispersion curves [46] can be obtained and shown in Figure 3-8. The higher modes need not be considered as they contribute only beyond their respective cutoff frequencies, which are in general higher than the excitation frequencies from hammer impact (in the excitation frequency range, these higher modes are evanescent in nature and do not contain measurable reflections). While it is counterintuitive to expect that significant transverse accelerations can be observed from longitudinal waves generated from lateral impact, it turns out that these accelerations are not insignificant. The existence of such transverse accelerations is explained with the help of an idealized model of infinite pile in two dimensions. Even though this model is approximate, it provides us with a deeper understanding of the phenomenon and helps us justify the length estimation procedure followed later on in Section 3.5.

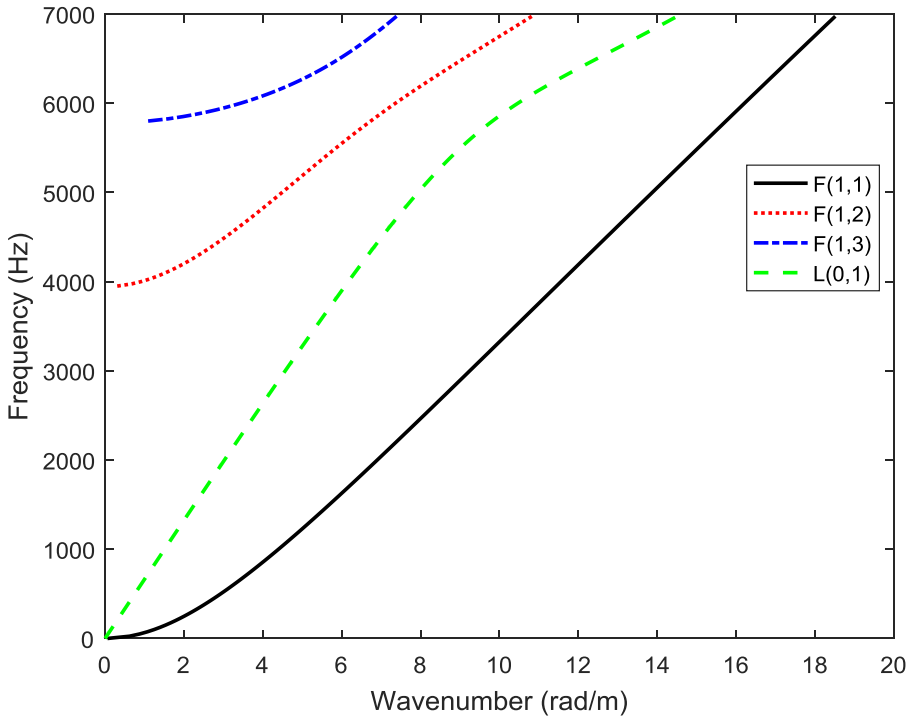

Figure 3-8: Dispersion curves for cylindrical pile as a waveguide.

3.4.1 Existence of secondary longitudinal modes

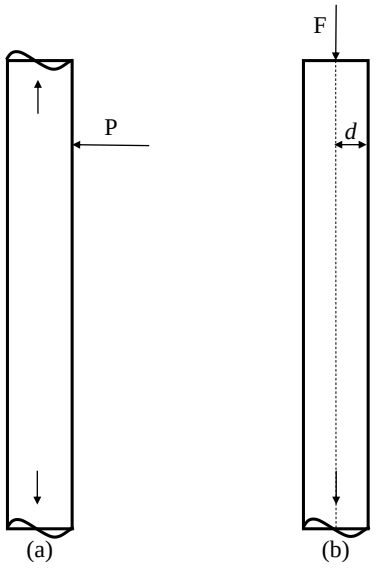

Figure 3-9: (a) Side impact (b) Top impact on pile.

The actual test resembles Figure 3-9(a) but as an intermediate step an impact at the top center producing symmetric waves in the pile (Figure 3-9(b)) is considered which will be used later to analyze the side impact case. This produces longitudinal waves of the general form

$$u_L = Ae^{ikz - i\omega t} \ . \tag{3.14}$$

The ratio of longitudinal (ε_L) and transverse (ε_T) strain is given by the Poisson's ratio (υ) and thus

$$\varepsilon_T = \upsilon \varepsilon_L \ . \tag{3.15}$$

Longitudinal strain can be obtained by taking the spatial derivative of Equation (3.14)

$$\varepsilon_L = iku_L \ . \tag{3.16}$$

Due to symmetric displacement field, the transverse displacement (u_L) on the surface of the pile can be obtained as

$$u_T = d\varepsilon_T \ , \tag{3.17}$$

where d is half the width of the pile. Thus, the ratio of transverse and longitudinal displacements is be given by

$$\left|\frac{u_T}{u_L}\right| = k\upsilon d = \frac{\omega\upsilon d}{c_L} = \alpha \ , \tag{3.18}$$

where ω is the frequency and c_L is the longitudinal wave velocity.

For a concrete pile of width 0.4 m (i.e. d =0.2 m), Poisson's ratio of 0.15, longitudinal wave propagation velocity of 4,200 m/s and in the range of frequency 1,000 Hz to 2,000 Hz where wiggles are obtained most commonly, the ratio of lateral to longitudinal acceleration (α) is between 0.05 and 0.09. This gives us the amplitude of lateral acceleration produced from a longitudinal impact. In reality, a lateral strike is imparted to the pile; to obtain the effect of the longitudinal wave generated from a lateral impact, we utilize the idea of reciprocity as elaborated below.

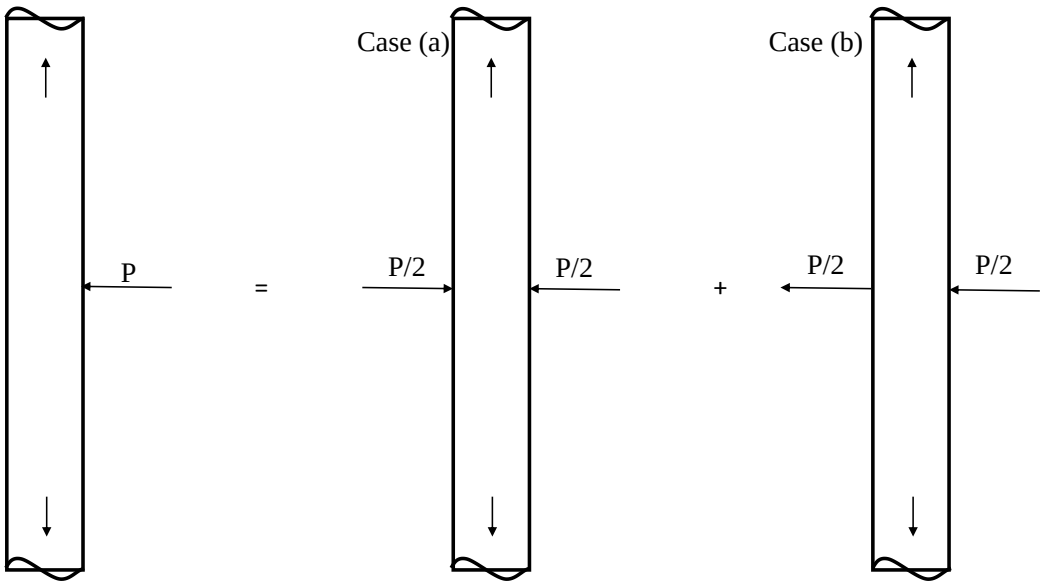

Figure 3-10: Lateral impact split into symmetric and antisymmetric loading.

Lateral impact on a pile shown in Figure 3-9(a) can be split into the sum of symmetric loading leading to symmetric longitudinal waves and anti-symmetric loading leading to transverse waves as shown in Figure 3-10. Transverse displacement due to the anti-symmetric loading (case (b)) can be obtained using the corresponding transverse impedance (Z_T) of the beam:

$$u_T^b = \frac{P}{2Z_T(i\omega)} \ . \tag{3.19}$$

Since impedance relates the force and velocity, to obtain displacements velocity is divided by $i\omega$. Thus, the load P is given by,

$$P = 2Z_T u_T^b \left(i\omega\right) \ . \tag{3.20}$$

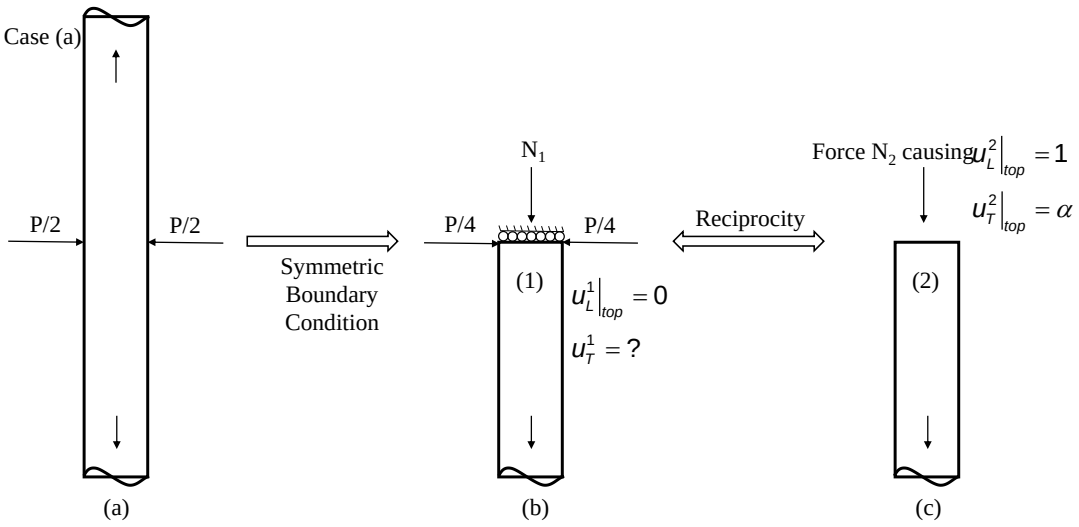

Figure 3-11: (a) Symmetric loading (b)System 1 by applying symmetric boundary conditions (c) System 2 for application of reciprocity.

To obtain the transverse displacement from the symmetric part of loading, the infinite beam is first split into half by horizontal axis of symmetry as shown in Figure 3-11b, with unknown reaction N_1, which can be solved with the help of Maxwell-Betti's reciprocity theorem. Specifically, consider two systems, system 1 in Figure 3-11b, and system 2 as shown in Figure 3-11c, which is same as the top impact case considered earlier in Figure 3-9(b). According to Maxwell-Betti's reciprocal theorem, work done by forces in system 1 on conjugate displacements in system 2 is the same as the work done by forces in system 2 on conjugate displacements in system 1, i.e.

$$N_2 * 0 = N_1 * 1 + 2 * \frac{P}{4} * (-\alpha) \Rightarrow N_1 = \frac{P\alpha}{2} \tag{3.21}$$

Longitudinal displacement from the symmetric loading is obtained using the longitudinal impedance (Z_L) and is given by,

$$u_L^a = \frac{N_1}{Z_L(i\omega)} \ , \tag{3.22}$$

which can be further simplified using Equation (3.21) as

$$u_L^a = \frac{\alpha Z_T u_T^b}{Z_L} \ . \tag{3.23}$$

Equation (3.23) give us the longitudinal displacement as a function of the transverse displacement but since the accelerations are measured only in the lateral direction, the effect of this longitudinal displacements in lateral direction needs to be considered. This comes from Poisson's effect considered in Equation (3.15). Using this equation, the ratio between the transverse displacements due longitudinal and transverse waves is given by,

$$\frac{u_T^a\big|_L}{u_T^b} = \frac{\alpha^2 Z_T}{Z_L} \ . \tag{3.24}$$

For purely longitudinal waves, the longitudinal impedance is

$$Z_L = A\sqrt{\rho E} \ , \tag{3.25}$$

where A is the cross sectional area, ρ is the density and E is the Young's modulus. Transverse impedance is more complicated and frequency dependent due to the dispersive nature of the waves. Considering the frequency range of interest, this can be approximated by shear wave equation, but with the effective shear area from Timoshenko beam theory. Thus the transverse impedance can be approximated as,

$$Z_T = A_S\sqrt{\rho G} \tag{3.26}$$

where G is the shear modulus and $A_s = \kappa A$ is the effective shear area. Substituting Equations (3.13), (3.25) and (3.26) in (3.24), and noting that the acceleration ratio is the same as the displacement ratio, we obtain,

$$\frac{a_T^L}{a_T^T} = \alpha^2 \frac{10(1+\upsilon)}{(12+11\upsilon)\sqrt{2(1+\upsilon)}} \ , \tag{3.27}$$

where a_T^L and a_T^T are the transverse accelerations due to longitudinal and transverse waves respectively, and α is given by Equation (3.18). For a representative Poisson's ratio of 0.15, the acceleration ratio appears to be between 0.0001 and 0.001. On the outset this seems very low and

does not affect the cycle period which is a consequence of initial wave arrival. On the other hand, soil plays a significant role in altering the relative content of longitudinal waves making their effect more significant as explained in the next subsection.

3.4.2 Differential attenuation of waves due to presence of soil

Soil surrounding the pile can play a significant role in attenuating the waves generated from the hammer impact. To better understand the phenomenon, a simple approach based on Winkler foundations model is utilized. Since the hammer impact produces low strain in the pile, effect of soil is included using (frequency-dependent) springs and dampers representing the soil resistance associated with its horizontal cross-section. Even though this approach is approximate, it is valid for the frequency range of interest since the associated length scales are larger than the pile diameter. Thus, the soil is assumed to be layered and under either plane strain or anti-plane shear, and the corresponding stiffness for longitudinal and transverse waves propagating in the pile are obtained separately as a function of the pile radius and soil properties. The pile is considered to be rigid compared to the soil, and always in contact with the soil. Thus, the effective dynamic stiffness from the soil can be obtained by solving the elastodynamic wave equation in soil for full space in 2D, assuming unit displacement boundary condition at the pile-soil boundary [47]. Using such an approach, the stiffness offered by soil for longitudinal waves propagating in the pile is given by

$$K_L = 2\pi G_s \frac{R\omega}{c_s} \frac{H_1^1\left(\frac{R\omega}{c_s}\right)}{H_0^1\left(\frac{R\omega}{c_s}\right)}, \tag{3.28}$$

where G_s is the shear modulus, R is the radius of the pile, c_s is the shear wave velocity given by $\sqrt{G_s/\rho_s}$, ω is the frequency, and $H_n^1(z)$ is n-th order Hankel function of first kind. It can be seen that the stiffness is complex-valued and frequency dependent. The real part of the stiffness acts like a spring and the imaginary part of the stiffness acts like a damper. Similar albeit more complicated expression for stiffness offered by soil for transverse waves propagating in the pile can be obtained for given pile radius and soil properties as a function of frequency ([47], [48]). Figure 3-12 shows the stiffness variation for representative soft/loose soil and hard/dense soil with properties shown in Table 3-3.

Table 3-3: Properties of soft and hard soil.

Soil Type	Density (Kg/m^3)	Young's Modulus (MPa)	Poisson's Ratio	Pressure Wave Velocity (m/s)	Shear Wave Velocity (m/s)
Soft/loose Soil	1800	105	0.3	280	150
Hard/dense Soil	2000	755	0.3	710	380

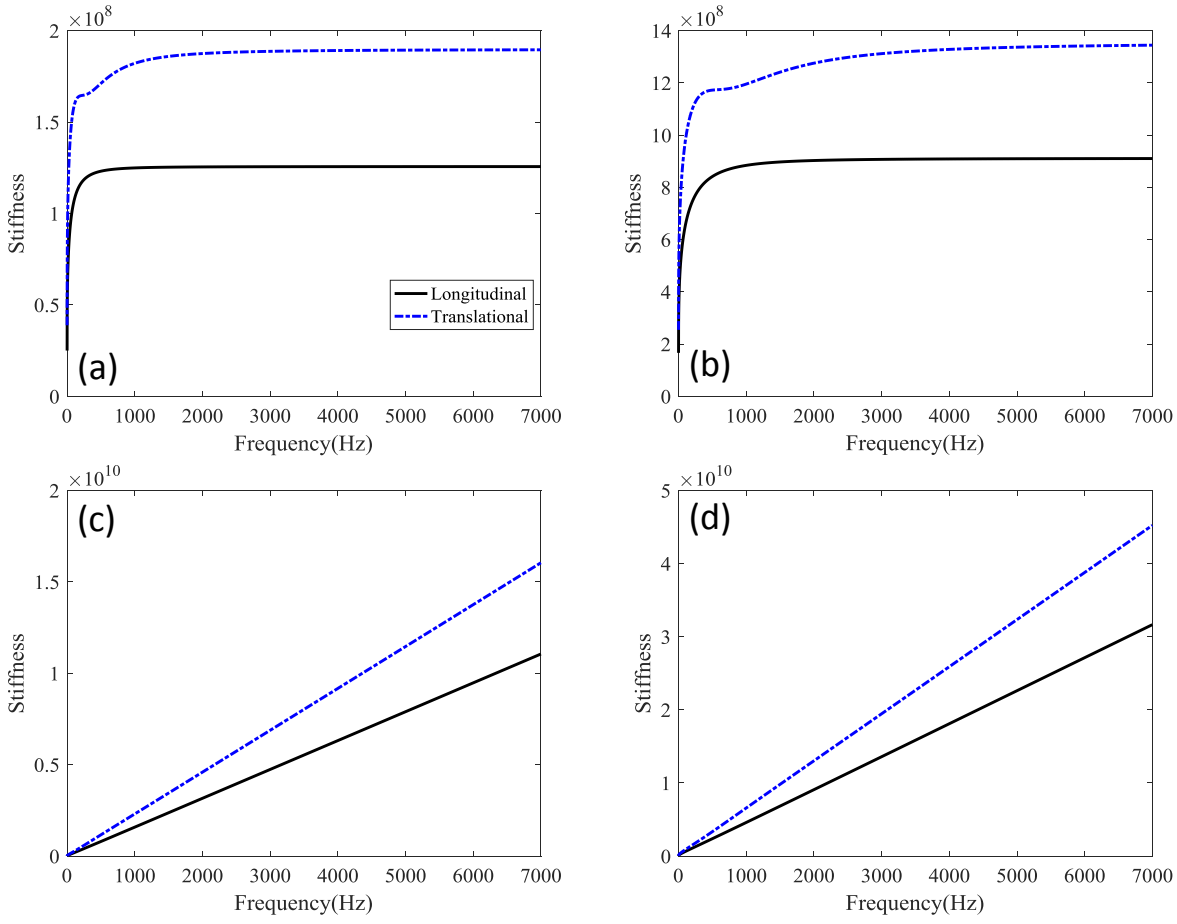

Figure 3-12: Soil stiffness (a) Soft soil (b) Hard soil.

The dynamic soil stiffness values in Figure 3-12 are used to model the pile for simple 1D shear and pressure waves (given the high frequencies, the flexural waves in Timoshenko beam

can be approximated as simple shear waves with appropriate correction for nonuniform shear within the cross section). Wavenumbers for longitudinal and shear waves can be calculated using

$$K_L = \sqrt{\frac{\rho_p A_p \omega^2 - K_L^{Soil}}{E_p A_p}} \ , \tag{3.29}$$

$$K_T = \sqrt{\frac{\rho_p A_p \kappa \omega^2 - K_T^{Soil}}{G_p A_p}} \ , \tag{3.30}$$

where ρ_p is the density of pile, E_p is the Young's modulus of pile, A_p is pile cross sectional area, K_L^{Soil} is the complex-valued longitudinal soil stiffness, G_p is the shear modulus of pile, K_T^{Soil} is the complex-valued transverse soil stiffness, κ is the Timoshenko shear coefficient and ω is the frequency. The corresponding attenuation coefficient associated with the bottom reflection $\left(e^{2L*imag(K_{L,T})}\right)$ for a fully embedded pile of length 15 m and radius 0.2 m is shown in Figure 3-13.

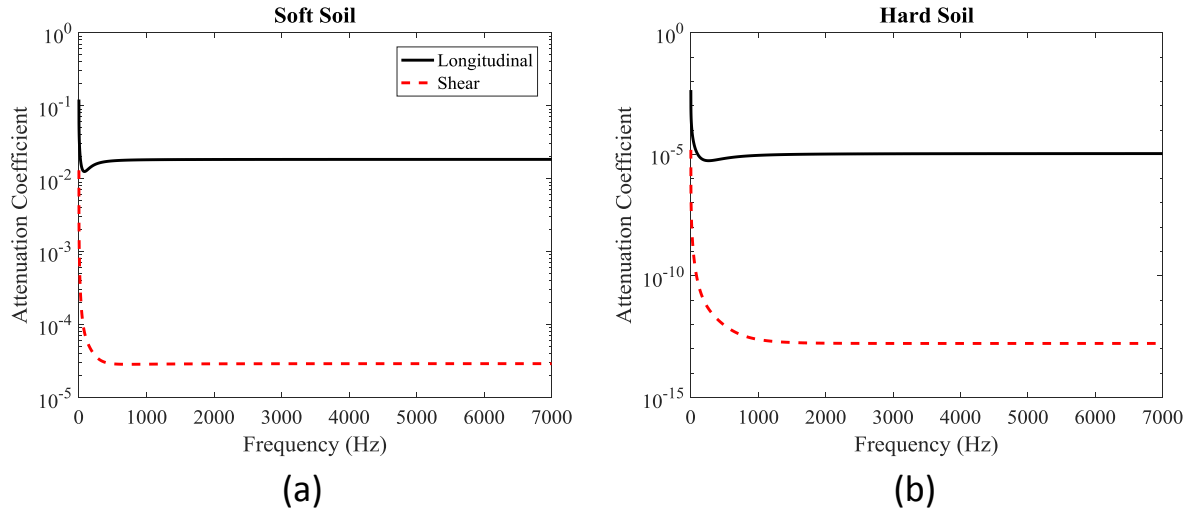

Figure 3-13: Attenuation coefficient (a) Soft Soil (b) Hard soil.

A more detailed guided wave modeling of embedded cylindrical shafts by Wang [42] and Hanifah [40] showed similar results. It is observed that the real part of the complex wavenumber

does not change in comparison to a free pile (without soil) while there is significant difference in imaginary part of wavenumber. Imaginary part of the complex wavenumber is higher for hard/dense soils corresponding to larger attenuation of the waves. This behavior is attributed to the impedance difference between pile and soil. The mismatch between longitudinal wave velocity in pile and shear wave velocity in soil is higher than that between shear/transverse waves in pile and longitudinal waves in soil. Thus, transverse waves in the pile encounter more radiation damping and are attenuated much faster than longitudinal as it can be seen in Figure 3-13. Since the piles were close to the coast, the soil conditions were saturated for a majority of embedded portion of soil. The degree of saturation of soil can have a significant effect on the pressure wave velocity in soil and has minimal effect on shear wave velocities. This would only make the attenuation of the transverse waves even more pronounced furthering the hypothesis of the dominance by longitudinal waves in the reflections recorded at the accelerometers.
In Equation (3.18), it was established that the ratio of amplitude of longitudinal wave to transverse waves generated from a lateral impact is small. However, as discussed in the previous paragraphs, the transverse waves decay significantly, three to eight orders of magnitude more than longitudinal waves (even for soft soil types in the field). Thus, the reflections from longitudinal waves dominate the measurements in the field settings, and EDAR analysis should accordingly be modified, as discussed in the next section.

3.5 Improved length estimation

EDAR methodology relies on estimating the cycle and wiggle periods from the phase and in doing so already separates the waves into initial arrival and reflections. Based on the analysis in the previous two sections, transverse waves dominate the initial arrival to the sensors, but longitudinal waves dominate the reflections in the field settings. This effect is captured in the modified EDAR methodology that entails the following steps:

1. Obtain average cycle period from a series of impacts for different hammers and sensors combinations.
2. An infinite Timoshenko beam is used to optimize for Young's modulus of the pile by matching the average cycle period. The cross-sectional area of the pile, distance between the sensors which are measured on site are required. The density of pile material and Poisson's ratio are assumed based on pile type.

3. Longitudinal wave velocity is calculated using the estimated Young's modulus and the other assumed material properties.
4. Wiggles are identified in the data and corresponding average wiggle periods are calculated as a function of frequency. Wiggle period and longitudinal wave velocities are used along with equation (3.7) to obtain a length estimate.

3.6 Final Field Validation

The data from the tests shown in Section 0 was reanalyzed using the procedure described in Section 3.5. Detailed analysis of the data by separating the initial arrival (cycle period) and reflections (wiggle period) is presented in this section. EDAR plot apart from the reflections coming from the pile tip also contain effects from other reflections (ex. top reflections as shown in Figure 3-14). This could affect the cycle and wiggle periods. In order to mitigate these effects, cycle and wiggle periods are obtained by averaging over several impacts and between different sensors combinations.

3.6.1 Material properties from cycle period

EDAR plot for a sensor spacing of 0.62 for three different impacts are shown in Figure 3-14. Cycle period, which is primarily a consequence of the initial wave arrival at the two sensors, appears to have some variability. This is attributed to factors such as the reflection from the top, near field effects and wiggle interference at the location of cycle period (effect of other boundaries is currently under investigation and will be presented as a part of future work). Nevertheless, the average cycle period, from different sensor combinations, is utilized to obtain the Young's modulus of the pile as described in the previous section. Cross-sectional properties are measured at the field and the exact distance between the sensors is known. The density of concrete is assumed to be the typical value of 2400 Kg/m^3, and the Poisson's ration is assumed to be three different values, 0.1, 0.15 and 0.2, representing the typical range of 0.1 to 0.2. Young's modulus is obtained by optimizing for the cycle period using an infinite Timoshenko beam with measured cross sections and distance between the sensors.

The cycle period for each sensor combination is averaged over a set of five different impacts. It can be observed from Figure 3-15 (a) and (b) that the cycle period can be estimated with minimal variation from different sensor combination. The Young's modulus back-calculated from these average cycle periods is used to estimate the wave velocity and is shown in

Figure 3-15(c) and (d), as a function of sensor combinations for an assumed Poisson's ratio of 0.15. The estimated Young's modulus from different sensors combinations was within 5% of the Young's modulus estimated from the design strength of concrete. The wave velocities obtained from different sensor combinations for the piles were within 3% variation between the extreme values. Additionally, it can be observed from Figure 3-15(e) that the estimated longitudinal wave velocity is not very sensitive to the value of the Poisson's ratio with less than 5% difference between the extreme values. This average velocity estimate is to be used along with the wiggle period obtained in the following section to calculate the length of the pile.

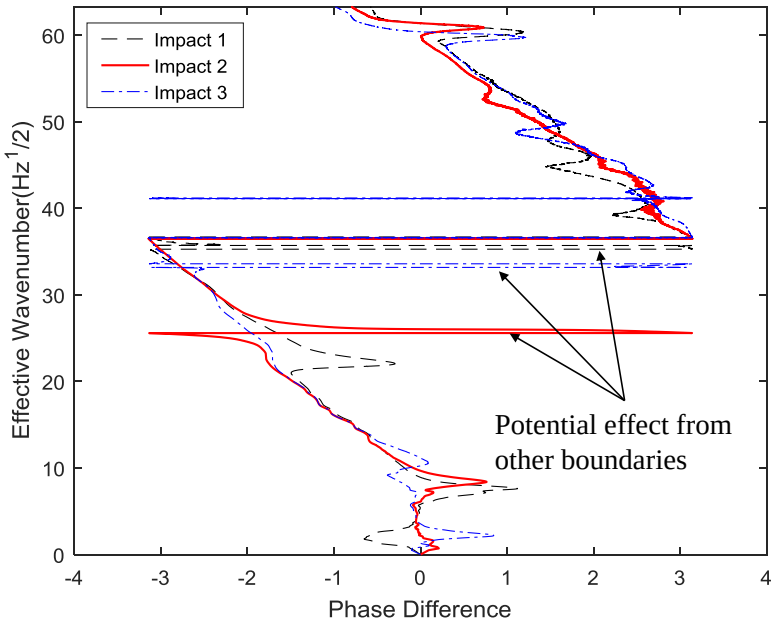

Figure 3-14: Top effect on EDAR plot and cycle period.

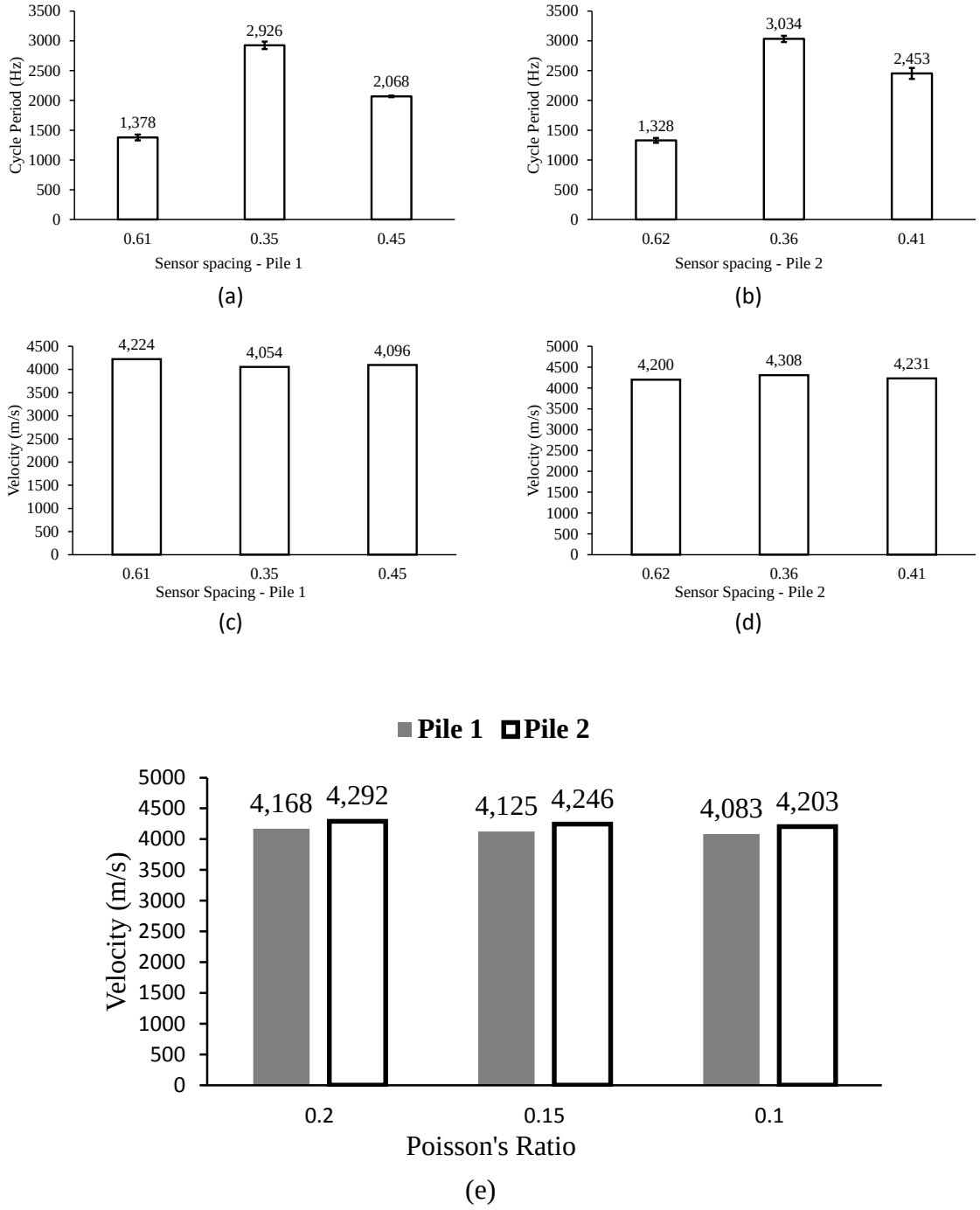

Figure 3-15: (a) Variation in cycle period for Pile 1 (b) Variation in cycle period for Pile 2 (c) Variation in velocity for Pile 1 as a function of sensor spacing for Poisson's ratio 0.15 (d) Variation in velocity for Pile 2 as a function of sensor spacing for Poisson's ratio 0.15 (e) Longitudinal wave velocity estimate from cycle period using Timoshenko beam model.

3.6.2 Length estimate from wiggle period

The length estimates shown in Figure 3-7 were calculated from individual wiggles but often these wiggles appear in clusters and thus, instead of individual wiggles, averages were calculated. Doing this reduced the scatter seen in Figure 3-7 and the overall average of the wiggles is used to obtain the final length estimate. Length estimate is obtained using equation (3.7) with longitudinal wave velocity corresponding to poisons ratio of 0.15, and is presented in Table 3-4. The average length estimates are within 5% error margin and the overall average for both piles have less than 2% error.

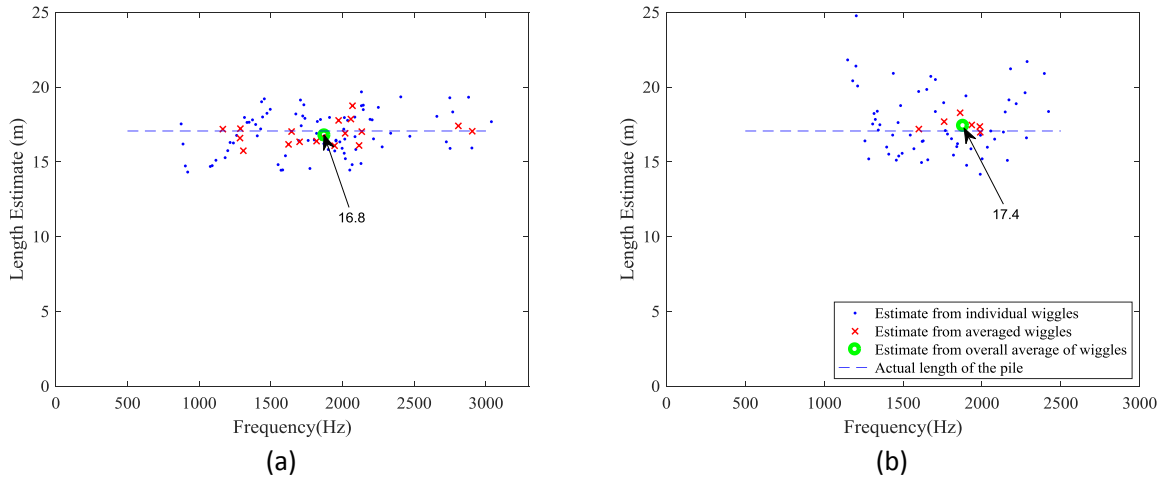

Figure 3-16: Average length estimate (a) Pile 1 (b) Pile 2.

Table 3-4: Improved length estimates.

		Average wiggle (linear frequency)	Length estimate (using wiggle period)	Total length (distance from sensor midpoint to top added)	Error
Overall average	Pile 1	138.5	15.4	16.8	-1.6 %
	Pile 2	135.1	15.3	17.4	2 %
Average (<1500 Hz)	Pile 1	135.2	15.3	16.7	-2.2 %
	Pile 2	133.9	15.7	17.8	4.3 %
Average (>1500 Hz)	Pile 1	140.3	15.4	16.8	-1.6 %
	Pile 2	134.2	15.1	17.2	0.8 %

3.7 Summary and Conclusions

EDAR, effective dispersion analysis of reflections, was recently developed to estimate the length of embedded depth of pile foundations. EDAR showed superior accuracy in laboratory settings, but direct application to field conditions resulted in significant errors. This paper presents a modification to EDAR methodology based on a rather counterintuitive observation that the reflected waves captured in field conditions are from longitudinal waves and not from transverse waves (even though the lateral hammer impact creates predominantly transverse waves). This is due to the differential attenuation caused by the radiation damping coming from compacted soil in field conditions. The modified EDAR methodology resulted in significant improvement in estimated pile depths with errors less than 5%. Ongoing and future enhancements of EDAR include (a) extension to other pile types, e.g. concrete filled steel tubes and timber piles, (b) understanding the influence of hammer characteristics as a function of pile type to increase the likelihood of obtaining good EDAR plots, (c) understanding the effects of top reflections and near field effects to reduce the scatter in material property estimation and thus the estimated pile depth. The outcomes of these investigations will be reported in future publications.

Chapter 4

Experimental aspects of EDAR

Over the past few decades several advancements have been made in terms of the equipment used for dynamic testing. Sensors and data acquisitions systems have become better and smaller with minimal noise and power requirements. Choosing the right equipment for the application of interest is critical in order to accurately measure the response. Important characteristics considered for the selection of equipment is briefly described. Additionally, the impact characteristics also depend on the hammer used to strike the pile and qualitative study based on the response spectrum of the measured data is presented in this chapter.

4.1 Accurate measurement of pile response

The main components required for the accurate measurement of pile response are, accelerometers, data acquisition system (DAQ), processing center (computer or tablet), accessories to connect the systems and a hammer to impact the pile and generate a response in the desired frequency range. A typical setup with all the components is shown in Figure 4-1. Details about the hammers used is presented later in Section 4.2. A windows based tablet computer was used to acquire and power the equipment for testing. Thus the entire system is very portable and does not require any external power which makes it easier to test in the field. Extensive research was conducted on the available data acquisition system technology and accelerometers and the following were chosen based on the key aspects described.

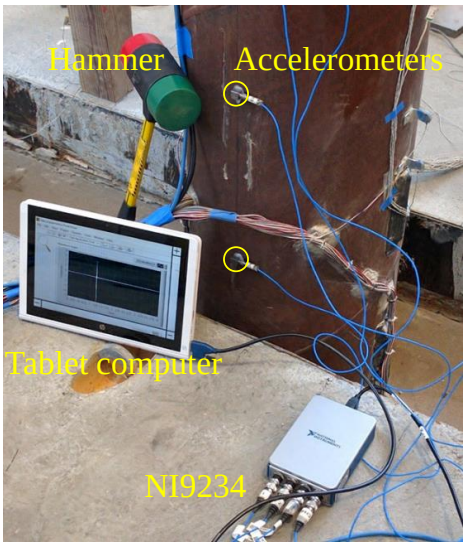

Figure 4-1: Typical setup and equipment.

4.1.1 Accelerometers

The sensors used to measure the response of the pile to the hammer impact were piezoelectric accelerometers. When stress is applied on the piezoelectric crystal, a high impedance electric charge is produced proportional to the stress applied, which is caused by the acceleration. The main characteristics that need to be considered before selecting an accelerometer are sensitivity, bandwidth and mounting, which are described below.

Sensitivity of an accelerometer is given at a specific reference frequency and is the factor that is used to convert voltage into acceleration. It is generally given in units of mV/g and the output voltage of the accelerometer is given by the product of acceleration and sensitivity. Sensitivity has an inverse relationship with the acceleration measurement range of the sensor. Thus, typically, lower sensitivity accelerometers are used to measure high amplitude and vice versa. Further, sensors must be selected based on the amplitude of the acceleration that will be generated from a hammer impact in order to avoid them from overloading.

Bandwidth is the range of frequency that can be measured with high accuracy using a specific accelerometer. This is important as the sensors need to be selected based on the application under consideration and the frequencies excited. In the context of EDAR, one needs to ensure that the bandwidth should include the range of frequencies where wiggles are expected.

In many laboratory and field tests performed as a part of this research, this range is typically between 500 Hz and 3000 Hz.

Proper mounting of the sensors is critical to acquire accurate pile response in the entire range of frequencies where wiggles are expected. Several mounting methods are considered, e.g. handheld, magnetic or adhesive, can be used. Handheld can measure only specific frequency ranges generally between 500Hz and 1000Hz and is mostly used in hard to mount application and initially identify potential location where the sensor can be permanently mounted. Magnetic mounting is a convenient means of attaching the sensor, but the choice of magnet and mounting surface are critical for reliable measurements. Adhesives can provide both temporary and permanent mount based on the choice of adhesive (wax, hot glue and super glue) and generally provide better high-frequency response. These require minimum preparation of the surface and often provide reliable connection to the structure. Based on these advantages, adhesive mounting was chosen for EDAR application. Hot glue was used in laboratory setting and sensors with stud mounts were used in field setting with super glue.

Two single-axis accelerometers shown in Figure 4-2 were used after taking into consideration all the above characteristics. Their specifications are shown in Table 4-1. The main difference between the sensors were their frequency range of measurement. 353C33 is capable of measuring up to 10,000 Hz while 333B32 can only measure up to 3,000Hz. Also, 353C33 can be stud mounted which makes it convenient to be used with super glue adhesive mounting. Given that EDAR plot appears to have usable wiggles mostly below 3,000 Hz, both accelerometers appear to be sufficient and hence, were used for the testing.

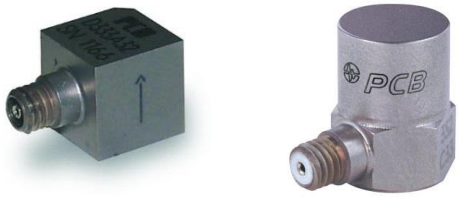

(a) (b)

Figure 4-2: Accelerometers (a) 333B32 (b) 353C33.

Table 4-1: Accelerometer specifications.

Property	**333B32**	**353C33**
Sensitivity	100mV/g	100mV/g
Measurement Range	50 g	50 g
Frequency Range	2 to 3000 Hz	0.5 to 10000 Hz
Broadband resolution	0.00015 g rms	0.00015 g rms
Transverse Sensitivity	≤ 5%	≤ 5%

4.1.2 Data acquisition system (DAQ)

The main purpose of a data acquisition is to covert the analog signal from the sensors into digital data which is done with the help of an analog to digital converter (ADC). Four channel DAQ, NI9234 from National Instruments with a 24 bit ADC resolution and 51.2 KS/s sampling rate was selected for this application. These DAQs are directly compatible with accelerometers and powered through USB connection to the computer. LabVIEW software is used to control the DAQ in the computer. Based on the sensors used and experimental requirements, the maximum frequency of interest was around 10 kHz. Based on the Nyquist theorem, a minimum of 20 kHz sampling rate is required. Using NI9234 the response was oversampled at the maximum rate of 51.2 kHz which reduces the signal-to-noise ratio of the signal.

4.1.3 Signal processing

One of the important aspect for obtaining better results is the handling of noise in the system. Every system will encounter noise of different origins, which cannot be avoided. One way to overcome this is to improve the signal to noise ratio (SNR). This can be done by oversampling during the test or later using specific noise filtering techniques. Pile response is measured only for a short time, typically 2 to 4 seconds, and the waves might not be attenuate completely within this time. Since, the data is predominantly processed in the frequency domain, an exponential window [49] is applied which reduces the noise in the frequency domain. Further, once the EDAR plot is obtained, it can be smoothed to facilitate easy peak picking for estimating the wiggle periods.

4.2 Hammer characteristics and producing a good impact

Multiple hammers with different sizes and interchangeable rubber tips of varying hardness, as shown in Figure 4-3, were used to impact the pile. Several factors such as the hammer weight, tip size (diameter), pile material and tip hardness play a key role in the frequency content generated on impact. Inherently, the process of impacting with a hammer is a nonlinear and localized phenomenon affected by surface interactions. Quantitative understanding of the impact characteristics would require a deeper knowledge of both hammer and structure properties which are often variable and unavailable; characterizing these properties would be more complicated than the main objective of pile NDE [50]–[52]. Thus, a more qualitative approach based on the frequency response obtained from the hammer impact was studied to further gain insight and identify the best hammer type and tip for difference scenarios. Six hammer tips have been used during the testing in the laboratory as well as the field tests. These tips include the hard (LH) and soft (LS) tips of the large sledge hammer and Hard (SH), Medium Hard (SMH), Medium (SM) and Tough (ST) tips of the small sledge hammer. Specifications about all the hammers used are presented in Table 4-2. Since the small sledge hammer was not equipped with a load cell to measure the force, a smaller instrumented hammer with hard (ISH), medium (ISM), soft (ISS) and super soft (ISSS) was used only to evaluate the impact force spectrum for different hammer tips (we recognize that the amplitude may be affected based on the hammer type, but we hypothesize that the frequency content is not affected).

Impact force from instrumented hammers were measured for an impact to a solid concrete pile surface. The time domain and frequency domain plots are shown in Figure 4-4 along with the average time duration for each of the tips. The time domain plot shows the difference between the impact duration for each of the tips and this translates to the frequency domain as well. The larger hammer impacts produces a force larger than the upper limit of the force transducer and thus sometimes the hammer signal is cut off at 22,240 N which is not a limitation as the hammer force is not used in the analysis. Nevertheless, the variation of the impact for the same hammer tip as well as between hammer tips can be seen in the scatter plot (Figure 4-4 (c)). Impact duration of various tips were as expected; softer tips had longer duration of impact and harder tips had sharper impulse with shorter impact durations. The smaller hammers are in general easier to operate with a more precise control on the impact application.

In contrast, the larger hammers are capable of providing a larger impact due to their weight but harder to control owing to the same reason.

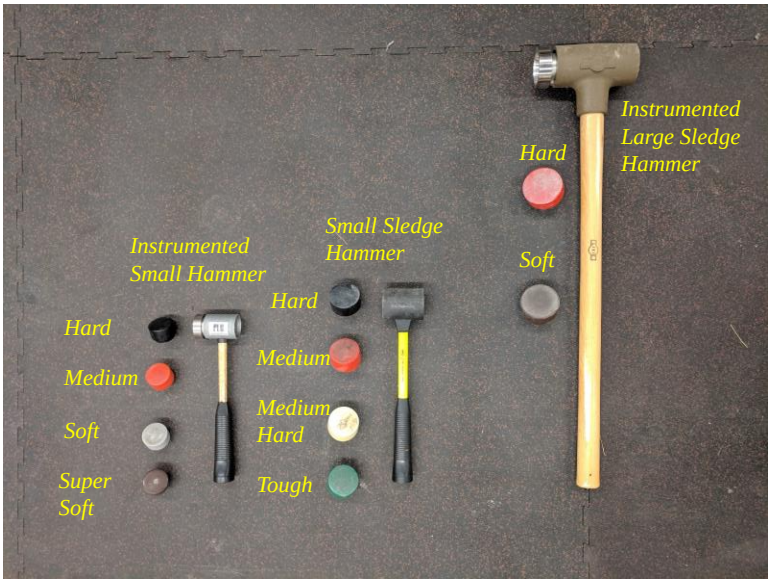

Figure 4-3: Different hammers used for testing.

Table 4-2: Hammer specifications.

Hammer/Specification	Mass (kg)	Head Diameter (cm)	Measurement Range
Large Sledge Hammer	5.5	7.62	±22240 N
Small Sledge Hammer	2	6.35	NA
Instrumented Small Hammer	1.1	5.08	±22240 N

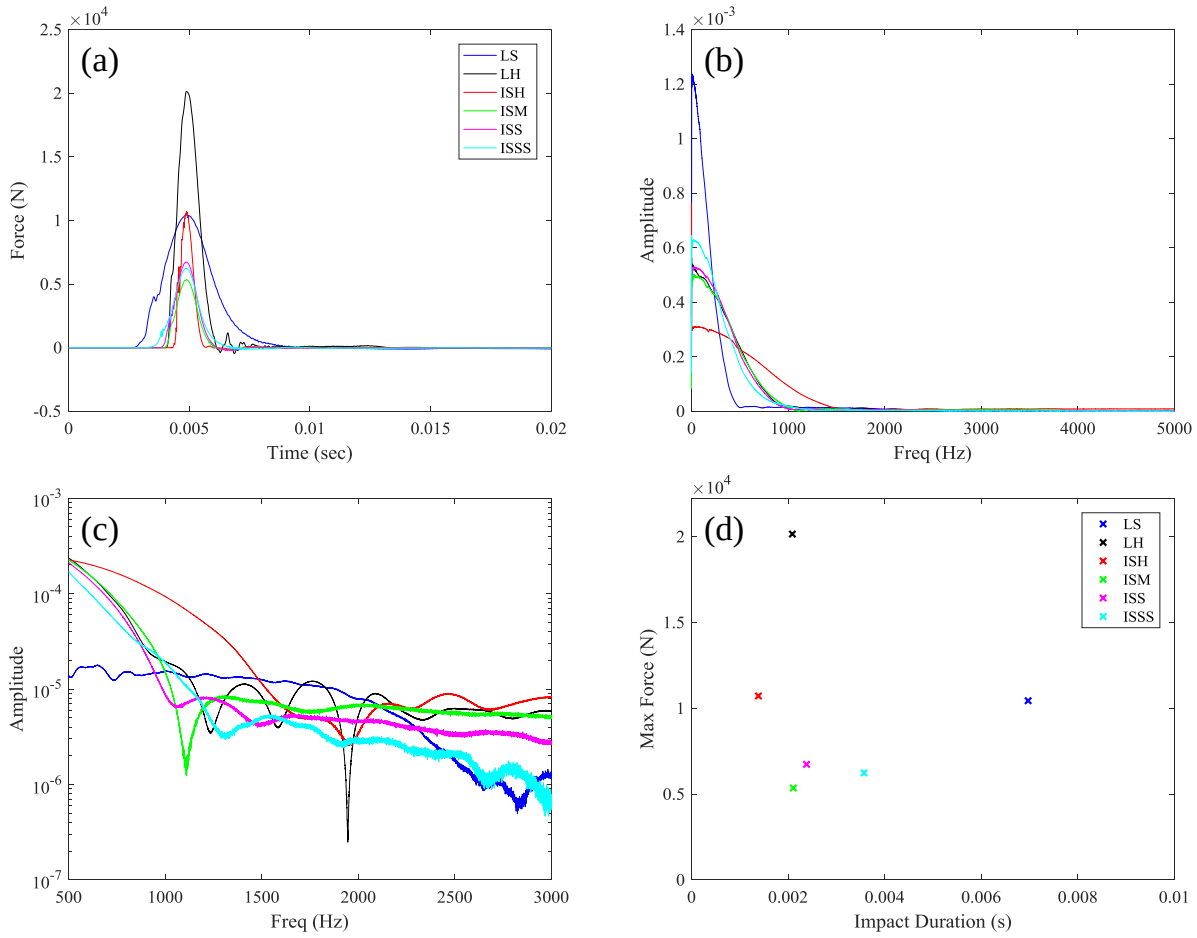

Figure 4-4: (a) Time-domain and (b) Frequency-domain representation of the force (c) Frequency content of the force from 500 to 3,000 Hz in logarithmic scale (c) Duration of impact vs maximum force.

While the hammer type and tip did not play a significant role in the results obtained in the lab (Section 3.2.2), observations from field testing of different piles were different. Based on pile type and material, data from certain hammer tips were more consistent and repeatable. For example, using ST tip produced for Outer Banks (OBX) piles produced better EDAR plots at higher success rates compared to the other tips with clear and consistent wiggles across a broad range of frequency. Similarly, for the concrete-filled steel tubes (CFST) tested in Portage, Alaska, SH and LH seemed to produce better EDAR plots compared to other tips. While this was observed it did not entirely mean that the other tips were unsuccessful in producing good EDAR plots but their success rate was lower in comparison. In order to explain these specific behaviors

some preliminary exploration of the data focused on the frequency content generated by the impact was studied. Six different impacts were processed for four different hammer tips for each of the pile type and are shown in Figure 4-5 and Figure 4-7. Additionally, all the impacts were averaged for each tip and presented in Figure 4-6 and Figure 4-8. Predominantly wiggles were obtained from field tests in the range of 1,000Hz to 3,000Hz. For the solid concrete piles, except for LS, rest of the tips had higher amplitude in the frequency range of interest. Even though ST, LH and SH tips were comparable in the frequency range of interest, only ST seemed to produce good data at a higher success rate. LS excited frequencies in this range is better for the Portage CFST. Counterintuitively, LS had higher amplitude than LH. LS was comparable to SH up to around 2,000Hz which is an indication of why LS worked better for CFST.

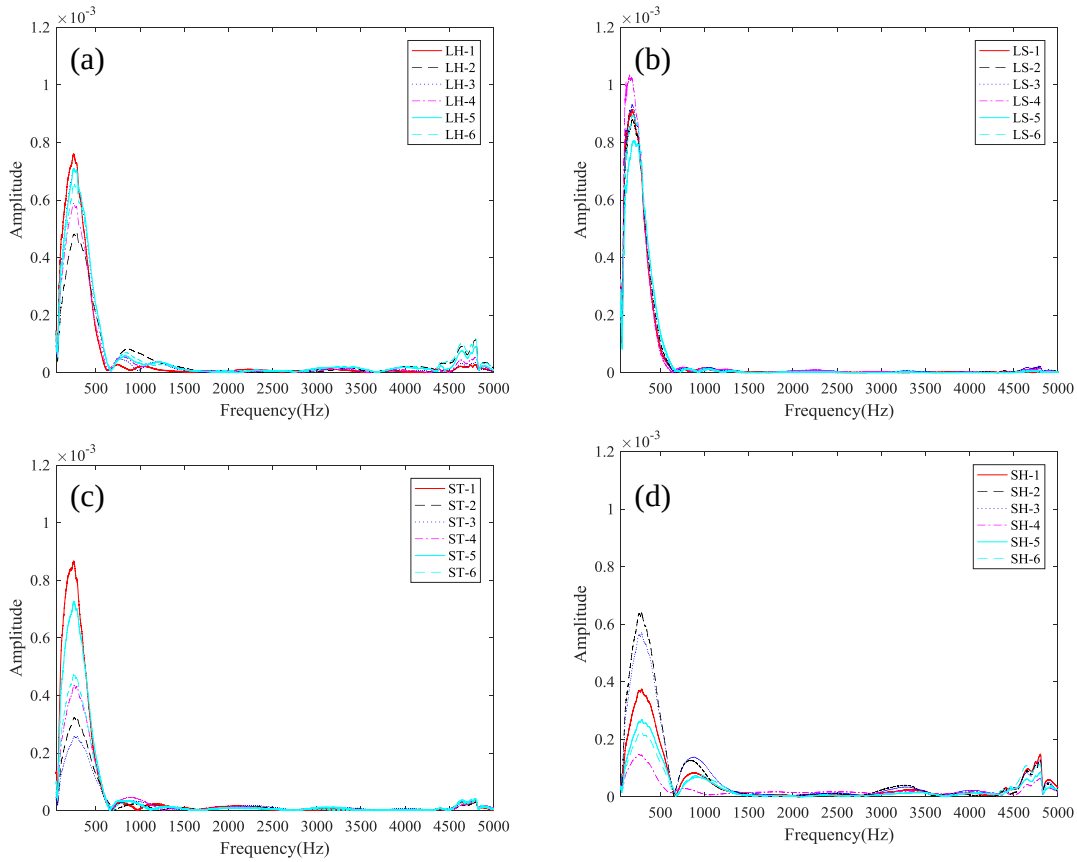

Figure 4-5: Outer Banks solid concrete pile (a) Large hammer hard tip (LH) (b) Large hammer soft tip (LS) (c) Small hammer hard tip (SH) (d) Small hammer tough tip (ST).

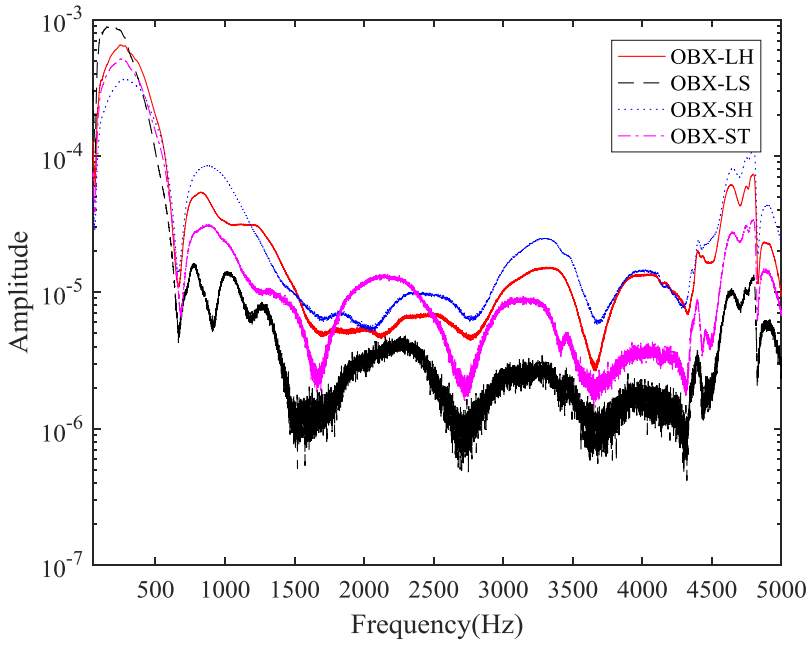

Figure 4-6: Average frequency from multiple impacts – Outer Banks pile.

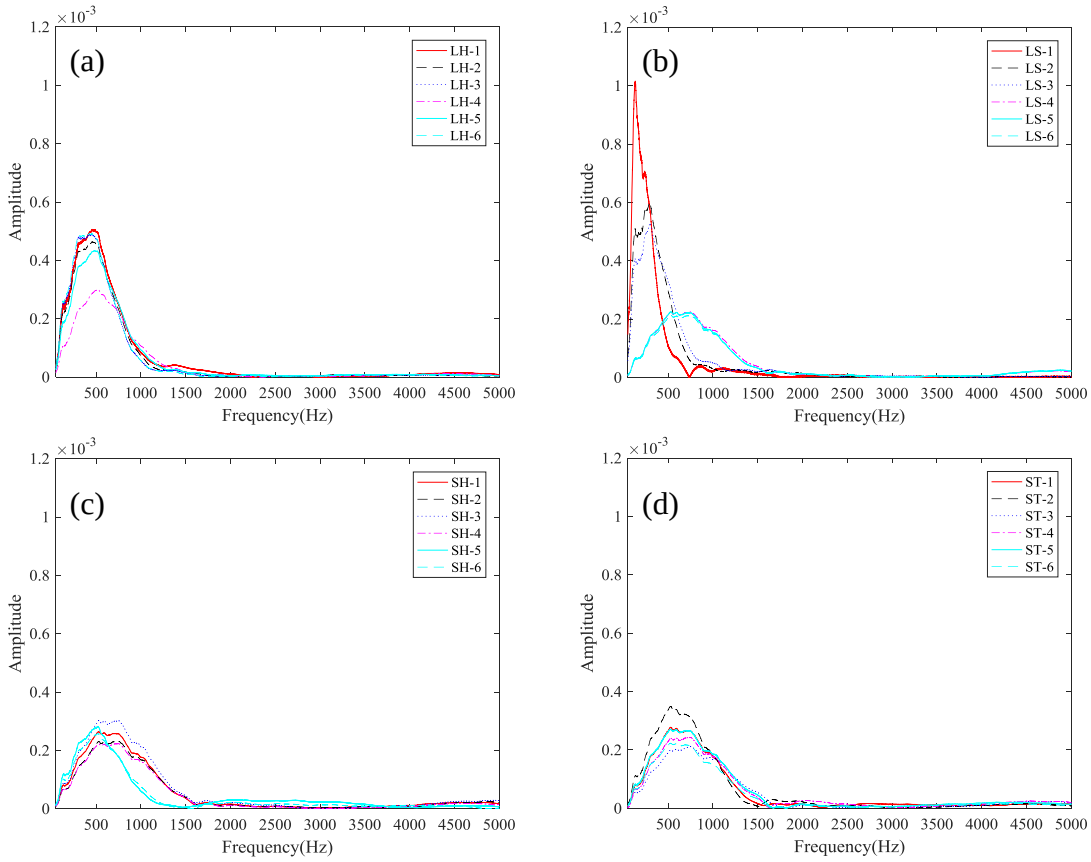

Figure 4-7: Portage CFST pile (a) Large hammer hard tip (LH) (b) Large hammer soft tip (LS) (c) Small hammer hard tip (SH) (d) Small hammer tough tip (ST).

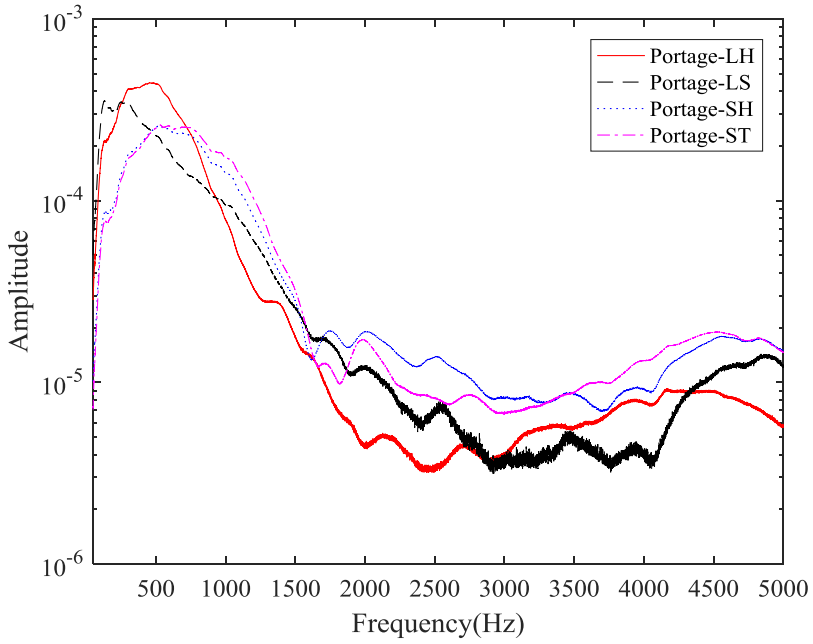

Figure 4-8: Average frequency from multiple impacts – Portage pile.

Although, this gives us an insight into the range of the frequencies excited for different hammer tips, this does not explain why wiggles are found only in specific impacts in the EDAR plot. The inherent randomness of the impact also plays an important role in obtaining good EDAR plots. Depending on the site and access to pile, impacting the pile might be difficult in certain situations. Applying a crisp purely lateral impact is often not possible. Two consecutive impacts one without wiggle (Impact 1) and one with wiggles (Impact 2), were analyzed. The resulting comparison in time, frequency domains and EDAR plots are shown in Figure 4-9. Even though impact 2 in the plot had lower acceleration amplitude meaning that it had the weaker impact of the two, it had better EDAR plot with cleaner wiggles. Looking at the time domain, there is significant difference in between the two impacts. Impact 1 has an extra peak at the beginning when compared to Impact 2 which looks cleaner. The amplitude spectrum in the frequency domain also shows more excitation over the frequency range of interest but this does not lead to a better EDAR plot for Impact 1. Also, the amplitude spectrum from the two sensors in Impact 2 are comparable while there is significant difference for Impact 1. Even though this was just one of the impacts, it is evident that higher excitation in frequency ranges of interest does not guarantee a good EDAR plot.

In summary, the hammer and impact characteristics seem to play an important role in obtaining EDAR plots with wiggles and this has to be studied and understood further for different pile types. While this analysis explains the observations from the field tests, it does not fundamentally explain the reason for a particular tip and impact leading to better EDAR plots. Currently, initial testing and analysis involving all the hammer tips is utilized for selecting the best hammer tip and type that suits the pile under consideration.

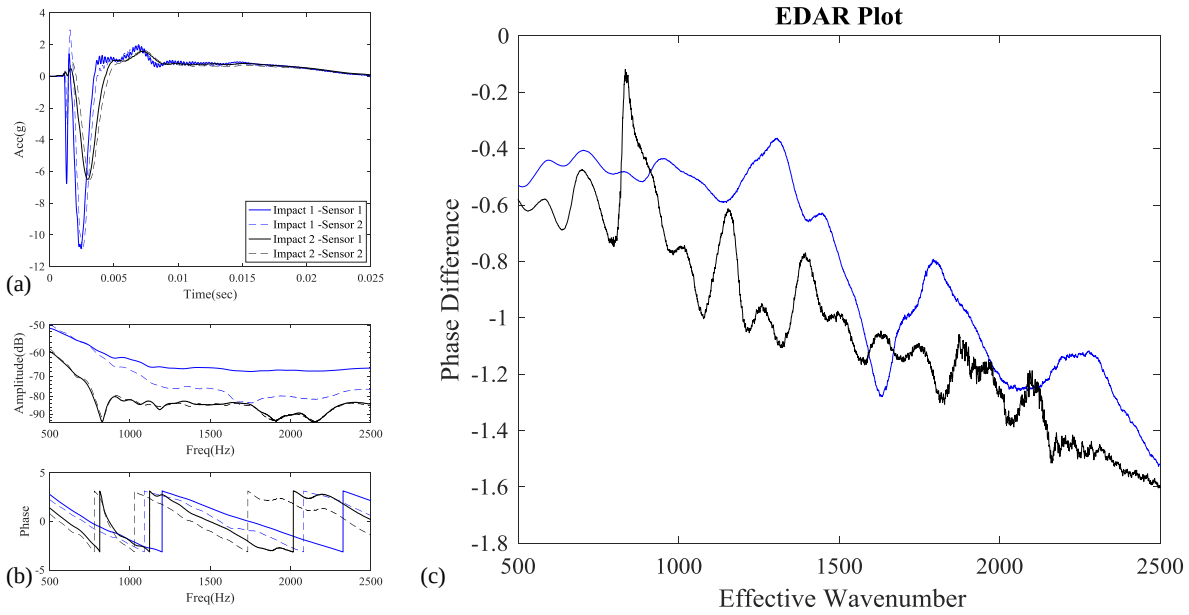

Figure 4-9: Comparison of good and bad impacts.

Chapter 5

Pile test results, Improvements and Extension of EDAR

Mainly three different types of pile were tested: hollow steel pipe piles, concrete filled steel tubes (CFST) and solid concrete piles. While the results were promising for CFST and solid concrete piles, the tests on the hollow steel pipe piles were unsuccessful and require further work. The results for pile tests are presented in this chapter.

5.1 Hollow steel pipes

A hollow steel pipe pile at a bridge site near Tryon Road, Raleigh was tested. Due to the hollow nature of the pile, ringing of steel from the impact highly polluted the data, making it difficult to process the data and obtain meaningful EDAR plots as shown in Figure 5-1. Nevertheless, some of the characteristics features of EDAR can still be observed in Figure 5-1(d) but supplemental understanding of the hollow steel behavior is essential before the results can be processed. Based on this, further analysis based on the frequencies excited and more sophisticated signal processing methods are required to handle this behavior and is beyond the scope of this research. The current development of the method is limited to solid concrete piles and CFST.

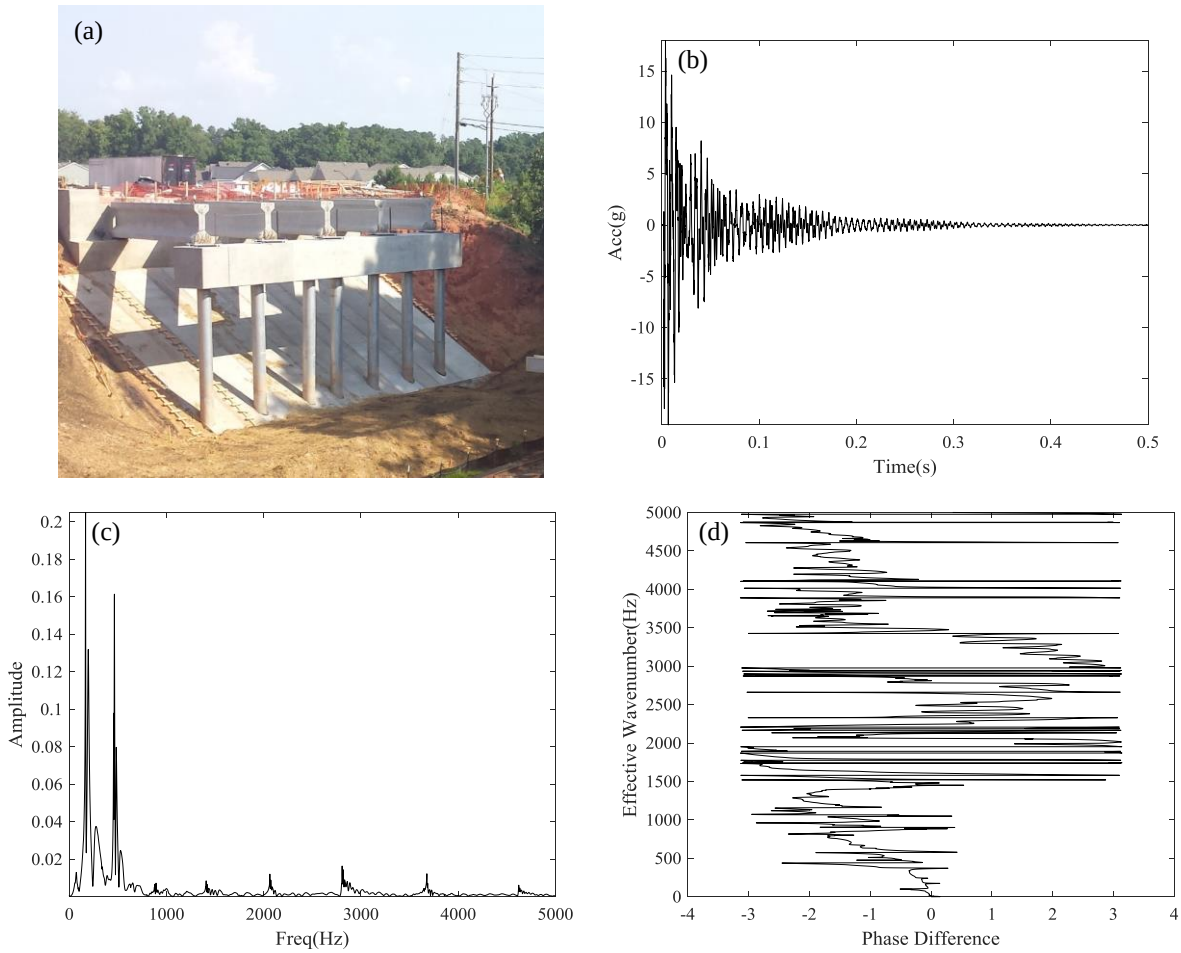

Figure 5-1: (a) Hollow steel pipe piles (b) Acceleration history showing ringing (c) Frequency domain of the acceleration (d) EDAR plot.

5.2 Concrete filled steel tubes (CFST) in laboratory

Pile were tested in the laboratory setting at the Constructed Facilities Laboratory at North Carolina State University (NCSU) with a unique opportunity to test the pile during different stages of cyclic lateral load tests [38]. The results presented in Sections 2.4 and 3.2.2 were conducted on intact piles before application of any cyclic lateral loads. One of the main differences between the laboratory and field testing is the soil surrounding the pile. The soil is relatively loose and less saturated in the laboratory condition when compared to the field conditions. The EDAR test was conducted before and after the seismic performance test which involved lateral displacements of increasing displacement until eventual failure of the pile. A unique soil pit was used with the ability to liquefy soil to embed the pile and subsequently drain

the water. Due to this process, the soil was not well compacted and the lateral displacements of the pile compacted the soil around it and reduced the interaction boundary of pile and soil as shown in Figure 5-3(a). As the test was conducted before and after this soil behavior, there were some differences obtained in EDAR plot and the length estimates which are summarized in this section. EDAR testing was conducted after various levels of lateral displacement of the pile top (0, 0.1 and 0.2 m), and with more separation between the pile and soil, the wiggle periods started to become more pronounced as shown in Figure 5-2. This is mainly attributed to the leakage of the waves into the soil. The waves generated from the lateral impact were predominantly found to be flexural in nature and as shown in Section 3.4.2, attenuation of flexural/ transverse waves is highly influenced by the presence of soil surrounding the pile. This particular observation is useful in the analysis of field data as often multiple wiggle like oscillation can be seen in EDAR. Not all of these oscillations correspond to reflection from the pile tip and given that the soil pile boundary is intact and better than lab conditions, the wiggles with lesser amplitude can be picked for the length estimation process. This same procedure was applied later in section 0 for analyzing CFST pile in the field.

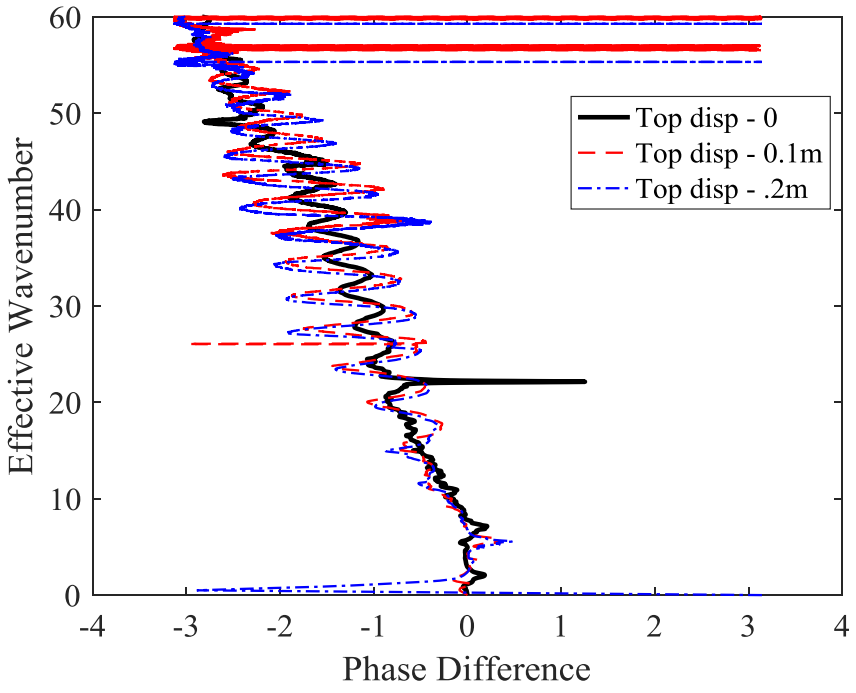

Figure 5-2: EDAR plot during different stages of testing.

Cycle period obtained from a sensor spacing of 0.61 m, wiggle periods obtained using Timoshenko wavenumber as the effective wavenumber axis and the length estimates obtained compare very well with the actual length of 6.31 m as shown in Figure 5-4. While the wiggle amplitudes were significantly different for the different stages of testing, only little difference was observed in the length estimates obtained from the corresponding wiggle and cycle periods. Nevertheless, effect of soil in laboratory is not as significant as observed in the field where the longitudinal modes become more prevalent in the reflection due to the differential attenuation.

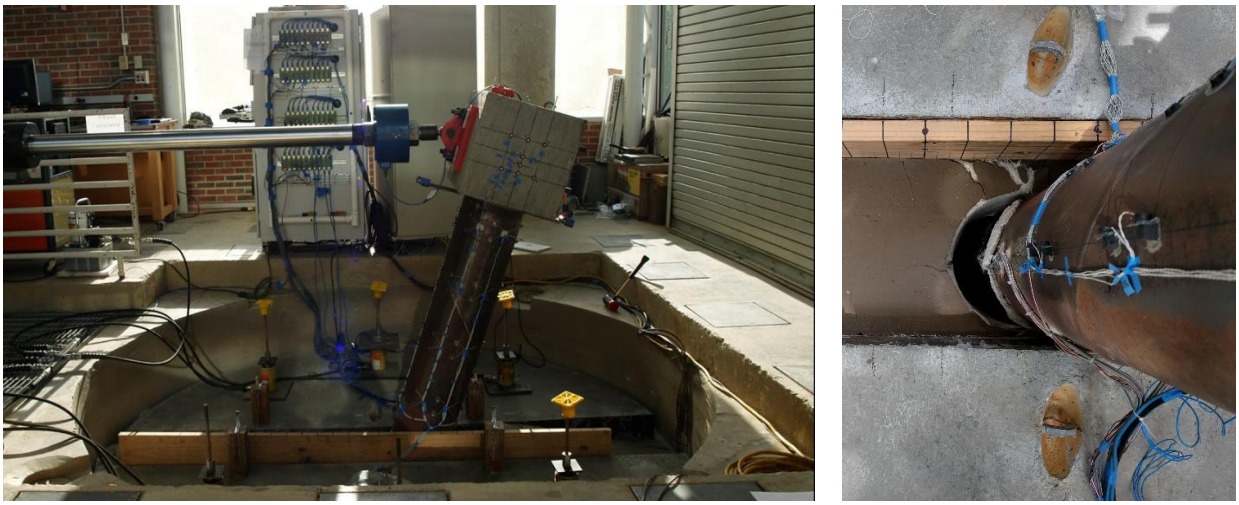

(a) (b)

Figure 5-3: (a) Lateral testing [38] and (b) soil compaction on the pile sides reducing pile soil interaction.

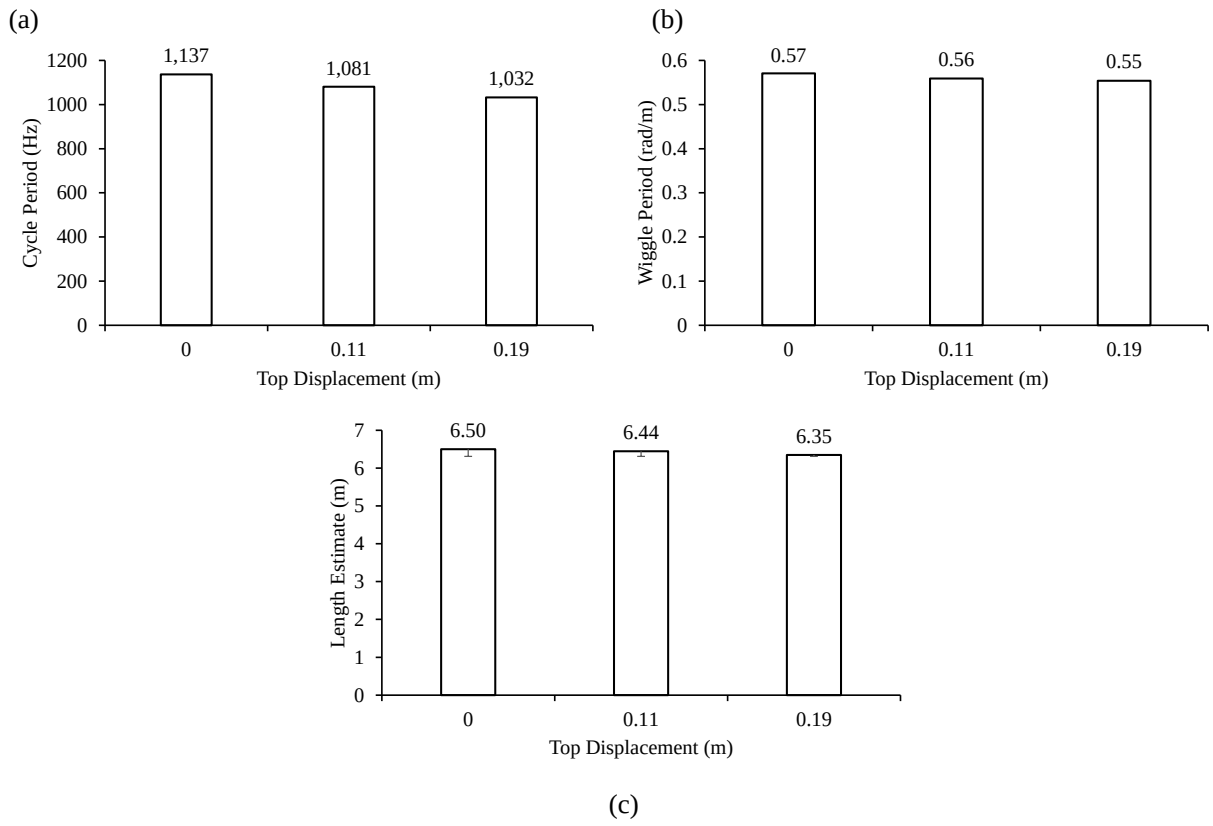

Figure 5-4: (a) Average cycle periods (b) average wiggle periods (b) average length estimates obtained.

5.3 CFST in field conditions – Portage pile and preliminary analysis

Similar to the piles tested in laboratory, CFST with comparable cross-sectional properties were tested in field condition in Portage, Alaska. A picture of the pile tested is shown in Figure 5-5(a).

Figure 5-5: (a) Bridge in Portage, AK (b) Sensor locations and spacing.

Unlike the lab piles, the external surface of the field pile had ageing related aberrations and thus, surface preparation was done before installing the sensors to ensure sufficient coupling of the sensors to the pile. In order to analyze the data using Timoshenko beam theory, modulus, density and Poisson's ratio for both the materials of the composite pile are required. This is more of a challenge for the field pile compared to the lab pile, as often these details are not readily available due to missing records. This requires gathering as much information through field reconnaissance and making some informed guesses. Steel being a less uncertain material compared to concrete, its properties found in the literature are used. For the pile under concern, after discussion with field engineers from AKDOT, ASTM A36 structural steel properties was considered to be a reasonable assumption. Also, external dimeter of the steel can be measured but unless the steel tubes terminate before reaching the cap, their thickness cannot directly be evaluated. Standard weight steel pipes with a wall thickness of 6.35 mm, typical of the time the

bridge was constructed, were assumed. Similar to the approach for Outer Banks pile the density and Poisson's ratio are assumed, and the Young's modulus is obtained using the cycle period (Section 3.5). All the material properties are summarized in Table 5-1. The concrete modulus obtained using the average cycle period (1207 Hz sensor spacing of 0.6 m) and an infinite composite Timoshenko beam model similar to Section 3.6.1.

Table 5-1: Properties of Portage pile.

Material	Inner diameter (m)	Outer diameter (m)	Young's Modulus (GPa)	Density (Kg/m^3)	Poisson's Ratio
Concrete	0	0.3112	37.66	2400	0.15
Steel	0.3112	0.3239	200	7800	0.26

Particularly, data obtained using the small hammer hard tip and large hammer soft tip produced consistent and repeatable EDAR plots. The data was analyzed based on the assumption of flexural waves and similar to the observation from Outer Banks piles, the length was underestimated as shown in Table 5-2.

Table 5-2: Portage pile length estimates based on flexural waves assumption.

Hammer	Average Length Estimate (m)	Actual Length (m)	Error
SH	5.4	9.1	-41 %
LS	6		-34%

Even though Portage piles are older (approximately 50 years) and might have deteriorations that could affect EDAR estimates, the underestimation was comparable to that observed for Outer Banks. These piles were embedded in soil with an embedment length of 7.2 m and due to the creek under the bridge, the soil is saturated. As shown earlier 3.4.2, this could lead to significant attenuation of the flexural waves leading to a reflection dominated by

longitudinal waves, similar to the results obtained for Outer Banks piles shown in Section 3.3. The modified results are shown Figure 5-6 and Table 5-3.

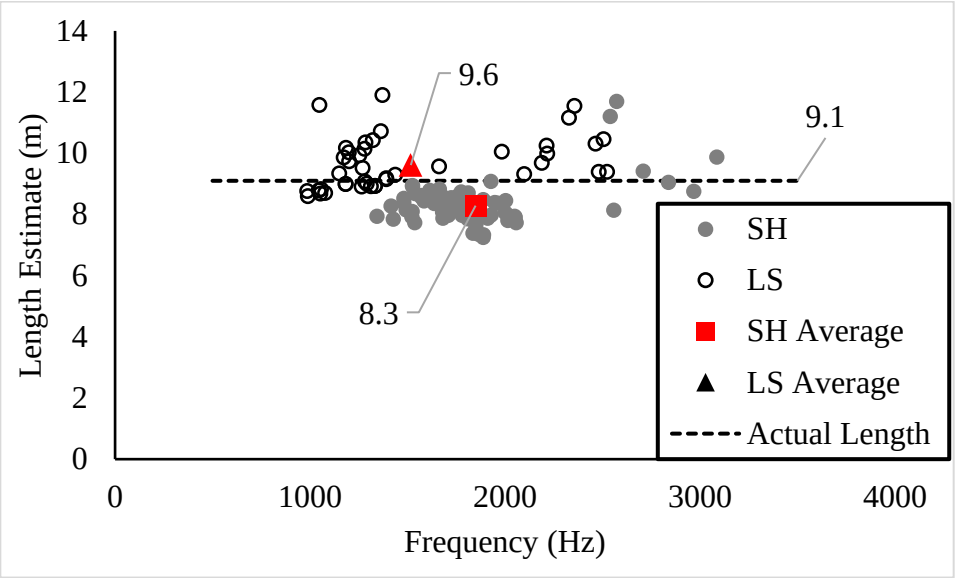

Figure 5-6: Improved length estimates for Portage pile with scatter and average.

Table 5-3: Improved length estimated – Portage pile.

Hammer	Average Length Estimate (m)	Actual Length (m)	Error
SH	8.3	9.1	-9%
LS	9.6		5.5 %

It can be observed that the length estimates resulting from longitudinal wave assumption are more accurate, with less than 10%. Scatter in the obtained length estimates is reduced by averaging the wiggles. One of the potential reasons for the non-uniform wiggles is due to the effect of other boundaries. Unlike the pile test results from lab piles and Outer Banks piles, the Portage pile terminated in a full constructed pile cap. This could have an effect on the EDAR

plots and subsequently on the cycle and wiggle periods. Effect of the top and bottom boundaries is discussed in the following section.

5.4 Effect of top and bottom boundaries

Sensitivity of EDAR method to the boundary conditions of the pile is the fundamental concept that is used to extract length information from the pile's response to a hammer impact. The waves generated on hammer impact get reflected from the pile tip which in turn are responsible for the wiggles. Likewise, other boundaries as well as damage (Section 5.5) in the pile also influence the EDAR plot and this knowledge is critical to the length estimation process. In a general sense, the waves generated from the hammer impact interact with all the boundaries which include the pile soil interface, pile tip and pile top. Depending on the structure, frequency content and modes of wave propagation, one or more of these boundary effects can be found in the EDAR plot. Pile foundations typically transfer load either through friction or end bearing and sometime a combination of both. Most commonly pile foundations are constructed using steel concrete or timber. For the case of friction piles or floating pile, the pile tip is suspended in the soil medium while end bearing piles terminate in the bedrock. Either way, the impedance contrast between the pile material or the soil (looser soil or bedrock) leads to the wave getting reflected at the pile tip. Similar to the wiggles produced due to wave reflection from the bottom of the pile, wiggle like disturbances due to other boundaries are also present in the EDAR plot. These disturbances can likely have adverse effects on the length estimation process from the EDAR methodology as they can interfere with the cycle and wiggle period that correspond to bottom reflections. Often, as described in Section 2.3.3, these effects could be discarded during the analysis and additionally, by averaging the cycle and wiggle periods obtained from multiple impacts and sensors combinations. Even though averaging reduces the effects from other boundaries, a more thorough approach to directly understand these effects is necessary.

Top boundary, whether free or fixed in a cap, can have an effect on the EDAR. One of the critical aspect of EDAR and its characteristics is the location of the impact. Typically to obtain EDAR plot with wiggles coming from the bottom boundary, the hammer strike is imparted between the top sensor and pile cap. The location of impact determines the characteristics of the EDAR plot. A Timoshenko beam with dimensions shown in Figure 5-7 and properties given in Table 5-4 is analyzed for two cases of impact: Impact above the top sensor

and impact below the bottom sensor. The bottom and top of the pile are attached with a half-space (HS), properties of which can be varied to simulate either an infinite pile in one or both directions or fixed, free or flexible boundary. Also, material damping is introduced by using a complex modulus (imaginary part is set as 2.5% of the modulus value).

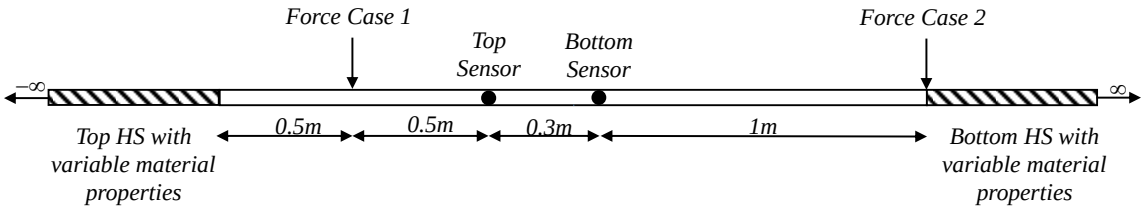

Figure 5-7: Theoretical Timoshenko beam with a bottom HS.

Table 5-4: Properties of the composite Timoshenko beam.

Material	Inner diameter (m)	Outer diameter (m)	Young's Modulus (GPa)	Density (Kg/m^3)	Poisson's Ratio
Concrete	0	0.2921	37.66	2400	0.15
Steel	0.2921	0.3048	200	7800	0.26

Impact Case 1:

The pile is impacted in between the pile top and the top sensor similar to the regular EDAR procedure. The properties of the bottom HS are matched with that of the pile and the top HS properties are set to a large value to simulate a fixed end. This isolates the effect of top reflections. Figure 5-8(a) shows the EDAR plot obtained from the response obtained at the sensor locations. Similar to the wiggles obtained from the bottom reflection, larger oscillations with wider periods are obtained. Nevertheless, these can be usually ignored, since data from multiple impacts is analyzed and six EDAR plots are obtained from four sensors for each impact. This can also be observed in experimental data and an example is shown in Figure 5-8(b) where you can also see the wiggles coming from the bottom reflections.

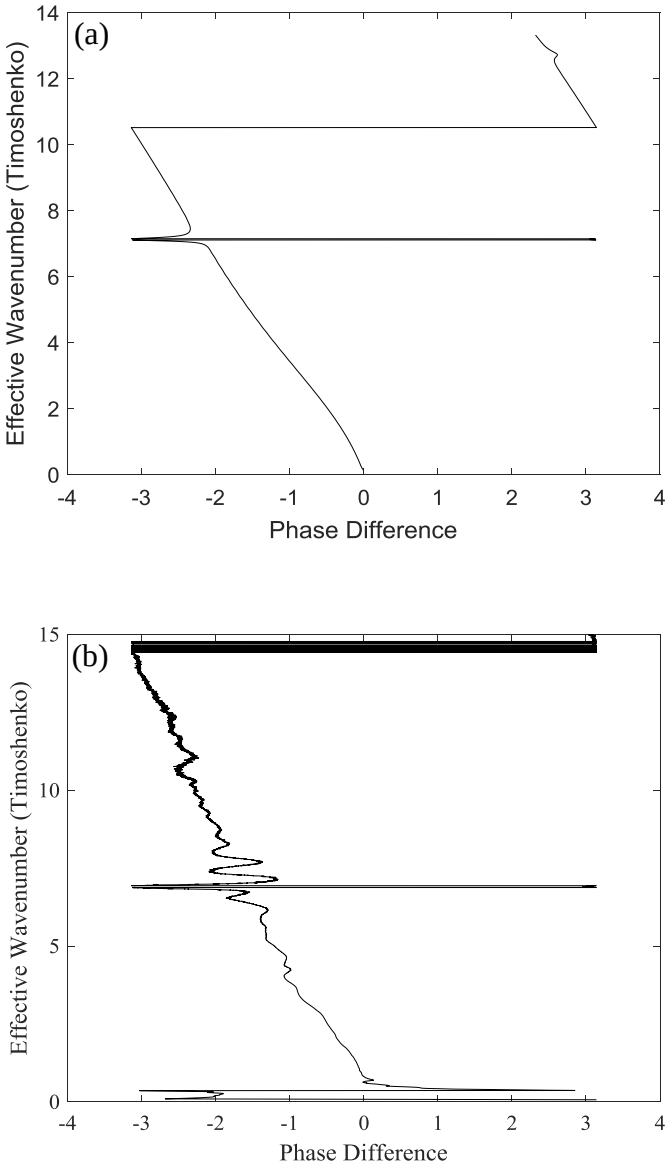

Figure 5-8: (a) Theoretical EDAR plot with sudden spike due to top reflection (b) Experimental EDAR plot from Portage pile test showing similar characteristics.

Impact Case 2:

The pile generally terminates in a cap at the top. The impedance difference between the pile and the cap might not be significant as the pile-soil boundary, since the cap and pile are most likely made of the same material (with exceptions for steel and timber piles). In order to evaluate the sensitivity of EDAR to the top boundary, the location of impact was varied to make the

effects from the top boundary significant. The cycle period is still a consequence of the arrival of the wave at the two accelerometer locations and as long as the distance between the sensors is unchanged, the cycle period is fairly unchanged. However, even though the wiggles are fundamentally same, they look different and the effect of the top boundary is pronounced.

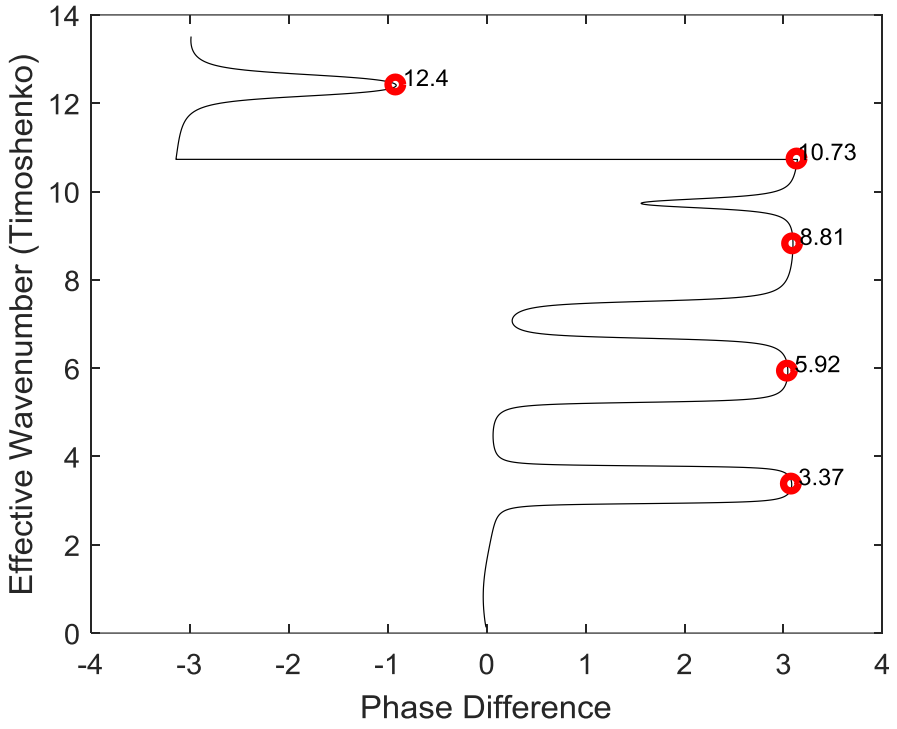

Figure 5-9: Impact below bottom sensor resulting in amplification of tops effects.

In fact, these wiggles can be used to obtain the distance to the top of the pile just like earlier, by using the cycle period, wiggle period and the sensor spacing. The average wiggle period can be calculated from the peaks shown in Figure 5-9 using which a length estimate of 1.19 m is obtained. The distance from the sensor midpoint to the pile is 1.15 m and thus, a very accurate estimate is obtained well within 5% error. One of the main reasons for the error is the broad nature of the wiggles and subsequent peak picking. A similar test was conducted on the Portage pile (Section 5.3) with the hammer strike between the bottom sensors and the soil surface. The resulting EDAR plot obtained for a sensor spacing of 0.25 matched well with a theoretical one-dimensional Timoshenko beam model. Using cycle period and average wiggle

period, length estimate obtained was 1.42 m which compared well with the actual length of 1.31 m (8% error). These results are preliminary, and further work is needed to make the estimate accurate as EDAR formulation approximates the two periods in the phase difference coming from the distance between the sensors to the boundary and considers the average length (Section 2.3.1.2). While this works for the pile tip as the distance between the sensors is small compared to the distance from the sensor to the tip, the same is not true for the top. The wiggles being wider could also influence the cycle period. Additionally, this shows that significant energy from the wave gets reflected back into the pile at the top boundary (pile-cap interface) and thus effect of waves transmitted into the cap and reflecting back from other boundaries is expected to be minimal. Nevertheless, this can be used in conjunction with the regular procedure (impact case 1), to obtain additional information about unknown pile material properties as the distance to the pile top is known and will be explored as a part of the future work.

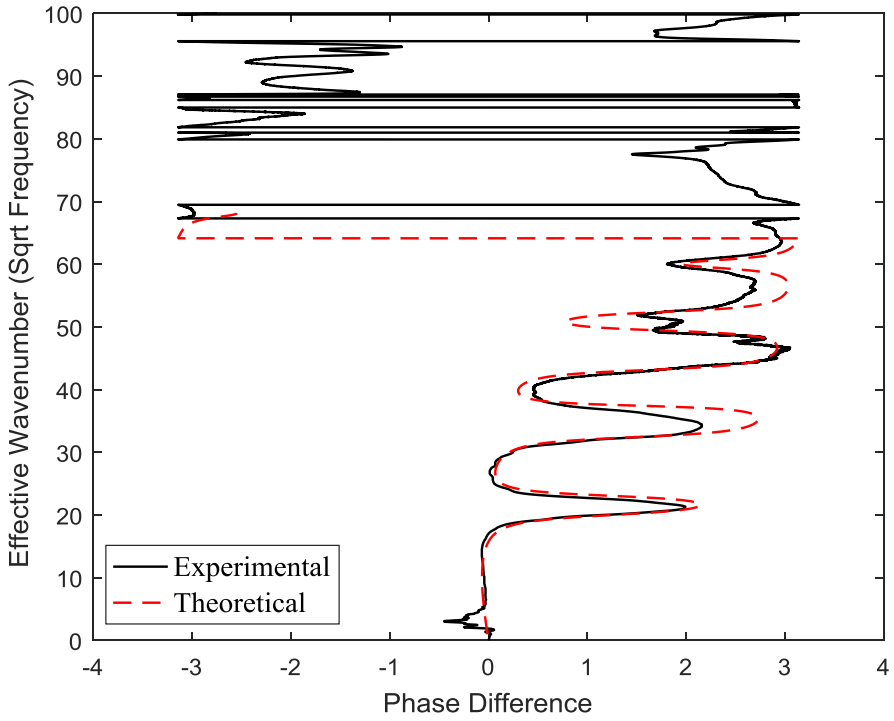

Figure 5-10: Comparison of experimental and theoretical EDAR plots obtained from hammer strike below the bottom sensor.

5.5 Preliminary work for detection of discontinuity

EDAR methodology was predominantly validated by Concrete Filled Steel Tubes (CFST) in the lab and solid concrete piles in the field. These piles were newly constructed with no significant deteriorations or discontinuities at the time of testing. While the results are promising, it is not uncommon for existing bridges to have deteriorated due to ageing and/or contain some discontinuities. This situation has been studied by several researchers (e.g. [13], [53]–[56])with standards existing for some methods [57]. Discontinuities can be of varying degrees and similar to the pile tip, the waves get scattered/reflected when they encounter any inhomogeneity as they travel. Thus, it is important to understand the effect of discontinuities on EDAR plot and eventually on the length estimates obtained.

We had the opportunity to test a pile with known damage in the laboratory setting. The cyclic lateral load test (Section 5.2) was continued until the CFST buckled and often a combination of concrete crushing, steel rebar fracture and steel tube fracture was observed. EDAR testing was conducted after the pile failure and the data obtained was analyzed. For this specific pile tested, it was determined, after pulling the pile out of the soil pit, that tube fracture, tube local buckling, reinforcement bar buckling had occurred as shown in the Figure 5-11. The section with the largest buckling was found to be at an average length of 2.31 m from the bottom of the cap.

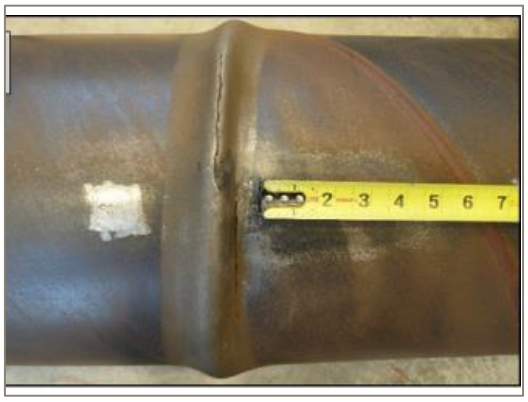

Figure 5-11: Local tube buckling and fracture in the laboratory pile [38].

5.5.1 Preliminary Theoretical Study

Firstly, theoretical study was performed through a Bernoulli-Euler beam modelled with an internal hinge, to better understand its effects on EDAR. Hinges cannot carry any moment and using this and condensing the dynamic stiffness matrix of a beam, corresponding stiffness matrix of a beam element with hinge can be obtained. Similar to earlier studies, half-spaces (HS) were added to both the top and bottom in order to isolate the effects coming from various boundaries in the problem and is shown in Figure 5-12. The top HS properties are matched to that of the pile while the bottom HS is matched to that of the pile first to obtain only the effect of the hinge and then later modulus is set to a very high value to simulate a fixed end at the pile bottom.

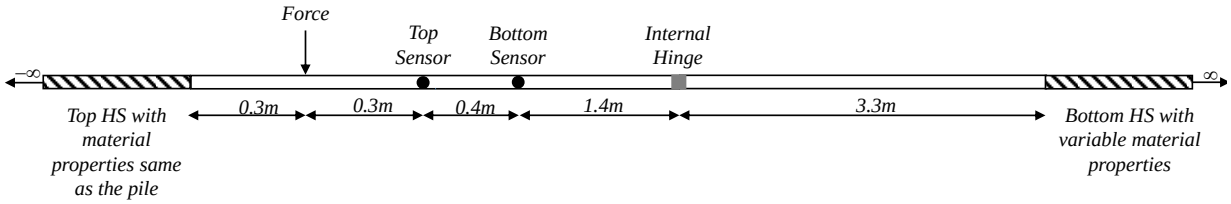

Figure 5-12: BE beam with internal hinge.

Case 1: Effect of the hinge

The bottom HS properties are matched to that of the pile and thus, the waves get reflected only from the hinge and the corresponding EDAR plot obtained is shown in Figure 5-13. It can be immediately observed that the reflection from the hinge produce similar wiggle like behavior and the period of the wiggle is expected to be larger than the ones coming from the bottom as the distance travelled by the wave is lesser. Wiggle and cycle period calculated gave an average length estimate of 1.56 m which compared very well with the distance from the midpoint of the sensors to the hinge location of 1.6 with an error of 2.5%.

Case 2: Combined effect of the hinge and bottom

Now the bottom HS modulus was set to a large value to simulate a fixed end and the corresponding EDAR plot obtained is shown in Figure 5-14. Since the wave gets reflected and transmitted at the internal hinge, EDAR plot displays characteristics of both the bottom and the hinge. Both smaller as well as larger oscillations can be observed in the EDAR plot which

correspond to the reflection from the pile bottom and hinge respectively. In order to effectively obtain the wiggle period and subsequently the lengths, the phase difference is processed further to extract the two period of oscillation using its Fourier components. Phase difference only up to the first cycle is cut separately and slope corrected to conduct Fourier analysis for extracting the two period as shown in Figure 5-15. The first two dominant peaks are used to obtain corresponding wiggle period. It is important to note that the distance from the midpoint of the sensor to the hinge and bottom is 1.6 m and 4.9 m respectively, Thus, using this method, both the distances were extracted from the EDAR plot.

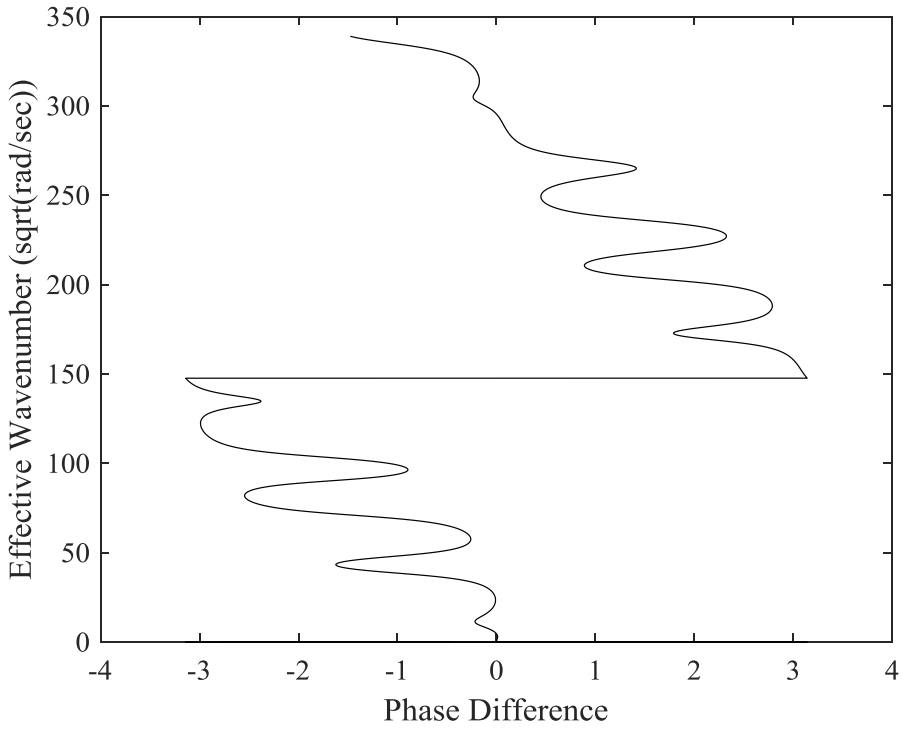

Figure 5-13: EDAR plot obtained for reflection only from the hinge.

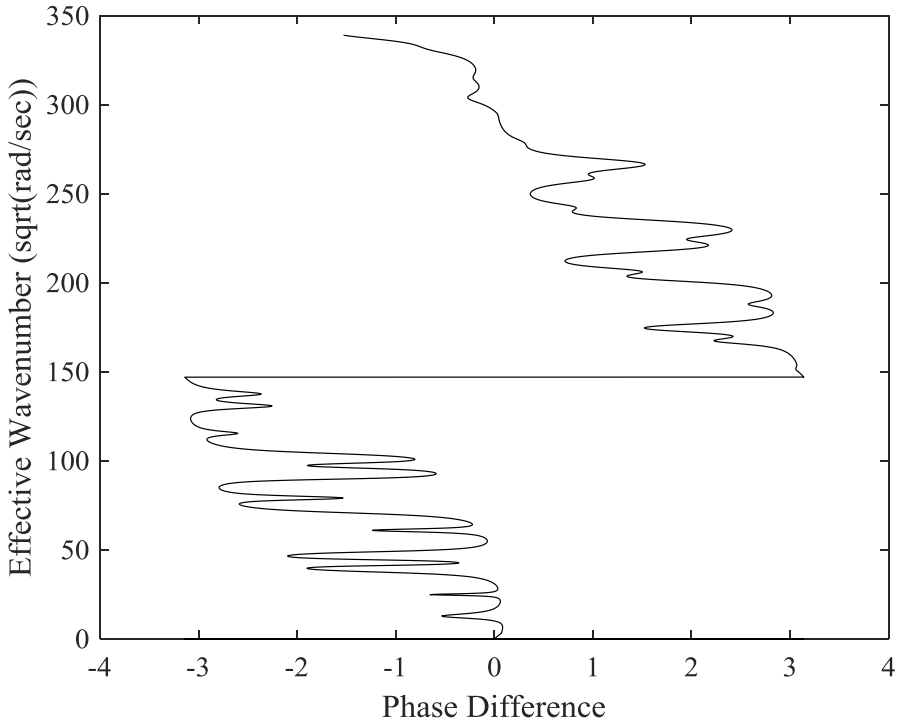

Figure 5-14: EDAR plot obtained from combined bottom and hinge reflection.

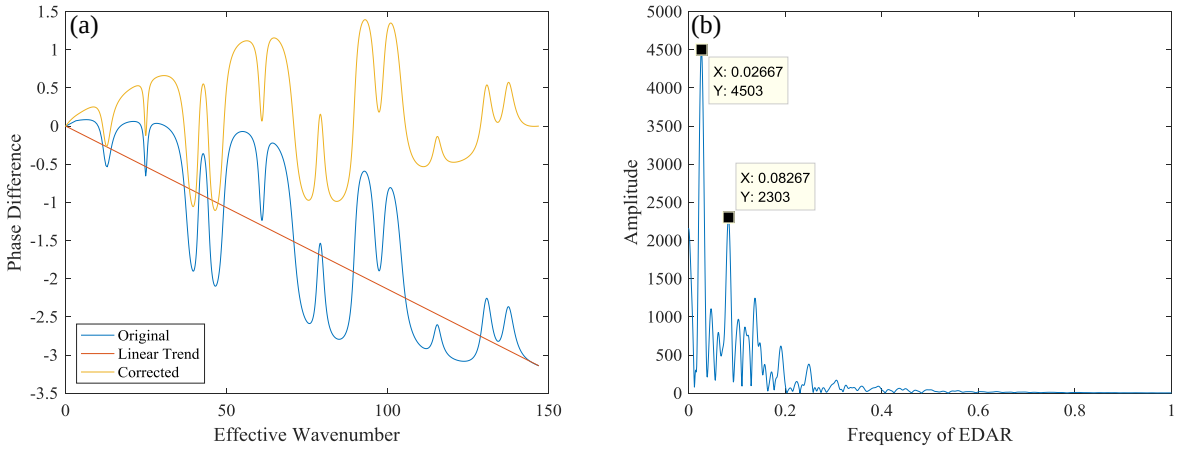

Figure 5-15: Processed phase difference to extract the various periods (a) Slope corrected phase difference (b) Fourier components of the corrected phase difference.

Table 5-5: Length estimates from processed phase difference.

Frequency of phase difference	Wiggle period	Length estimate
0.027	37.04	1.59
0.083	12.05	4.88

5.5.2 Analysis of Laboratory Data

As mentioned earlier, CFST was tested after local buckling and steel fracture. EDAR plots obtained from the pile while it was intact and after failure are shown Figure 5-16.

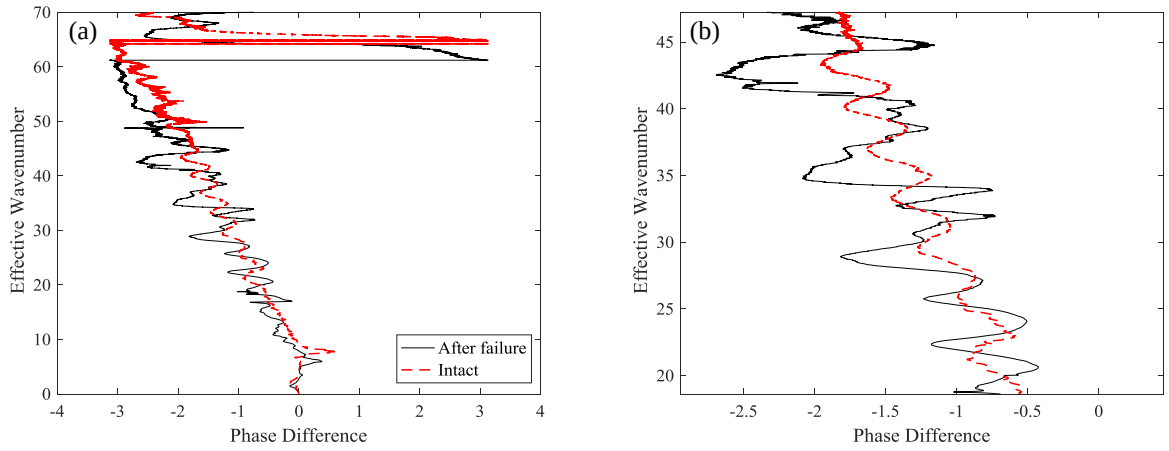

Figure 5-16: EDAR plot obtained for CFST – Comparison between intact and failed pile.

Clearly, there was significant differences between the two plots. While theoretical analysis of EDAR for identifying damage from the frequency spectrum of EDAR showed promise, actual measurements contain noise from various sources. To perform an analysis similar to case 2 only a specific range in the effective wavenumber axis is considered. This range is to be established such that the noisy part of the phase is ignored to obtain only the portion that contain clear wiggle. Otherwise, clear peaks as observed in Figure 5-15(b) cannot be observed. Additionally, the effect of top reflection shown in Section 5.4 also polluted the phase difference. Nevertheless, for the data obtained from the failed pile, patterns similar to the theoretical case in the phase

difference were processed to obtain the different periods. A most plausible location of damage at an average distance of 2.5 m from the bottom of the cap was identified from the analysis (with effective wavenumber obtained using Timoshenko beam theory) while the actual location of the significant damage was at a distance of 2.3 m. Even though this is promising, further development and detailed analysis of the phase may increase the potential of using EDAR to identify locations of damage. The ability of EDAR procedure to identify location of damage or discontinuity depends greatly on the type of damage and how much of energy gets reflected and transmitted. Frequency content also plays an important role as a hammer impact is capable of producing only lower frequencies and thus smaller damage locations cannot be identified but larger and significant damage locations can be potentially identified.

Chapter 6

Summary and Conclusions

A new surface-based nondestructive testing method called effective dispersion analysis of reflection (EDAR) has been developed to address the long standing problem of unknown foundation. EDAR is based on incorporating the wave dispersion characteristics to obtain a length estimate by simplifying the visualization of reflections of the wave generated through a hammer impact. The difference in the phase of the response recorded at two accelerometers is periodic in nature with two characteristics periods named cycle and wiggle. Phase difference is processed as a function of a newly defined quantity called the effective wavenumber to successfully extract the length information. Effective wavenumber is essentially a scaled wavenumber and defined based on the type of wave generated. The power of the method comes from its ability to deal with dispersive flexural waves. Additionally, it provides an alternate methodology to analyze longitudinal waves thus making it capable of analyzing both nondispersive and dispersive waves.

Underlying theory of EDAR methodology and the length estimation process is originally derived using one dimensional bar and Bernoulli-Euler (BE) beam models. The method is easily extendable to higher order beam theories such as Timoshenko beam theory or guided wave theory by defining the effective wavenumber as the actual wavenumber obtained from the models. Successful practical application of EDAR requires access to the pile with a sufficient exposed length (at least 0.6 to 0.9 m) for installation of a minimum of two sensors and hammer strike. The method was validated in laboratory using concrete filled steel tubes (CFST). Length estimates obtained using BE beam theory were accurate only in the lower frequencies. Using Timoshenko beam theory increased accuracy is achieved over a larger frequency range with average length estimates within 5% error. Using BE theory does not require any additional knowledge about the pile materials for calculating effective wavenumber (defined as square root of frequency) but using Timoshenko beam theory requires knowledge about the pile materials to calculate the effective wavenumber. Careful examination of the frequencies in which the wiggles are observed can help in selecting the right beam theory to be used for the length estimation process.

Following the success in the laboratory conditions, EDAR methodology was extended to field piles. Unlike laboratory conditions, obtaining usable data was more challenging and various aspects including the equipment and the hammer impact were studied for better understanding. Nonetheless, data with observable wiggles was obtained and initial analysis results led to underestimation of the pile length. After further analysis this was attributed to the differential attenuation of flexural and longitudinal waves from soil, which exists for compacted soil in field conditions (and not in loose soil conditions in the lab). Due to the differential attenuation, transverse waves attenuate by several orders of magnitude compared to longitudinal waves, making the (secondary) longitudinal waves dominating the reflections. Thus, an improved EDAR procedure was established by separating the effects of initial arrival and reflected waves using the cycle and wiggle periods. Improved EDAR methodology resulted in less than 5% error for solid concrete piles tested and less than 10% error for CFST in field conditions. Field piles tested are believed to have embedment sufficient enough to attenuate most of the transverse waves generated. In other situations, involving shorter length piles and loose soil conditions can lead to existence of both longitudinal and flexural waves and effect of this on the EDAR analysis needs to be evaluated through further field testing and analysis. While the results obtained are very promising, limitations pertaining to all surface-based methods also apply for EDAR. The method still relies on being able to record an identifiable reflection from the pile tip which in turn manifests as wiggles in the EDAR plot. Also, complex foundation elements such as splices, embedded caps etc. could complicate identification of pile tip leading to false length estimates.

Essentially, EDAR is sensitive to boundary conditions and depending on the orientation of the sensors and impact, different boundaries exhibit distinct characteristics in the EDAR plot. Characteristics of two important boundaries: pile top and tip were evaluated for different impact cases, theoretically using one dimensional Timoshenko beam model. While other boundaries can affect the length estimation process, with careful consideration these can be leveraged to obtain additional information about the pile such as material properties and improve the accuracy of the length estimates. Further analysis and accurate modelling of the pile, soil and pile boundaries in the problem is essential to improve the analysis methodology and potentially explain the scatter observed in the wiggle periods calculated from actual testing.

EDAR was implemented for CFST and solid concrete piles as a part of this thesis with encouraging results. EDAR appears to be extendable to other pile types (e.g. timber, steel H

piles) in the future. The piles tested were relatively intact in most cases with the actual lengths known for comparison with the estimates obtained. The known length was essential to establish sufficient confidence in the methodology but in actual field conditions complex situations involving different pile materials, pile size, soil types, defects and deteriorations cannot be avoided, and the pile lengths are unknown. Piles with larger cross sections may have additional effects due to the wave reflections from the pile sides and this needs to be evaluated before EDAR can be extended for larger piles. Preliminary theoretical work on the effect of discontinuity on the EDAR procedure was done using a BE beam with an internal hinge. An additional analysis tool based on looking at the Fourier spectrum of the phase difference was established to extract the different wiggle periods as a result of reflection from both the pile tip as well as the hinge. Based on the observations, test results from a damaged pile in the lab were analyzed. The estimated damage location was promising, and further development may lead to the potential of using EDAR to identify damage location in addition to estimating length. This can be key to extending the method for drilled shafts as they are expected to have non-uniform cross section with imperfections along the length.

Potential future work, apart from continued exploration of the previously mentioned areas, include: (a) incorporation of a statistical framework to obtain an interval for the length estimate rather than point estimates which in turn involves understanding the different uncertainties associated with the entire process, i.e. data acquisition and analysis as well as discrepancies and inherent assumptions in the underlying models; (b) use of multi-axis accelerometers to increase the occurrence of wiggles; (c) alternate impact strategies including direction and location such as pile caps; (d) use of individual phase from each accelerometer in addition to phase differences to enhance the results.

REFERENCES

[1] ASCE, “Infrastructure Report Card 2017,” 2017.

[2] V. Schaefer R. and Jalinoos Frank, “Characterization of Bridge Foundations Workshop Report No. FHWA-HRT-13-101,” 2013.

[3] S. Mclemore *et al.*, “Unknown Foundation Bridges Pilot Study,” *Fed. Highw. Adm. Florida Dep. Transp.*, 2010.

[4] L. D. Olson, P. E. Marwan, and F. Aouad, “NCHRP 21-5 Research Results on Determination of Unknown Bridge Foundation Depths,” *Int. Water Resour. Eng. Conf.*, 1998.

[5] F. Rausche, “Non-Destructive Evaluation of Deep Foundations,” 2004.

[6] J. F. Levy, “Sonic pulse method of testing Cast-in-Situ concrete piles,” *Gr. Eng.*, vol. 3, p. 17–19., 1970.

[7] A. G. Davis, C. S. Dunn, and CEBTP., “From Theory to Field Experience with the Non-Destructive Vibration Testing of Piles.,” *Proc. Inst. Civ. Eng.*, vol. 57, no. 4, pp. 571–593, 1974.

[8] F. Rausche, G. G. Goble, and G. E. Likins, “Dynamic Determination of Pile Capacity,” *J. Geotech. Eng.*, vol. 111, no. 3, pp. 367–383, 1985.

[9] H. F. C. Chan, “Non-destructive testing of concrete piles using the sonic echo and transient shock methods,” *Diss. Univ. Edinburgh*, 1987.

[10] Y. Lin, M. Sansalone, and N. J. Carino, “Impact-Echo Response of Concrete Shafts,” *Geotech. Test. Journal, GTJODJ*, vol. 14, no. 2, pp. 121–137, 1991.

[11] M. Hussein, W. Wright, and B. Edge, “Low Strain Dynamic Testing of Wood Piles Supporting an Existing Pier,” *Struct. Congr. XII*, pp. 940–945, 1994.

[12] A. G. Davis, “Nondestructive Evaluation of Existing Deep Foundations,” *J. Perform. Constr. Facil.*, vol. 9, no. 1, pp. 57–74, 1995.

[13] J.-L. Briaud, J.-L. Briaud, M. Ballouz, G. Nasr, and S. J. Buchanan, “Defect And Length Predictions By NDT Methods For Nine Bored Piles,” *Deep Found. 2002 An Int. Perspect. Theory, Des. Constr. Perform.*, pp. 173–192, 2002.

[14] B. Jozi, U. Dackermann, R. Braun, J. Li, and B. Samali, “Application and improvement of conventional stress-wave-based non-destructive testing methods for the condition assessment of in-service timber utility poles,” *Australas. Conf. Mech. Struct. Mater.*, pp. 9–12, 2014.

[15] H. Wang and C.-H. Hu, “Identification on Unknown Bridge Foundations Using Geophysical Inspecting Methods,” *e-Journal Nondestruct. Test.*, vol. 20(11), pp. 905–912, 2015.

[16] R. A. Douglas and J. D. Holt, “Determining length of installed timber pilings by dispersive wave propagation methods,” *Cent. Transp. Eng. Stud. Dept. Civ. Eng. North Carolina State Univ.*, 1994.

[17] R. Y. Kim, R. S. Ranjithan, P. J. Donato, and C. M. Murphy, “Nondestructive Evaluation of the Structural Condition of Timber Piles - Volumes 1 and 2,” *Final Report, North Carolina Dep. Transporatio, FHWA/NC/2000-004*, 2000.

[18] G. J. Rix and L. J. Jacobs, “Nondestructive determination ofpile tip elevation using modal analysis,” vol. 3400, pp. 522–530, 1998.

[19] H. Wang, T. P. Chang, and J. J. Wang, “Response analysis of concrete piles subjected to lateral impact,” *J. Mar. Sci. Technol.*, vol. 18, no. 6, pp. 848–859, 2010.

[20] B. Jozi, “Condition Assessment of In-Service Timber Utility Poles Utilizing Advanced

Digital Signal Processing and Multi-Sensors Array," *Diss. Univ. Technol. Sydney*, no. February, 2015.

[21] A. T. M. Farid, "Prediction of unknown deep foundation lengths using the Hilbert Huang Transform (HHT)," *HBRC J.*, vol. 8, no. 2, pp. 123–131, 2012.

[22] M. Subhani, J. Li, B. Samali, and N. Yan, "Determination of the embedded lengths of electricity timber poles utilizing flexural wave generated from impacts," *Aust. J. Struct. Eng.*, vol. 14, no. 1, pp. 85–96, 2013.

[23] S.-H. Ni, J.-L. Li, Y.-Z. Yang, and Z.-T. Yang, "An improved approach to evaluating pile length using complex continuous wavelet transform analysis," *Insight - Non-Destructive Test. Cond. Monit.*, vol. 59, no. 6, pp. 318–324, 2017.

[24] J.-Y. Zhang, L.-Z. Chen, and J. Zhu, "Theoretical basis and numerical simulation of parallel seismic test for existing piles using flexural wave," *Soil Dyn. Earthq. Eng.*, vol. 84, pp. 13–21, 2016.

[25] J. T. Coe and B. Kermani, "Comparison of Borehole Ultrasound and borehole radar in evaluating the length of two unknown bridge foundations," *DFI J. - J. Deep Found. Inst.*, vol. 10, no. 1, pp. 8–24, Jan. 2016.

[26] E. Niederleithinger, "Improvement and extension of the parallel seismic method for foundation depth measurement," *Soils Found.*, vol. 52, pp. 1093–1101, 2013.

[27] K. F. Lo, S. H. Ni, Y. H. Huang, and X. M. Zhou, "Measurement of unknown bridge foundation depth by parallel seismic method," *Exp. Tech.*, vol. 33, no. 1, pp. 23–27, 2009.

[28] D. A. Sack, S. H. Slaughter, and L. D. Olson, "Combined Measurement of Unknown Foundation Depths and Soil Properties with Nondestructive Evaluation Methods," *Transp. Res. Rec. J. Transp. Res. Board*, no. 1868, pp. 76–80, 2004.

[29] M. S. Hossain, ; M S Khan, ; J Hossain, ; G Kibria, and T. Taufiq, “Evaluation of Unknown Foundation Depth Using Different NDT Methods,” *J. Perform. Constr. Facil.*, vol. 27, no. 2, pp. 209–214, 2013.

[30] S. M. Sayed, M. Asce, H. N. Sunna, and P. R. Moore, “Rational Alternative to Positive Discovery of Pile-Supported Bridges with Unknown Foundation Depth,” 2012.

[31] M. S. Hossain, ; M S Khan, J. Hossain, G. Kibria, and T. Taufiq, “Evaluation of Unknown Foundation Depth Using Different NDT Methods,” *J. Perform. Constr. Facil.*, vol. 27, no. 2, pp. 209–214, 2011.

[32] J.-L. Briaud *et al.*, “Unknown Foundation Determination for Scour,” *Texas Dept, Transp. Texas Transp. Institue, Coll. Station. TX*, 2012.

[33] Yousefpour, Negin, Medina-Cetina, Zenon, Briaud, and Jean-Louis, “Evaluation of Unknown Foundations of Bridge Subjected to Scour - Physically Driven Artificial Neural Network Approach,” *Transp. Res. Rec. J. Transp. Res. Board Transp. Res. Board Natl. Acad.*, no. 2433, pp. 27–38, 2014.

[34] L. D. Olson, F. Jalinoos, and M. F. Aouad, “Determination of Unknown Subsurface Bridge Foundations,(NCHRP 21-5 Interim Report Summary),” *Geotech. Eng. Noteb. Issuance GT-16. Fed. Highw. Adm. Washington, DC*, 1998.

[35] Sarkar K.H., Islam M.S., Yasmin T., and Sarna S.A., “Determination of unknown bridge foundation depths with parallel seismic (PS) systems,” in *IABSE-JSCE*, 2015.

[36] E. J. Mercado and M. W. O’Neill, “Methods to measure scour depth and the depth of unknown foundations,” in *The 3rd International Conference on Applied Geophysics-Geophysics*, 2003.

[37] S. Rashidyan, “Characterization of Unknown Bridge Foundations,” *Diss. Univ. New Mex.*,

2017.

[38] D. A. Realpe, “Seismic Performance and Displacement Capacity of RCFST Drilled Shafts.,” *Diss. North Carolina State Univ.*, 2017.

[39] R. J. Finno, “1-D Wave Propagation Techniques in Foundation Engineering,” in *The Art of Foundation Engineering Practice Congress*, 2010, pp. 260–277.

[40] A. Hanifah, “A theoretical evaluation of guided waves in deep foundations.,” *Diss. Northwest. Univ.*, 2000.

[41] H. C. Chao, “An Experimental Model for Pile Integrity Evaluation using a Guided Wave Approach,” *Diss. Northwest. Univ.*, 2002.

[42] H. Wang, “Theoretical Evaluation of Embedded Plate-Like and Solid Cylindrical Concrete Structures with Guided Waves,” *Diss. Northwest. Univ.*, 2004.

[43] J. J. Lynch, “Experimental verification of flexural guided waves in concrete cylindrical piles,” *Diss. Northwest. Univ.*, 2007.

[44] V. Samu and M. Guddati, “Nondestructive Method for Length Estimation of Pile Foundations through Effective Dispersion Analysis of Reflections,” *Manuscr. Submitt. Publ.*, 2018.

[45] G. R. Cowper, “The shear coefficient in Timoshenko’s beam,” *Trans. ASME J. Appl. Mech.*, vol. 33, no. 4, pp. 335–340, 1966.

[46] A. Vaziriastaneh, “On the Forward and Inverse Computational Wave Propagation Problems.,” North Carolina State University, 2016.

[47] V. Samu, “Estimation of Embedded Length of Pile Foundation using Flexural Wave Model,” 2014.

[48] M. Novak, T. Nogami, and F. Aboul-Ella, “Dynamic Soil Reactions for Plane Strain

Case," *Jounal Eng. Mech. Div.* , pp. 953–959, 1978.

[49] K. McConnell and P. Varoto, *Vibration testing: theory and practice*. 1995.

[50] W. G. Halvorsen and D. L. Brown, "Impulse Technique for Structural Frequency Resposne Testing," *Sound Vib.*, vol. 11, no. 11, pp. 8–21, 1977.

[51] M. French, "What makes a Good Impact Function?," *Exp. Tech.*, vol. 23, no. 6, pp. 33–35, 1999.

[52] D. L. Brown, R. J. Allemang, and A. W. Phillips, "Forty Years of Use and Abuse of Impact Testing : A Practical Guide to Making Good FRF Measurements," *Exp. Tech. Rotating Mach. Acoust.*, vol. 8, pp. 221–241, 2015.

[53] F. Rausche, G. E. Likins, and M. Hussein, "Pile Integrity by Low and High Strain Impacts," *Third Int. Conf. Appl. Stress. Theory to Piles*, vol. Vol. 25, 1988.

[54] B. H. Hertlein and A. G. Davis, *Nondestructive Testing of Deep Foundations*. Wiley, 2006.

[55] S. Wu, J. Lai, B.-H. Yang, and C.-F. Cheng, "Integrity Testing of Model Piles with Pile Cap," in *International Symposium Non-Destructive Testing in Civil Engineering*, 2015.

[56] J.-P. Ertel, E. Niederleithinger, and M. Grohmann, "Advances in Pile Integrity Testing," *Near Surf. Geophys.* , vol. 14, pp. 503–512, 2016.

[57] "ASTM D5882-26 Standard Test Method for Low Strain Impact Integrity Testing of Deep Foundations." 2016.